SUPERSONIC FLOW ABOUT CONES AT LARGE ANGLES OF ATTACK

Clive Fletcher

REPORT NO. FM-74-8
GRANT NO. AFOSR 72-2318
May 1974

COLLEGE OF ENGINEERING
UNIVERSITY OF CALIFORNIA, Berkeley

UNCLASSIFIED

SECURITY CLASSIFICATION OF THIS PAGE (When Data Entered)

REPORT DOCUMENTATION PAGE	READ INSTRUCTIONS BEFORE COMPLETING FORM
1. REPORT NUMBER: AFOSR - TR - 76 - 0148	2. GOVT ACCESSION NO. / 3. RECIPIENT'S CATALOG NUMBER
4. TITLE (and Subtitle): SUPERSONIC FLOW ABOUT CONES AT LARGE ANGLES OF ATTACK.	5. TYPE OF REPORT & PERIOD COVERED: INTERIM Rept. / 6. PERFORMING ORG. REPORT NUMBER
7. AUTHOR(s): C. A. J. FLETCHER; FM-74-8	8. CONTRACT OR GRANT NUMBER(s): AF-AFOSR-2318-72
9. PERFORMING ORGANIZATION NAME AND ADDRESS: UNIVERSITY OF CALIFORNIA, BERKELEY; DEPARTMENT OF MECHANICAL ENGINEERING; BERKELEY, CALIFORNIA 94720	10. PROGRAM ELEMENT, PROJECT, TASK AREA & WORK UNIT NUMBERS: 681307; 9781-02; 61102F; 9781Ø2
11. CONTROLLING OFFICE NAME AND ADDRESS: AIR FORCE OFFICE OF SCIENTIFIC RESEARCH/NA; BUILDING 410; BOLLING AIR FORCE BASE, D C 20332	12. REPORT DATE: May 1974 / 13. NUMBER OF PAGES: 130 (133p.)
14. MONITORING AGENCY NAME & ADDRESS (if different from Controlling Office)	15. SECURITY CLASS. (of this report): UNCLASSIFIED / 15a. DECLASSIFICATION/DOWNGRADING SCHEDULE

16. DISTRIBUTION STATEMENT (of this Report)

Approved for public release; distribution unlimited.

17. DISTRIBUTION STATEMENT (of the abstract entered in Block 20, if different from Report)

18. SUPPLEMENTARY NOTES

19. KEY WORDS (Continue on reverse side if necessary and identify by block number)

SUPERSONIC CROSSFLOW
CONICAL FLOW
INVISCID FLOW
NUMERICAL METHOD
G T T METHOD
METHODS OF CHARACTERISTICS
VORTICAL SINGULARITY
INTERNAL SHOCK
COMPARISON WITH EXPERIMENT

20. ABSTRACT (Continue on reverse side if necessary and identify by block number)

A numerical method is presented which is applicable to the supersonic inviscid flow about cones inclined at such angles of attack that a substantial region of supersonic crossflow exists ($M_{cr} > 1$). The method is based partly on the method of characteristics. The method produces results that compare favorably with experimental data and with the results of other numerical methods. The numerical method has produced results in the range: free stream Mach number, $M_\infty = 3$ to 16; incidence, $\alpha = 10^\circ$ to 50°, nose cone angles, $\theta_b = 5^\circ$ to 30°. These results demonstrate similar trends with M_∞, α and θ_b as obtained for subsonic crossflow.

DD FORM 1 JAN 73 1473 EDITION OF 1 NOV 65 IS OBSOLETE

400426

UNCLASSIFIED

SECURITY CLASSIFICATION OF THIS PAGE (When Data Entered)

Mach numbers ($M_{cr} < 1$) by Babenko et al. (BVLR method). From the numerical data and from the equations of motion at the body surface it appears that the vortical singularity will remain attached to the body if the crossflow is just supersonic no internal shock will occur and if, in addition, θ_b is small the vortical singularity will be situated just above the body surface. For larger M_{cr} the supersonic crossflow region is terminated by an internal shock and the vortical singularity occurs further from the body.

GRANT NO. AFOSR 72-2318
REPORT NO. FM-74-8
May 1974

SUPPORTED BY
THE U.S. AIR FORCE
OFFICE OF SCIENTIFIC RESEARCH

SUPERSONIC FLOW ABOUT CONES AT LARGE ANGLES OF ATTACK

Clive Fletcher

FACULTY INVESTIGATOR:

M. Holt, Professor of Aeronautical Sciences

UNIVERSITY OF CALIFORNIA

Department of Mechanical Engineering
Berkeley, California 94720

ACKNOWLEDGMENT

The author is particularly indebted to Professor M. Holt for his continuing encouragement, advice and support. In addition, the author is grateful to Dr. P. Kutler of NASA-Ames Research Center, who provided the raw data that permitted a comparison (Figs. 8 to 10) with the shock capturing technique to be made. Also the author is grateful to Dr. J. M. Lyons of Aerospace Corporation, who provided the numerical data on which Fig. 12 is based.

ABSTRACT

A numerical method is presented which is applicable to the supersonic inviscid flow about cones inclined at such angles of attack that a substantial region of supersonic crossflow exists ($M_{cr} > 1$). The method is based partly on the method of Gilinskii, Telenin and Tinyakov and partly on the method of characteristics. The method produces results that compare favorably with experimental data and with the results of other numerical methods.

The numerical method has produced results in the range: free stream Mach number, M_∞ = 3 to 16; incidence, α = 10° to 50°; nose cone angles, θ_b = 5° to 30°. These results demonstrate similar trends with M_∞, α and θ_b as obtained for subsonic crossflow Mach numbers ($M_{cr} < 1$) by Babenko et al (BVLR method).

From the numerical data and from the equations of motion at the body surface it appears that the vortical singularity will remain attached to the body if the crossflow remains subsonic. If the crossflow is just supersonic no internal shock will occur and if, in addition, θ_b is small the vortical singularity will be situated just above the body surface. For larger M_{cr} the supersonic crossflow region is terminated by an internal shock and the vortical singularity occurs further from the body.

TABLE OF CONTENTS

LIST OF FIGURES

LIST OF SYMBOLS

a	local sound speed
a	coefficient used in equation (5.24)
a_{ik}	coefficient used in equation (4.2)
a_*	critical sound speed
A	variable defined after equation (2.27)
A	variable defined after equation (5.19)
b	variable defined after equation (5.9)
b	coefficient used in equation (5.24)
B	Bernoulli constant, equation (2.10)
B	variable defined after equation (2.19)
B	variable defined after equation (2.27)
B	matrix of the coefficient u_o^k, equation (4.4)
B	variable defined after equation (5.14)
c	coefficient used in equation (5.24)
C	variable defined after equation (2.27)
C	variable defined after equation (5.15)
C_p	pressure coefficient, $C_p = (p - p_\infty)/\frac{1}{2} U_\infty^2$
d_{ij}	elements of the matrix D, equation (4.8)
$\underline{d}_i$	independent vector directions, Appendix A
D	coefficient matrix defined by equation (4.7)
D	variable defined after equation (2.27)
D	variable defined after equation (5.16)
D_1, D_2, D_3, D_4	variables defined by equation (4.13)
D_5	variable defined after equation (4.18)

E	variable defined after equation (2.32)
E	variable defined after equation (5.20)
E	variable defined by equation (6.7)
F	variable defined after equation (2.32)
F	variable defined after equation (5.20)
F	sum of the squares of the normal velocity at the body surface, equation (4.21) and Appendix A.
FCH	error at point 3, equation (5.27)
G	variable defined after equation (5.21)
G	variable defined by equation (6.7)
H	variable defined after equation (5.21)
H	variable defined by equation (6.7)
I	variable defined by equation (6.7)
J	variable defined by equation (6.7)
k	variable used in the analytic function representation, equation (4.1)
k	general characteristic direction
k_c	particular characteristic direction
k_s	streamline direction
K	constant in the entropy definition, equation (2.9)
K	matrix of function values, equation (4.3)
K_1, K_2, K_3	variables defined by equation (4.13)
K_4	variable defined after equation (4.18)
m	order of the analytic function representation, equation (4.1)
M	Mach number
M_{cr}	crossflow Mach number, $((v^2 + w^2)/a^2)^{1/2}$

M_r	radial Mach number, u/a
M_s	Mach number on the surface at the vortical singularity, equation (3.1)
M_∞	free stream Mach number
n_1, n_2, n_3, n_4	variables defined after equation (2.13)
N	number of rays used to find the ξ derivative in the leeward region
p	pressure
p_i	variable defined after equation (A.7)
p_o	stagnation pressure
p_s	pressure at the surface at the vortical singularity, equation (3.1)
p_∞	free stream pressure
q_{cr}	crossflow velocity
q_i	coefficient relating $\underline{\delta}$ to $\underline{d}$ in equation (A.6)
r	radial coordinate
$\hat{R}$	universal gas constant
s	entropy
s_i	scaling factor used in equations (A.8) and (A.9)
s_o	entropy reference level
S	entropy parameter, p/ρ^γ
S_s	value of entropy parameter on body surface
u	radial velocity component
u_k	first approximation to $\gamma_k^{\,1}$, equation (A.11)
$u_k^{\,o}$	coefficients of the analytic function representation, equation (4.1)

U_∞ free stream velocity

v normal velocity component

v_k normal velocity component at the body on the kth ray

v_k second approximation to γ_k^i, equation (A.12)

v_{n_1} upstream normal velocity of the internal shock, equation (6.8)

v_{ns} normal velocity on downstream side of the internal shock, equation (6.8)

w circumferential velocity component

x distance from characteristic to the mesh point m,n, equation (5.23)

X variable defined by equation (5.25)

Greek Letters

α angle of attack; incidence

β characteristic direction

β_{cr} crossflow Prandtl-Glauert parameter, $(M_{cr}^2 - 1)^{1/2}$

γ specific heat ratio

γ_i^k approximate rate of change of the normal velocity on the kth ray with a change in the shock location on the ith ray, Appendix A

$\underline{\delta}$ correction to the shock location, Appendix A

ϵ angle between normal to shock surface and a meridian plane, ϕ = const., after equation (2.13)

ϵ distance from the vortical singularity, equation (3.3)

η circumferential coordinate defined by equation (2.15)

$\Delta\eta$ step size in the η direction

θ angular coordinate measured from the cone axis

θ_b	cone nose angle, location of the body surface
θ_s	angular location of the outer shock
λ	angular distance between the internal shock and the leeward line of symmetry
λ	scalar multiplying $\underline{\delta}$, Appendix A
λ_m	value of λ which makes F in equation (A.1) a minimum
μ	constant related to specific heat ratio, after equation (2.3)
ξ	coordinate defined, by equation (2.16), to transform the region between the body surface and the outer shock into a rectangle.
$\Delta\xi$	step size in the ξ direction
ρ	density
σ	angular distance between the body surface and the outer shock, equation (2.17)
τ	coordinate defined, by equation (2.25), to transform the region between the internal shock and the leeward line of symmetry into a rectangle
$\Delta\tau$	step size in the τ direction
ϕ	circumferential coordinate measured from the windward line of symmetry
ϕ_{is}	location of the internal shock
ϕ_{max}	fifth ray of the windward region; upstream boundary of the shoulder region
ϕ_{sep}	circumferential location at which flow separates from surface of cone, Section 3.1

ψ	circumferential coordinate centered at the vortical singularity

Subscripts

c	characteristic direction
m	ξ location in the characteristics grid, Section 5
n	η location in the characteristics grid, Section 5
o	indicates a line on which solution has been found, Section 5
o	stagnation conditions
s	conditions at shock
θ,ϕ,ξ,η	partial differentiation with respect to these variables
1	conditions obtained from characteristic solution, equation (6.8)
1,2, 4	intersection of characteristic directions with the line $\eta = \eta_o$, Section 5
3	mesh point at which a solution is sought, Section 5
∞	free stream conditions
_	underline indicates vector
–	overbar indicates dimensional quantity, Section 2.0

1.0 INTRODUCTION

The study of supersonic inviscid flow past inclined cones is attractive because it shares with two dimensional flow a dependence on only two independent variables (conical flows are independent of the distance from the apex), while revealing detailed flow behavior that is typical of more complex, inclined slender bodies. The analysis of viscous flow past cones in a supersonic stream is also simplified by the conical nature of the inviscid outer flow (Bashkin, 1968).

Historically the first attempt to obtain a numerical solution for the flow about an inclined cone was made by Stone (1948,1952). Stone's solutions, for purely inviscid flow, allowed for second order incidence effects. Kopal (1947,1949), using Stone's method, produced tables of the flow variables for supersonic flow about cones inclined at small angles of attack. However, Ferri (1951) indicated that Stone's method had an inherent error. Stone's solutions were based on the assumption that all flow variables, including entropy, were periodic in the circumferential angle, ϕ. Such an assumption is incorrect at the body surface where the entropy must be constant (since the body surface is a local stream surface). To correct this situation, Ferri introduced the concept of a vortical layer adjacent to the body surface. Across the vortical layer the streamlines vary from approximately normal to the surface at the outer edge of the layer to parallel to the body at the inner edge of the layer. All the streamlines eventually meet at a singular point on the body situated on the leeward line of symmetry. At this "vortical" singularity the entropy is multi-

valued. More references, dealing specifically with the vortical (or entropy) layer and the vortical singularity, are given in Section 3.1. It now appears (see Section 8) that the entropy layer is only significant for small angles of attack, for which the vortical singularity is attached to the body surface.

The next stage in the application of more sophisticated numerical methods to the inclined cone problem was the advent of the "inverse methods" of Briggs (1960) and Stocker and Mauger (1962). The inverse methods were a significant improvement over previous methods in that the inverse methods solved the full non-linear, inviscid equations. In the inverse method the shock location is prescribed and the equations of motion are integrated until the normal velocity component is zero. This defines the body location. Inverse methods work well for small angles of attack but lead to inaccurate body shapes at large angles of attack.

The method of integral relations (MIR) has been applied to the flow around inclined cones (Chushkin and Shchennikov, 1960; Brook, 1964; and Ndefo, 1968), but with limited success, even though application of MIR to the related blunt body problem was successful (Van Dyke, 1958, and Belotserkovskii, 1966). In the application of MIR to inclined cones the flow variation in a direction normal to the body is represented analytically. The governing partial differential equations then reduce to ordinary differential equations in the circumferential direction.

The first finite difference method to obtain a solution for an inclined cone was given by Babenko et al. (1964). In this

method (BVLR) the axial coordinate is treated as a timelike variable, thus rendering the governing equations hyperbolic in character. BVLR will handle bodies of arbitrary shape, but is restricted to angles of attack for which the vortical singularity remains attached to the body and for which an internal shock does not occur. A similar method with similar limitations is described by Moretti (1967). More recently shock-capturing methods (Kutler and Lomax, 1970) have been developed which permit internal shocks to occur without having to make any local modifications to cope with the shocks. This is done by deliberately introducing dissipative terms into the finite difference representation of the partial differential equations. The result is to distribute the shock effect over a number of adjoining cells. The shock capturing method, like BVLR, will treat bodies of quite general shape. When applied to the inclined cone problem the shock capturing technique produces results in good overall agreement with other methods. However, for angles of attack at which the vortical singularity moves away from the body surface the dissipative nature of the shock capturing technique replaces the entropy jump at the vortical singularity with an entropy gradient from the outer shock to the body (see Section 7.3).

More recently solutions of the inclined cone problem have been obtained (Helliwell and Lubard, 1973), solving an approximation to the full Navier-Stokes equations, in which the viscous diffusion terms in the axial direction are ignored. Although a solution to the complete viscous flow field is obtained, the method is restricted to small to moderate angles of attack and is

very time consuming.

The methods to be used in the present report fall into a similar category to the MIR method, in the sense that considerable computer time is saved by reducing the governing partial differential equations to ordinary differential equations. The different methods used here are determined by the particular flow behavior in different parts of the flow regime (Fig. 4). In the windward region the method of Gilinskii, Telenin and Tinyakov (1964) is used. The basis of the GTT method is to represent the flow variation in the circumferential direction analytically and to integrate the resulting ordinary differential equations from the outer shock to the body. The choice of the direction of the analytic representation may be contrasted with that used in the MIR method. The integration from the outer shock to the body is repeated, iterating on the outer shock shape for each integration, until the boundary condition of zero normal flow at the body surface is satisfied. The GTT method or variations of it have been applied to the inclined cone problem by Bazzhin and Chelysheva (1967), Jones (1968), Holt and Ndefo (1970), and Klunker, South and Davis (1971). The last reference contains a very comprehensive bibliography of previous work.

When the crossflow is supersonic (Fig. 4), the method of characteristics can be employed to extend the flow in the circumferential direction. The first attempt to apply the method of characteristics to conical flow was due to Maslen (1951), who looked at the flow past an inclined delta wing. Bazzhin, Trusova and Chelysheva (1968) have applied the method of characteristics

to the inclined cone problem.

Unfortunately, since the method of characteristics has no forewarning of downstream conditions there is no way that the boundary condition of zero circumferential velocity on the leeward side of symmetry can be satisfied by using this method alone. Physically the crossflow at the leeward line of symmetry will be subsonic anyway. This failure of the method of characteristics to satisfy this boundary condition suggests the occurrence of an internal shock which will effectively terminate the characteristics region (Fig. 4). Previously attempts have been made (Fowell, 1956 and Babaev, 1962) to allow for the occurrence of an internal shock for the related inclined delta wing problem.

In this report the region between the internal shock and the leeward line of symmetry has been treated by using a modified form of the GTT method. For the leeward region the direction of integration is the circumferential direction. Repeated integrations are made, adjusting the location of the internal shock, until the condition of zero circumferential velocity at the leeward line of symmetry is satisfied.

The related problem of viscous boundary layer flow over an inclined cone in a supersonic free stream was first investigated by Moore (1953). Solutions have more recently been found using the method of integral relations (Bashkin, 1968) and by implicit finite difference techniques (Dwyer, 1971, and Boericke, 1971).

The inclined cone in supersonic flow has also been studied experimentally by Holt and Blackie (1956), Tracy (1963), Avduevskii and Medvedev (1966), Rainbird (1968), Feldhuhn, Winkelmann and

Pasiuk (1971), and Yahalom (1971). The last reference contains a comprehensive bibliography of previous studies.

The present studies are restricted to attached, inviscid supersonic flow at such angles of attack that a substantial region of supersonic crossflow occurs. Also, only circular cones have been considered. Previous investigators (Bazzhin, 1971; Jones, 1968; and Klunker et al., 1971) have also considered elliptic cones and delta wings. The extension of the present method to these cases would be quite straightforward; the major effect would appear through equation (2.17), where θ_b would then be a function of ϕ.

In Section 2 the basic equations are given, along with boundary conditions and required coordinate transformations. The physical nature of the flow field, based mainly on the experimental evidence cited above, is described in Section 3.1 and used to determine the boundaries of the numerical methods, as indicated in Section 3.2. Sections 4, 5, and 6 contain specific descriptions of the numerical methods used in the windward, shoulder and leeward regions (Fig. 4), respectively. The numerical computations are discussed in Section 7. The discussion includes accuracy, execution time, and comparisons with other numerical methods and experimental results. Section 8, based primarily on the numerical studies of this report, gives a physical description of the flow field about cones inclined at large angles of attack, and describes the variation of the flow behavior with changes in the free stream Mach number, incidence, and nose angle. Also in Section 8 lift-off of the vortical singularity and its relation to

the occurrence of an internal shock are discussed.

2.0 FORMULATION OF THE PROBLEM

In this report, spherical coordinates $\{ \begin{matrix} r, \theta, \phi \\ u, v, w \end{matrix} \}$ are used with r measured from the cone apex, θ measured from the cone axis, and ϕ measured from the windward line of symmetry. If $\bar{u}$, $\bar{v}$, $\bar{w}$ are the dimensional velocity components (Fig. 1), then non-dimensionalization with respect to ρ_∞, the free stream density, and a_*, the critical velocity, gives

$$u = \bar{u}/a_* \quad , \quad v = \bar{v}/a_* \quad , \quad w = \bar{w}/a_* \quad ,$$

$$\rho = \bar{\rho}/\rho_\infty \quad \text{and} \quad p = \bar{p}/\rho_\infty a_*^2 \quad . \tag{2.1}$$

In order to describe the flow conditions completely, only the following flow parameters need be specified: free stream Mach number M_∞, angle of attack α, and cone nose angle θ_b. To link the free stream Mach number with the non-dimensionalized variables defined by (2.1), the following expressions can be obtained from the Bernoulli equation (2.10):

$$U_\infty^2 = \frac{M_\infty^2}{\mu^2 \cdot M_\infty^2 + (2/\gamma+1)} \tag{2.2}$$

and

$$p_\infty = \frac{\gamma+1}{2\gamma} \left[1 - \mu^2 \cdot U_\infty^2\right] \quad , \tag{2.3}$$

where

U_∞ is the non-dimensional free stream velocity

p_∞ is the non-dimensional free stream pressure

and $\mu^2 = (\gamma-1)/(\gamma+1)$.

2.1 Equations of Motion

As long as a shock wave is attached to the apex of the cone the flow variables are independent of r and the flow is said to be conical. With this assumption the equations of motion for steady flow of an inviscid, non-conducting fluid become:

Conservation of Mass:

$$v_\theta + \frac{1}{\sin\theta} \cdot w_\phi + \frac{v}{\rho} \cdot \rho_\theta + \frac{w}{\rho \sin\theta} \cdot \rho_\phi + 2u + v \cot\theta = 0 \quad , \tag{2.4}$$

Conservation of 'r' Momentum:

$$v \cdot u_\theta + \frac{w}{\sin\theta} \cdot u_\phi - (v^2 + w^2) = 0 \quad , \tag{2.5}$$

Conservation of 'θ' Momentum:

$$v \cdot v_\theta + \frac{w}{\sin\theta} \cdot v_\phi + \frac{1}{\rho} \cdot p_\theta + u \cdot v - w^2 \cdot \cot\theta = 0 \quad , \tag{2.6}$$

Conservation of 'ϕ' Momentum:

$$v \cdot w_\theta + \frac{w}{\sin\theta} \cdot w_\phi + \frac{1}{\rho \sin\theta} \cdot p_\phi + u\,w + v\,w \cot\theta = 0 \quad , \tag{2.7}$$

Conservation of Energy:

$$v \cdot p_\theta + \frac{w}{\sin\theta} \cdot p_\phi - a^2 (v \cdot \rho_\theta + \frac{w}{\sin\theta} \cdot \rho_\phi) = 0 \quad , \tag{2.8}$$

where the sound speed, $a^2 = \gamma p/\rho$.

The form of the energy equation (2.8) used here comes from the conservation of entropy in the absence of any dissipative

processes. The equation connecting pressure, density and entropy,

$$\frac{p}{\rho^{\gamma}} = k\, e^{(\gamma-1)(s-s_o)/\hat{R}} = S \quad , \tag{2.9}$$

will be used to define the entropy parameter, S, which is conserved along streamlines (except when crossing shock waves). From the equations of motion one algebraic equation, the steady Bernoulli equation, can be obtained,

$$\frac{\gamma p}{(\gamma-1)\rho} + \frac{1}{2}(u^2 + v^2 + w^2) = B \tag{2.10}$$

The Bernoulli constant B is constant throughout the flow field, for the fluid properties assumed. B can be evaluated from (2.3) as

$$B = \frac{1}{2\mu^2} \quad . \tag{2.11}$$

A combination of equations (2.4) - (2.8) and (2.10) will be solved for u, v, w, ρ, and p on the surface of a sphere, defined by r = constant.

2.2 Boundary Conditions

The flow field, in which a solution is to be sought, is bounded by the body, $\theta = \theta_b$, the shock, $\theta = \theta_s(\phi)$, and the windward and leeward lines of symmetry ($\phi = 0$ and 180°, respectively). At the cone surface the normal velocity must be zero,

$$v = 0 \quad \text{and} \quad v_\phi = 0 \quad \text{on} \quad \theta = \theta_b. \tag{2.12}$$

At the shock, which is a conical surface, the flow properties are given in terms of the free stream conditions and the shock slope,

θ_{s_ϕ} by the Rankine-Hugoniot shock relations:

$$u_s = U_\infty n_1 \quad ,$$

$$v_s = n_3 \tan \varepsilon - n_4 \quad ,$$

$$w_s = n_3 + n_4 \tan \varepsilon \quad , \qquad (2.13)$$

$$\rho_s = U_\infty n_2 \cos^2 \varepsilon / n_4 \quad ,$$

$$p_s = \frac{2}{(\gamma+1)} U_\infty^2 n_2^2 \cos^2 \varepsilon - \frac{(\gamma-1)}{2\gamma} (1 - \mu^2 U_\infty^2) \quad ,$$

where

$$\tan \varepsilon = \theta_{s_\phi} / \sin \theta_s \quad ,$$

$$n_1 = \cos \alpha \cos \theta_s - \sin \alpha \sin \theta_s \cos \phi \quad ,$$

$$n_2 = \cos \alpha \sin \theta_s + \sin \alpha \cos \theta_s \cos \phi + \sin \alpha \sin \phi \tan \varepsilon \quad ,$$

$$n_3 = U_\infty (\sin \alpha \sin \phi - n_2 \sin \varepsilon \cos \varepsilon) \quad ,$$

and $$n_4 = (1 - \mu^2 U_\infty^2 (1 - n_2^2 \cos^2 \varepsilon)) / U_\infty n_2 \quad .$$

The angle ε lies between the inward directed normal to the shock surface and the local meridian plane, ϕ = constant. The derivation of the shock relations shown above (2.13), is given by Ndefo (1969).

At the plane of symmetry, ($\phi = 0$ and $180°$),

$$w, \; w_\theta, \; u_\phi, \; v_\phi, \; \rho_\phi, \; p_\phi, \text{ and } \theta_{s_\phi} = 0 \quad . \qquad (2.14)$$

2.3 Transformation of the Coordinates

Initially the region bounded by the body, the shock, and the

plane of symmetry will be transformed into a rectangle (Fig. 2) using the following relations,

$$\eta = \phi/\pi \tag{2.15}$$

$$\xi = (\theta_s(\phi) - \theta)/\sigma(\phi) \quad , \tag{2.16}$$

where

$$\sigma(\phi) = \theta_s(\phi) - \theta_b \quad . \tag{2.17}$$

Noting that

$$\left(\frac{\partial}{\partial\theta}\right)_\phi = -\frac{1}{\sigma}\left(\frac{\partial}{\partial\xi}\right)_\eta \quad , \tag{2.18}$$

and

$$\left(\frac{\partial}{\partial\phi}\right)_\theta = \left(B\left(\frac{\partial}{\partial\xi}\right)_\eta + \left(\frac{\partial}{\partial\eta}\right)_\xi\right)/\pi \quad , \tag{2.19}$$

where

$$B = \pi\left(\frac{1-\xi}{\sigma}\right)\theta_{s_\phi} \quad ,$$

direct substitution into (2.4) - (2.8) leads to:

$$-\frac{1}{\sigma}v_\xi + \frac{B}{\pi \sin\theta}w_\xi + \frac{E}{\rho}\rho_\xi + \frac{1}{\pi \sin\theta}\left(w_\eta + \frac{w}{\rho}\rho_\eta\right) + 2u + v\cot\theta = 0 \quad , \tag{2.20}$$

$$E\,u_\xi + \frac{w}{\pi \sin\theta}u_\eta - (v^2 + w^2) = 0 \quad , \tag{2.21}$$

$$E\,v_\xi - \frac{1}{\rho\sigma}p_\xi + \frac{w}{\pi \sin\theta}v_\eta + uv - w^2\cot\theta = 0 \quad , \tag{2.22}$$

$$E\,w_\xi + \frac{B}{\rho\pi \sin\theta}p_\xi + \frac{1}{\pi \sin\theta}\left(w\,w_\eta + \frac{1}{\rho}p_\eta\right) + uw + vw\cot\theta = 0 \quad , \tag{2.23}$$

$$E(p_\xi - a^2\rho_\xi) + \frac{w}{\pi \sin\theta}(p_\eta - a^2\rho_\eta) = 0 \quad , \tag{2.24}$$

where

$$E = \frac{B\,w}{\pi \sin\theta} - \frac{v}{\sigma} \quad .$$

Equations (2.20) - (2.24) are used as the starting point for the Windward Region (Section 4) and the Shoulder Region (Section 5). In the Leeward Region (Section 6), a further transformation is made to make the region bounded by the body, the outer shock, the internal shock, and the leeward line of symmetry a rectangle (Fig. 3). In this case the same ξ coordinate as defined in (2.16) is used. Instead of η, a new coordinate τ is defined as follows,

$$\tau = \frac{\phi - \phi_{is}(\theta)}{\lambda(\theta)} \qquad (2.25)$$

where

$$\lambda(\theta) = \pi - \phi_{is}(\theta)$$

and

$\phi_{is}(\theta)$ is the location of the internal shock.

θ,ϕ coordinates can be transformed to ξ,τ coordinates by making use of

$$\left(\frac{\partial}{\partial\phi}\right)_{\theta} = A\left(\frac{\partial}{\partial\xi}\right)_{\tau} + B\left(\frac{\partial}{\partial\tau}\right)_{\xi} \qquad (2.26)$$

and

$$\left(\frac{\partial}{\partial\theta}\right)_{\phi} = C\left(\frac{\partial}{\partial\xi}\right)_{\tau} + D\left(\frac{\partial}{\partial\tau}\right)_{\xi} \quad , \qquad (2.27)$$

where

$$A = \frac{\theta_{s_\phi}(1-\xi)}{\sigma}$$

$$B = \frac{1}{\lambda}$$

$$C = -\frac{1}{\sigma}$$

$$D = -\frac{\theta_{is_\theta}\,(1-\tau)}{\lambda} \quad .$$

Substitution into equations (2.20) - (2.24) gives

$$C\,v_\xi + D\,v_\tau + \frac{B}{\sin\theta}\,w_\tau + \frac{A}{\sin\theta}\,w_\xi + \frac{E}{\rho}\,\rho_\xi + \frac{F}{\rho}\,\rho_\tau + 2u + v\cot\theta = 0 \quad , \tag{2.28}$$

$$E\,u_\xi + F\,u_\tau - (v^2+w^2) = 0 \quad , \tag{2.29}$$

$$E\,v_\xi + F\,v_\tau + \frac{C}{\rho}\,p_\xi + \frac{D}{\rho}\,p_\tau + uv - w^2\cot\theta = 0 \quad , \tag{2.30}$$

$$E\,w_\xi + F\,w_\tau + \frac{A}{\rho\sin\theta}\,p_\xi + \frac{B}{\rho\sin\theta}\,p_\tau + uw + vw\cot\theta = 0 \quad , \tag{2.31}$$

$$E\,(p_\xi - a^2\,\rho_\xi) + F\,(p_\tau - a^2\,\rho_\tau) = 0 \quad , \tag{2.32}$$

where

$$E = C\,v + \frac{A}{\sin\theta}\,w$$

$$F = D\,v + \frac{B}{\sin\theta}\,w \quad .$$

3.0 PHYSICAL DESCRIPTION OF THE FLOW AND NUMERICAL METHODS USED

It has been the author's intention to obtain a numerical solution that is as physically realistic as possible. Therefore before indicating the numerical methods used a description will be given of the physical nature of the flow. In addition, attention will be drawn to certain physical features which suggest natural boundaries for local numerical methods, e.g., the occurrence of an internal shock terminates the region in which a solution can be found by the method of characteristics.

3.1 Physical Description of the Flow

As indicated in the introduction, this report is restricted to those flows in which the crossflow becomes supersonic, $M_{cr} = [(v^2+w^2)/a^2)]^{1/2} > 1$. Qualitatively the crossflow about an inclined cone in a free stream of Mach number M_∞ will be similar to the flow about a two dimensional cylinder in a free stream of $M_\infty \sin \alpha$, where α is the inclination of the cone to the free stream (Fig. 1). For a two dimensional cylinder the flow will first become locally supersonic on the surface of the cone at a circumferential angle of approximately 90°. Both experiments and the Janzen-Rayleigh analysis indicate that the corresponding free stream Mach number will be 0.4. Thus the crossflow about an inclined cone should be supersonic if $M_\infty \sin \alpha > 0.4$. For a substantial area of supersonic crossflow to occur it is desirable that $M_\infty \sin \alpha \gg 0.4$. The two approaches are either to make M_∞ large or to make α large. However, large incidence generally leads to flow separation from the cone surface and a region near the leeward generator in which the flow behavior is dominated by

viscous effects. Since only the inviscid Navier-Stokes equations are treated in this report no prediction of flow separation can be made. The other approach of increasing M_∞ will eventually lead to the occurrence of real gas effects which will cause the flow behavior in the region where the shock is strongest, i.e., at the windward line of symmetry, to depart from the flow behavior implied by the assumption of the perfect gas relations. Generally it is possible to cover a larger range of free stream Mach numbers, and still obtain physically realistic solution, than it is to cover a range of incidences. The only other parameter that can influence the inviscid flow about inclined cones is the cone nose angle, θ_b (Fig. 1). The ratio α/θ_b becomes a useful parameter with which to describe the flow. Although separation and viscous effects become more important with increasing incidence, such effects are suppressed by increasing θ_b. Avduevskii and Medvedev (1966) have obtained the following correlation between separation angle (ϕ is measured from the windward line of symmetry (Fig. 1)) and θ_b for $\alpha/\theta_b > 1$.

θ_b	5°	10°	15°	30°
ϕ_{sep}	118°	130°	138°	145°

As long as $M_\infty > 5$ and $\alpha/\theta_b > 1$ this correlation is independent of both M_∞ and α. Thus the region in which viscous effects are significant becomes smaller as θ_b is increased. The conditions $M_\infty > 5$ and $\alpha/\theta_b > 1$ will also imply the crossflow typically becomes supersonic. For flow conditions in which the region of supersonic crossflow extends from the body to the outer shock it is

to be expected that the flow adjacent to the body will expand (pressure will reduce and M_{cr} will increase) with increasing ϕ. Consequently, in order for the crossflow Mach number to be zero at $\phi = 180°$ at the body the occurrence of an internal shock is anticipated. In this case the cause of the internal shock is the need to satisfy the symmetry condition at $\phi = 180°$. The location of this shock can be found by solving the inviscid equations of motion. The internal shock is weak but will cause some pressure rise. The impingement of such a shock wave on a boundary layer in the presence of a supersonic (upstream) free stream is unstable in that the local inviscid/viscous interaction causes the streamwise pressure gradient to increase and the boundary layer to separate. Thus the separation is "self-induced" (Berger, 1971). The separation of the boundary layer causes the inviscid flow behavior to change and the physically measured separation point (Feldhuhn, et al., 1971; Rainbird, 1968) is considerably upstream of the location of the internal shock predicted by an inviscid analysis. However, the experimental studies of Avduevskii and Medvedev (1966), Tracy (1963), and Yahalom (1971) indicate that the internal shock often consists of two branches joined far from the body. The upstream branch is associated with the separation of the boundary layer and the downstream branch appears to be responsible for reducing the circumferential velocity component, w, so that the symmetry condition ($w = 0$) can be satisfied at $\phi = 180°$. Thus it might be expected that the occurrence of an internal shock predicted from the solution of the inviscid Navier-Stokes equations is equivalent to the downstream branch of the internal shock that

has been measured experimentally.

Ferri (1951) has demonstrated that at some point (called the vortical singularity) in the flow the entropy will be multivalued. If the projection of the stream surfaces is made onto the surface of a sphere of constant radius and with a center coincident with the apex of the cone, the result is a series of lines along which the entropy remains constant (except when crossing a shock wave). These lines will be referred to as streamlines throughout the rest of this report. The vortical singularity is the point at which all streamlines meet.

For small angles of attack the vortical singularity lies on the surface of the cone at $\phi = 180°$. Under certain conditions, e.g., large incidence, the vortical singularity leaves the surface of the body and moves in the direction of the external shock along the line $\phi = 180°$. Melnik (1967) obtained a criterion for the vortical singularity to leave the surface, namely,

$$P_{\phi\phi} < -2\gamma \cdot p_s \cdot M_s^2 \cdot \sin^2 \theta_b \qquad (3.1)$$

where p_s and M_s refer to the pressure and Mach number at the vortical singularity.

When the vortical singularity is attached to the body the streamlines adjacent to the body are very close together, particularly as the vortical singularity is approached. This leads to a considerable entropy gradient normal to the body. Previous analyses of this "entropy layer" by Cheng (1962), Holt (1954), Melnik (1967), Munson (1965), and Woods (1962), all indicate that the pressure remains constant across the entropy layer.

At an isolated vortical singularity (i.e., for large incidence),

$$v = w = w_\theta = v_\phi = 0 \tag{3.2}$$

Some of these conditions follow from the location of the vortical singularity on the leeward line of symmetry. In the immediate neighborhood of the vortical singularity let

$$v = w = w_\theta = v_\phi = O(\varepsilon) \ , \tag{3.3}$$

where ε is the distance from the vortical singularity. Substitution into equations (2.3) and (2.4) indicates that even if v_ϕ and w_θ are $O(1)$ then p_ϕ and p_θ are $O(\varepsilon)$. Thus as the vortical singularity is approached p_θ and $p_\phi \to 0$ and hence p remains continuous and constant at the vortical singularity.

At the vortical singularity the following equations are available,

$$p = \rho^\gamma S \tag{3.4}$$

and

$$\frac{\gamma p}{(\gamma-1)\rho} + \frac{u^2}{2} = B \ , \tag{3.5}$$

since $w = v = 0$.

If it is assumed that $S = S(\psi)$, where ψ is a circumferential angle for a coordinate system centered at the vortical singularity, then differentiating (3.4) with respect to ψ, and noting that p is locally constant, leads to

$$-\frac{\gamma}{\rho} \cdot \rho_\psi = \frac{S_\psi}{S} \ . \tag{3.6}$$

and, if use is made of (3.5),

$$(\gamma-1)\, u \frac{u_\psi}{a^2} = \frac{\rho_\psi}{\rho} = -\frac{S_\psi}{\gamma S} \quad . \tag{3.7}$$

If flow conditions are known at the outer shock then equation (3.7) gives the appropriate jumps in u and ρ when the vortical singularity is crossed. This is made use of in Section 6.

The occurrence of a vortical singularity is a result of entropy remaining constant along streamlines. However, that is only true for inviscid flow. Since the vortical singularity occurs in a location that is dominated by viscous effects, one might ask whether there is any experimental evidence for the occurrence of an isolated vortical singularity. In fact there is; the work of Feldhuhn et al. (1971) indicates a large isolated density gradient combined with $v = w = 0$ on the leeward line of symmetry just outside the separated flow region.

3.2 Numerical Methods Used

The overall strategy has been to use numerical methods that are as economical as possible, even if this entails greater algebraic complexity. Thus schemes that reduce the governing partial differential equations to ordinary differential equations have been used in preference to two or three dimensional finite difference codes which treat each independent variable in the same manner. Physical knowledge of the local flow behavior has been utilized to permit different numerical schemes to be employed in particular regions of the flow field.

The region adjacent to the windward line of symmetry

(Fig. 4) is similar to the two dimensional or axisymmetric blunt body problem. Because of this and the earlier work of Holt and Ndefo (1970) the GTT method (after Gilinskii, Telenin and Tinyakov (1964)) has been used to solve the windward region.

For most of the flow conditions $(M_\infty, \alpha, \theta_b)$ examined in this report, the cross flow Mach number, M_{cr}, exceeds one at $\phi = 90°$. If $M_{cr} > 1$ the governing equations (2.4) to (2.8), have a hyperbolic character and it is more efficient to extend the solution to large ϕ using a method of characteristics. In this report the method of characteristics given by Belotserkovskii and Chushkin (1965) has been used. The method of characteristics requires starting data on a non-characteristic line within the hyperbolic region. For most of the cases examined in this report $\phi = 90°$ has been used as the required non-characteristic line. This line forms the boundary between the windward and shoulder regions (Fig. 4).

If a characteristics solution is extended around the body no warning is obtained of the requirement of symmetry at $\phi = 180°$. Thus Bazzhin (1971) obtained solutions, using the method of characteristics, which gave a non-zero circumferential velocity component, w at $\phi = 180°$. As indicated in Section 3.1, an internal shock wave is expected to occur. The flow behind the internal shock will have a subsonic crossflow component, at least close to the body. Thus the method of characteristics cannot be extended beyond the internal shock.

For the leeward region (Fig. 4), the GTT method has been modified to integrate from the internal shock to the leeward line of symmetry ($\phi = 180°$), iterating on the location of the internal shock

until the condition of zero circumferential velocity at $\phi = 180°$ is satisfied. A second integration from the $\phi = 180°$ line to the internal shock and a third integration from the internal shock to the $\phi = 180°$ line have been made in order to establish the correct flow behavior adjacent to the isolated vortical singularity.

4.0 WINDWARD REGION

Because of the similarity of this region with the flow about two dimensional and axisymmetric blunt bodies it is natural to attempt to modify methods that have been successful for the blunt body. Thus previous investigators of the supersonic flow about inclined cones (Bazzhin and Chelysheva (1967), Holt and Ndefo (1970)) have followed the blunt body solutions of Gilinskii, Telenin and Tinyakov (1964) (GTT method). A basic feature of the GTT method is that the variation of the variables in one direction is represented analytically. For a cone, symmetry conditions suggest the use of Fourier series of the form, e.g.,

$$u(\xi,\eta) = \sum_{k=0}^{m-1} u_k^{o}(\xi) \cos k \pi \eta \qquad (4.1)$$

to represent the u variation in the η direction. If equations like (4.1) for the other flow variables are differentiated and substituted into (2.20) - (2.24) there results a system of (5xm) ordinary differential equations that can be integrated simultaneously in the ξ direction, along m rays of constant η (Fig. 5). At first sight it appears that at each ξ step use must be made of equations like (4.1) in order to obtain the local function values.

It is interesting to compare this state of affairs with the Method of Lines (Liskovets, 1965). In the Method of Lines, typically the η derivatives are given a finite difference representation. E.g., for the ith ray,

$$(u_\eta)_i = \sum_{k=0}^{m-1} a_{i_k} u_k \quad . \tag{4.2}$$

Since the coefficients a_k are known *a priori*, the resulting ordinary differential equations are in terms of the function values e.g., u rather than in terms of coefficients of a series (like $u_k^{\,o}(\xi)$ in (4.1)). It might be concluded that such a scheme is more economical. Jones (1968) and Klunker et al. (1971) essentially used the Method of Lines to solve the inclined cone problem. However, if equation (4.1) is generalized into a matrix equation it can be rearranged to look like equation (4.2). Writing (4.1) in the form

$$[U]_i = [K]_{i,k}\,[B]_k \tag{4.3}$$

where the elements of $[U]_i$ are the radial velocity components u_i on the ith ray, the elements of $[K]_{i,k}$ are the kth order cosine terms evaluated on the ith ray, $\cos(k\pi\eta_i)$ and the elements of $[B]_k$ are the unknown coefficients, $u_o^{\,k}(\xi)$.

It follows that

$$[B]_k = [K]^{-1}_{k,j}\,[U]_j \quad . \tag{4.4}$$

If equation (4.1) is differentiated with respect to η and put into matrix notation, the result is

$$[U_\eta]_i = [K_\eta]_{i,k}\,[B_k] \tag{4.5}$$

where the elements of $[U_\eta]_i$ are the η derivatives of the radial velocity components $(u_\eta)_i$ on the ith ray, and the elements of $[K_\eta]_{i,k}$ are the kth order sine terms evaluated as the ith ray, $-k\pi \sin(k\pi\eta_i)$. Substitution for $[B_k]$ into (4.5), from (4.4)

leads to

$$[U_\eta]_i = [K_\eta]_{i,k} [K]^{-1}_{k,j} [U]_j \quad . \tag{4.6}$$

Setting

$$[D]_{ij} = [K_\eta]_{i,k} [K]^{-1}_{j,k} \tag{4.7}$$

allows (4.6) to be written as

$$(u_\eta)_i = \sum d_{ij} u_j \tag{4.8}$$

where d_{ij} is an element of $[D]_{ij}$. From equations (4.1), (4.5), and (4.7) it is obvious that d_{ij} is a function, only, of the location of the ith ray and the type of analytic representation assumed. The similarity between equations (4.2) and (4.8) is self-evident. On the basis of this it will be assumed, in this report, that the GTT method and the Method of Lines are equivalent.

Three different forms for the coefficients d_{ik} have been tried:

1) An exact matching of the function values using a Fourier series, e.g., equation (4.1).
2) A least-squares matching of function values using a Fourier series of order m-2.
3) A fifth order finite difference representation, e.g., equation (4.2).

For a test case of 20° cone inclined at 30° to a free stream of Mach number 7.00 all three forms gave results that agreed within the accuracy of the method. For the results shown in this report the fifth order finite difference method was used because it

appeared to produce marginally more stable behavior of the iteration scheme for fixing the shock location. However, any conclusion of this nature is entirely subjective and may well be erroneous.

In Gilinskii, Telenin and Tinyakov (1964) it is pointed out that the method applied to an elliptic Cauchy problem is fundamentally unstable and that any disturbances will tend to grow like $\exp(m\xi)$. Consequently, neither m nor ξ can be allowed to be large. ξ is determined by equation (2.16) and varies between zero at the shock and one at the body. m is the total number of rays. If the range of interest of η is $\Delta\eta$ then the η step size is $\Delta\eta/(m-1)$ and the truncation error of representations like (4.2) is of order $[\Delta\eta/(m-1)]^{m-1}$. Therefore, for greater accuracy one would like to make m large, but the exponential disturbance growth suggests m small. In the present report five rays have been used ($m = 5$), this is typical of the number of rays used by the other investigators mentioned above. In order to reduce the growth of disturbances it was felt that the second method of representing the coefficients a_{ik} by matching the function values in a least squares sense might be advantageous. However, the loss of accuracy associated with the lower order of the least squares scheme had more influence than any possible gain in stability. Possibly had more rays been used the least squares scheme might have compared more favorably with the other two schemes.

Assuming a representation like (4.8) for the η derivatives allows equations (2.20) - (2.24) to be treated as a set of five simultaneous equations for u_ξ, v_ξ, w_ξ, ρ_ξ, and p_ξ. Further manipulation gives the following explicit form for the unknowns

u_ξ to p_ξ.

$$p_\xi = \frac{\gamma p [K_3 D_2 - D_1/\sigma] - K_2 [a^2 D_3 + D_4]}{[a^2(K_3^2 + 1/\sigma^2) - K_2^2]} , \qquad (4.9)$$

$$w_\xi = [\frac{B}{\rho\pi \sin\theta} p_\xi - D_2]/K_2 \qquad (4.10)$$

$$v_\xi = [\frac{1}{\rho\sigma} p_\xi + D_1]/K_2 \qquad (4.11)$$

$$u_\xi = [v^2 + w^2 - K_1 u_\eta]/K_2 \qquad (4.12)$$

where

$$\begin{aligned} K_1 &= w/\pi \sin\theta \\ K_2 &= B w/\pi \sin\theta - v/\sigma \\ K_3 &= B/\pi \sin\theta \end{aligned} \qquad (4.13)$$

$$D_1 = -(\frac{w}{\pi \sin\theta} v_\eta + u v - w^2 \cot\theta)$$

$$D_2 = -(\frac{w}{\pi \sin\theta} w_\eta + \frac{1}{\rho\pi \sin\theta} p_\eta + u w + v w \cot\theta)$$

$$D_3 = -\rho(\frac{1}{\pi \sin\theta} w_\eta + \frac{w}{\rho\pi \sin\theta} \rho_\eta + 2u + v \cot\theta)$$

$$D_4 = -\frac{w}{\pi \sin\theta}(p_\eta - a^2 \rho_\eta) \quad .$$

It can be seen that no explicit expression is given for ρ_ξ. The procedure used was to integrate equations (4.9) to (4.12) using a fourth order Runge-Kutta scheme and at each step ρ was obtained from the Bernoulli equation (2.10)

$$\rho = \gamma p/[(\gamma-1)(B - \tfrac{1}{2}(u^2 + v^2 + w^2))] \qquad (4.14)$$

On ray 1, the windward line of symmetry (Fig. 5), equations (4.9) to (4.12) can be considerably simplified, to give

$$p_\xi = -\gamma p v \sigma D_5/K_4 \tag{4.15}$$

$$w_\xi = 0 \tag{4.16}$$

$$v_\xi = \sigma [a^2 D_5/K_4 + u] \tag{4.17}$$

$$u_\xi = -v\sigma \quad , \tag{4.18}$$

where

$$K_4 = a^2 - v^2$$

and

$$D_5 = \frac{w_\eta}{\pi \sin\theta} + u + v \cot\theta \quad .$$

Since the windward line of symmetry is a streamline, along which entropy is conserved, the following result can be used

$$p = S_s \rho^\gamma \tag{4.19}$$

where S_s is evaluated at the shock. If this result is combined with the Bernoulli equation, there results

$$\rho = [(\gamma-1)(B - \tfrac{1}{2}(u^2 + v^2))/\gamma S_s]^{1/(\gamma-1)} \quad . \tag{4.20}$$

The pressure follows directly from equation (4.19). Thus only (4.17) and (4.18) need be integrated numerically on the windward line of symmetry and (4.15) is redundant.

The general procedure has been to specify a shock location, integrate simultaneously to the body, and test that the body boundary condition of zero normal velocity is satisfied. Due to the arbitrary initial choice of the shock location the normal velocity at the body will generally be non-zero. An iteration scheme is required to

systematically vary the shock location until the body boundary condition is satisfied. In the present report a minimization scheme due to Powell (1964) has been used. The following function representing the body boundary condition is defined

$$F = \sum_{k=1}^{m} v_k^2 \quad . \tag{4.21}$$

The shock is represented by the shock location at $\phi = 0$ and the shock slopes, θ_{s_ϕ} on the other four rays. Powell's method (which is described in more detail in Appendix A) seeks to modify the five parameters specifying the shock until F in equation (4.15) is then $F_{min} = 0$. The choice of specifying the shock shape by its slope differs from previous treatments of the inclined cone problem. The reason for this choice is that the flow solution depends directly on the shock slope through the shock relations (2.13). The shock location only appears indirectly through the scaling of ξ (2.16). It has been found that specifying the shock slope has allowed the iteration scheme to converge faster than it does if the shock location only is specified. This is probably due to a smaller error being introduced when the shock slopes are integrated to give the shock location than if the shock locations are numerically differenced to give the shock slope, bearing in mind Telenin's exponential growth factor.

Examination of the form of equations (4.10) to (4.12) indicates, that as the body is approached K_2 goes to zero and hence the equations are not well behaved. To overcome this a procedure similar to Jones' (1968) has been utilized. The equations have been integrated almost to the body and then the normal velocity has been

extrapolated to the body to test the boundary condition. Examination of equations (2.20) and (2.22) indicates that v_ξ and p_ξ are well behaved at the surface. Once a converged solution for the shock location has been obtained, the behavior at the surface can be determined by integrating along the surface from the windward line of symmetry, since the surface is a streamline. The following equations are available

$$u_\eta = \pi w \sin\theta \tag{4.22}$$

$$p = S_s \rho^\gamma \tag{4.23}$$

$$\frac{\gamma p}{(\gamma-1)\rho} + \frac{1}{2}(u^2 + w^2) = B \tag{4.24}$$

S_s, the entropy parameter at the surface is constant and equal to its value along the windward line of symmetry (i.e., a continuation of the surface streamline). S_s used in equations (4.19) and (4.23) is the same. Since p is obtained by extrapolation, equation (4.23) immediately gives ρ. Equation (4.22) is integrated along the surface with (4.24) used to give current values of w. Ndefo (1969) and Jones (1968) both report a significant change in entropy close to the surface. However, as can be seen from Fig. 19, there is no obvious entropy layer at the larger incidences treated here. This result was also noted by Bazzhin (1971).

In the present study a step-size of $\Delta\xi = 0.1$ was used. Initial results indicated that making the step size smaller than this (down to 0.01) caused no significant change in the solution. Increasing the step size to 0.2 did cause a change in the solution. For most of the solutions obtained in this report the GTT method

was applied in the range $0 \leq \phi \leq 90°$. For some larger incidence and Mach number cases in which the cross flow becomes supersonic earlier it was convenient to reduce the downstream boundary of the windward region to $\phi = 84°$ or less.

Before leaving this section it is of value to examine under what conditions the denominator of the expression for p_ξ (4.9) can go to zero. Let

$$\text{Den} = a^2(K_3^2 + \frac{1}{\sigma^2}) - K_2^2 \quad . \tag{4.25}$$

Substituting for K_3 and K_2 gives

$$\text{Den} = \left(\frac{B}{\pi \sin\theta}\right)^2 \left[1 - \left(\frac{w}{a}\right)^2\right] + \frac{a^2 - v^2}{\sigma^2} + \frac{2\, v\, w\, B}{\pi\sigma \sin\theta} \tag{4.26}$$

If we note that $M_{cr}^2 = (v^2 + w^2)/a^2$, equation (4.26) can be rearranged as

$$\text{Den} = \left[\left(\frac{B}{\pi \sin\theta}\right)^2 + \frac{1}{\sigma^2}\right]\left[1 - M_{cr}^2\right] + \left[\frac{v\, B}{\pi\, a \sin\theta} + \frac{w}{a\,\sigma}\right]^2 \quad . \tag{4.27}$$

It follows immediately that the denominator of equation (4.9) will remain well behaved as long as M_{cr} is less than one. If M_{cr} is greater than one then comparison with the characteristic equation (5.3) indicates that Den = 0 if

$$\left(\frac{\partial\theta}{\partial\phi}\right)_c = (1 - \xi)\, \theta_{s_\phi} \tag{4.28}$$

at any point on an integration ray (e.g., $\phi = 90°$).

At such a point p_ξ has the form

$$p_\xi = \frac{A}{B} = \frac{0}{0} \quad . \tag{4.29}$$

This is acceptable analytically because as $B \to 0$ the compatibility condition (5.7) requires that $A \to 0$ in such a manner that p_ξ remains well behaved. Numerically if the particular stage of the iteration is not close to the converged solution A will probably be small but non-zero as $B \to 0$ and the behavior of p_ξ will be singular. However, typical values of the shock slope, θ_{s_ϕ} suggest that equation (4.28) will not be satisfied for cross flows that are only moderately supersonic. Thus as the fifth ray (Fig. 5) is reasonably close to the sonic line no problem should arise.

5.0 SHOULDER REGION

Once the crossflow becomes supersonic $(a^2 < v^2 + w^2)$ it is appropriate to extend the solution for the windward region around the body (Fig. 4) using the method of characteristics. Earlier applications of the method of characteristics to the conical flow equation have been made by Maslen (1951) and Bazzhin et al. (1968). Maslen solved the flow about a flat plate, zero-thickness delta wing inclined at 12° to a free stream at Mach number of 3. Maslen used spherical coordinates, but as dependent variables used the crossflow velocity, $q_{cr} = (v^2 + w^2)^{1/2}$, the ratio $\alpha = v/w$, and the radial velocity component u. Also, Maslen followed the traditional method of defining an auxiliary grid (at whose intersections the solution is actually found) which follows the development of the characteristics themselves. Bazzhin has obtained solutions for inclined elliptic cones in the Mach number range 5 to 10, angles of incidence up to 50° and nose cone angles 10° to 20°. Bazzhin used a Cartesian coordinate system and considered the primitive variables u, v, w, p, and T. Superimposed on the Cartesian coordinate scheme Bazzhin (like Maslen) obtained solutions following a traditional lattice defined by the characteristic directions. Bazzhin also considered a second scheme in which a grid was defined by constant values of r and θ in a cylindrical coordinate system. Values at a downstream mesh point were obtained by projecting back characteristic lines through the mesh point. At the intersections of the characteristic with the upstream cell boundary (Fig. 6) the local flow variables can be found by interpolation. The characteristic relations can then

be used to connect the interpolated upstream values with the unknown downstream values at the mesh point.

In the present report spherical coordinates are used. Subsequently, to facilitate matching with the windward region, ξ,η coordinates are introduced. The same dependent variables are used here as were used in the windward region, e.g., u, v, w, ρ, and P. To allow easy transition from one region to another the second characteristic scheme of upstream interpolation has been used. This method is fully described in Belotserkovskii and Chushkin (1965).

5.1 Characteristic Relations

The method of characteristics, for two independent variables, is based on establishing directions (β) in the flow along which the equations of motion, (2.4) to (2.8), can be reduced to ordinary differential equations with β as the independent variable. β is related to the original independent variables, θ and ϕ by the relation

$$\sqrt{1 + k^2}\ \frac{\partial}{\partial \beta} = \frac{\partial}{\partial \phi} + k \frac{\partial}{\partial \theta} \qquad (5.1)$$

where $k = \partial\theta/\partial\phi$; thus k defines the characteristic direction. The system of equations (2.4) to (2.8) possesses five characteristic directions, of which three are the same; namely, the streamline direction defined by

$$k_s = v \sin \theta / w \quad . \qquad (5.2)$$

The other two directions are given by

$$k_c = (-vw \pm a^2 \beta_{cr}) \sin\theta/(a^2 - w^2) \qquad (5.3)$$

where $\beta_{cr} = ((v^2 + w^2)/a^2 - 1)^{1/2}$.

Corresponding to the five characteristic directions are five compatibility conditions that are satisfied on the characteristics. On a streamline,

$$u\,du + v\,dv + w\,dw + \frac{dp}{\rho} = 0 \quad . \qquad (5.4)$$

$$dp = a^2\,d\rho \quad , \qquad (5.5)$$

and

$$du = \frac{(v^2 + w^2)}{w} \sin\theta\,d\phi \quad . \qquad (5.6)$$

Equation (5.4) is just the Bernoulli equation (2.10), written in differential form; equation (5.5) follows from the fact that entropy is conserved along a streamline. Equation (5.6) is the radial momentum equation (2.5), written in differential form.

Along the characteristics,

$$w\,dv - v\,dw \mp \frac{\beta_{cr}}{\rho}\,dp = [(v^2+w^2)\cos\theta + u(v\sin\theta - w\,k_c)]d\phi \quad . \qquad (5.7)$$

The minus sign in front of β_{cr}/ρ in (5.7) corresponds to the plus sign in front of $a^2\,\beta_{cr}$ in (5.3).

In order to be compatible with the independent variables ξ,η used in the windward region, the above relations can be transformed. Equations (5.2) and (5.3) become

$$k_s = \left(\frac{\partial\xi}{\partial\eta}\right)_s = b - \frac{\pi}{\sigma}\,\frac{v\sin\theta}{w} \qquad (5.8)$$

and

$$k_c = \left(\frac{\partial \xi}{\partial \eta}\right)_c = b + \frac{\pi}{\sigma}\left[\frac{(v\,w \mp a^2\,\beta_{cr})}{a^2 - w^2}\sin\theta\right] , \qquad (5.9)$$

where $b = (\pi/\sigma)(1-\xi)\theta_{s_\phi}$.

Equations (5.4) and (5.5) remain unchanged but will be repeated along with (5.6) for completeness, thus

$$u\,du + v\,dv + w\,dw + \frac{dp}{\rho} = 0 , \qquad (5.10)$$

$$dp = a^2\,d\rho \qquad (5.11)$$

and

$$du = \frac{(v^2 + w^2)}{w}\pi \sin\theta\, d\eta . \qquad (5.12)$$

Equations (5.7) become

$$w\,dv - v\,dw \mp \frac{\beta_{cr}}{\rho}dp = [(v^2 + w^2)\cos\theta + u(v\sin\theta - \frac{w\sigma}{\pi}(b - k_c))]\,\pi d\eta . \qquad (5.13)$$

With reference to Fig. 6, equations (5.8) to (5.12) can be written in the form,

$$\xi_3 - \xi_4 = \frac{(B_3 + B_4)}{2}\Delta\eta , \qquad (5.14)$$

where $B = b - (\pi/\sigma)(v \sin\theta)/w$ and $\Delta\eta = \eta_3 - \eta_1$.

$$\xi_3 - \xi_2 = \frac{(C_3 + C_2)}{2}\Delta\eta , \qquad (5.15)$$

where $C = b + (\pi/\sigma)(v\,w + a^2\,\beta_{cr})\sin\theta/(a^2 - w^2)$.

$$\xi_3 - \xi_1 = \frac{(D_3 + D_1)}{2}\Delta\eta , \qquad (5.16)$$

where $D = b + (\pi/\sigma)(v\,w - a^2\,\beta_{cr})\sin\theta/(a^2 - w^2)$.

$$(u_3 + u_4)(u_3 - u_4) + (v_3 + v_4)(v_3 - v_4) + (w_3 + w_4)(w_3 - w_4) + \left(\frac{1}{\rho_3} + \frac{1}{\rho_4}\right)(p_3 - p_4) = 0 \quad . \tag{5.17}$$

$$(p_3 - p_4) = \frac{(a_3^2 + a_4^2)}{2}(\rho_3 - \rho_4) \quad . \tag{5.18}$$

$$(u_3 - u_4) = \frac{(A_3 + A_4)}{2}\Delta\eta \quad , \tag{5.19}$$

where $A = ((v^2 + w^2)/w)\,\pi \sin\theta$.

$$(w_3 + w_2)(v_3 - v_2) - (v_3 + v_2)(w_3 - w_2) + (E_3 + E_2)(p_3 - p_2) = (F_3 + F_2)\,\Delta\eta \quad , \tag{5.20}$$

where $E = \beta_{cr}/\rho$

and

$$F = \pi\,[(v^2 + w^2)\cos\theta + u(v\sin\theta - w\,\sigma\,(b - C)/\pi)] \quad .$$

Finally,

$$(w_3 + w_1)(v_3 - v_1) - (v_3 + v_1)(w_3 - w_1) + (G_3 + G_1)(p_3 - p_1) = (H_3 + H_1)\,\Delta\eta \quad , \tag{5.21}$$

where $G = -\beta_{cr}/\rho$

and

$$H = \pi\,[(v^2 + w^2)\cos\theta + u(v\sin\theta - w\,\sigma\,(b - D)/\pi)].$$

In such a form, the relationships (5.14) to (5.21) are second order finite difference equations and are to be solved

iteratively. At each step of the iteration, terms like $(a_3^2 + a_4^2)/2$ in (5.18) will be assumed known (i.e., the current values are inserted); the differential terms like $p_3 - p_4$ will be rearranged and solved as simultaneous algebraic equations. Generally three or four iterations were found adequate for convergence.

The precise procedure for solving equations (5.14) to (5.21) depends on the nature of the point 3 (Fig. 6). The three cases to be described are

1) when point 3 is an interior point,
2) when point 3 is at the shock,
3) when point 3 is at the body.

5.2 Point 3 as an Interior Point

With reference to Fig. 6a, points 1 and 2 are the intersections of the rearranged characteristics drawn through point 3 to intersect with the line $\eta = \eta_0$. The slopes of 1-3 and 2-3 are given by equation (5.9). Point 4 is the intersection of the streamline through 3 with the line $\eta = \eta_0$. The slope of 3-4 is given by (5.8). It is assumed that the flow variables have been determined $\eta = \eta_0$, i.e., that the variables are known (after interpolation) at 1, 2 and 4, and that a solution is required at 3.

To start the iteration, some estimate of terms like B_3 must be obtained. Belotserkovskii and Chushkin (1965) suggest initially setting the parameter at 3 equal to the parameter at the other end of the line, in this case setting $B_3 = B_4$. In this report the initial estimate of B_3 has been obtained by

extrapolating in the η direction, i.e.,

$$B_{3_{m+1}} = 2\,B_{3_m} - B_{3_{m-1}} \quad . \tag{5.22}$$

Initially point 4 is unknown. If B_4 is interpolated in terms of B_{n-1}, B_n and B_{n+1} (which are known), (5.14) becomes

$$x_4^2(B_{n-1} - 2B_n + B_{n+1}) + x_4(B_{n+1} - B_{n-1}) + 2B_n$$

$$= -4\,x_4\left(\frac{\Delta\xi}{\Delta\eta}\right) - 2\,B_3 \quad , \tag{5.23}$$

where $x_4 = (\xi_4 - \xi_3)/\Delta\xi$

and

$$\Delta\xi = \xi_n - \xi_{n-1} \quad .$$

This has the solution

$$x_4 = -b_4/2a_4 \pm (b_4^2/4a_4^2 - c_4/a_4^2)^{1/2} \quad , \tag{5.24}$$

where $a_4 = B_{n-1} - 2B_n + B_{n+1}$

$$b_4 = B_{n+1} - B_{n-1} + 4(\Delta\xi/\Delta\eta)$$

and

$$c_4 = 2\,B_n + 2\,B_3 \quad .$$

The correct root is the one that gives the smaller $|x_4|$. Once x_4 is determined, the function values follow from

$$X_{i_4} = [x_4^2(X_{n-1} - 2X_n + X_{n+1}) + x_4(X_{n+1} - X_{n-1}) + 2X_n]/2 \quad , \tag{5.25}$$

where

$$X = \begin{bmatrix} u \\ v \\ w \\ \rho \\ p \end{bmatrix} \quad , \text{ and } \quad \xi_4 = \xi_3 + x_4 \, \Delta\xi \quad . \tag{5.26}$$

In a similar manner we can find ξ_2 and ξ_1 and the function values at points 2 and 1. For each equation like (5.24) the correct root is that which leads to the smallest $|x|$ provided that x is of the correct sign, i.e., the correct side of point 3.

With conditions at 1, 2 and 4 determined and the first estimates of conditions at 3 determined from equations like (5.22), equations (5.17), (5.20) and (5.21) constitute three simultaneous equations for the unknowns v_3, w_3 and p_3. It is repeated that terms of the form $(v_3 + v_4)$ are treated as being known and that terms like $(v_3 - v_4)$ are treated as being unknown. u_3 follows from (5.19) and ρ_3 from (5.18). At this point the second estimate of conditions at 3 has been obtained.

Terms like A_3, B_3 can now be recomputed with the new values at 3. Consequently the locations of ξ_1, ξ_2, and ξ_4, as defined by equations (5.14) to (5.26), will now be different. Fresh estimates of locations 1, 2 and 4 can be obtained from equations like (5.23) to (5.26). In turn, solutions of (5.17) to (5.21) give the next iterate of conditions at 3. The process is repeated until successive variable values at 3 differ by an arbitrarily small number. The following expression has been used to get an overall estimate of the error at 3.

$$FCH = \left(\frac{u_{j+1} - u_j}{u_j} \right)^2 + \left(\frac{\rho_{j+1} - \rho_j}{\rho_j} \right)^2 + \left(\frac{p_{j+1} - p_j}{p_j} \right)^2$$

$$+ (v_{j+1} - v_j)^2 + (w_{j+1} - w_j)^2 \quad . \qquad (5.27)$$

The form of this equation has been chosen to keep the influence of the different variables roughly the same. Convergence was assumed if FCH was less than 10^{-8}. With hindsight, a more natural choice would have been to compute

$$\frac{\gamma p}{(\gamma-1)\rho} + \frac{1}{2}(u^2 + v^2 + w^2) \quad ,$$

and to compare it with the Bernoulli constant defined by equation (2.11).

5.3 Point 3 at the Shock

The basic parameter to be determined in this case is the shock slope, θ_{s_ϕ}, and only point 1 is available (Fig. 6b). Initially θ_{s_ϕ} is extrapolated from its value at m and m-1 following equation (5.22). Use of the shock relations (2.13) then allows calculation of u_3, v_3, A_3, etc., to be made. Following the procedure given in Section 5.2, the location of point 1 and the variable values at 1 can be determined. Equations (5.21) then connect three unknowns v_3, w_3, and p_3. However, all three are functions of a single variable $\theta_{s_{\phi_3}}$ through the shock relation (2.13). The idea of solving (5.21) for θ_{s_ϕ} using Newton's method was discarded when the prospect of analytically differentiating equation (5.21) with respect to θ_{s_ϕ} was contemplated. Instead the method of Regula Falsi (Abramowitz and Stegun, 1964)

has been used. The method is equivalent to Newton's method, except that the derivative is calculated numerically. Initially equation (5.21) is evaluated twice. Extrapolation is made to the value of θ_{s_ϕ} which would render (5.21) equal to zero. The method proceeds iteratively, using two values. At each iteration the value of θ_{s_ϕ} which causes (5.21) to be a maximum is discarded. If two values of θ_{s_ϕ} can be found that cause (5.21) to change sign, convergence is very rapid. Since solutions for θ_{s_ϕ} are available at m and m-1, etc., this is not difficult. Once the correct value of θ_{s_ϕ} at 3 has been obtained, the shock relations give u_3, v_3, w_3, ρ_3 and p_3. As in Section 5.2, the solution for conditions at 3 is iterated until there is no further change in the conditions at 3.

5.4 Point 3 at the Body Surface

This situation is shown in Fig. 6c. In this case v_3 is zero and point 4 coincides with point n-1, m. Initially conditions at 3 are extrapolated for, along the surface. A_3 and C_3 are determined and equation (5.15) is used to obtain the location of point 2 and the flow conditions at 2. Since v_3 is zero, equations (5.17) and (5.20) can be solved simultaneously to give w_3 and p_3. ρ_3 and u_3 follow from equations (5.18) and (5.19). The process is repeated, iteratively, until conditions no longer change.

5.5 General Comments

On each new line $\eta = \eta_1$ conditions must be solved for at the shock first because the shock location is required to

evaluate σ which appears in many of the equations of Section 5.1. Sequentially solutions at the interior points are obtained, and at the end of each sweep, conditions at the body are obtained.

Data to start the characteristics solution are provided by the solution in the windward region. Since the initial estimate of conditions at 3 uses two preceding values (see equation (5.22)), a second line of initial data has to be interpolated from the windward solution. Initial data are specified at 11 points matching the windward solution. It was found that the flow variables varied considerably, with ξ, just inside the shock and at the body. Consequently, two extra points at $\xi = 0.05$ and 0.95 were interpolated from the initial data. The solution in the shoulder region proceeds along 13 rays towards increasing η. The step size in the η direction, $\Delta\eta$, is controlled by the program. An initial step size of 0.002 was used. Every five steps $\Delta\eta$ was doubled, until the interpolation given by (5.23) and (5.24) indicated that the relevant characteristic had fallen outside the flow regime, in which case $\Delta\eta$ was halved. The minimum size allowed for $\Delta\eta$ has been 0.001. If the characteristic location 1, 2, or 4 does not fall in the range given by n-1,n and n+1 values of, say B, then fresh B_{n-1}, n, n+1 values are chosen to straddle the expected location of 1, 2 or 4.

As ϕ approaches 180° the value of M_{cr}, in the outer part of the flow adjacent to the shock, reduces and starts to approach unity. When this happens the characteristic directions

approach the η direction. This is also a problem if the local streamline direction differs too much from the ξ direction. The result of either situation is that the program tries to keep reducing the step size, $\Delta\eta$. How this situation is overcome to allow a solution to be extended to the leeward sonic line will be described in the next section.

5.6 Extension of the Characteristics Solution to the Leeward Sonic Line

The first ray for which one of the characteristics 1-3 or 2-3 does not intercept the previous line of known data, $\eta = \eta_0$, is the ray $\eta = 0.05$, which is adjacent to the shock. There are three reasons for this. Firstly, the crossflow Mach number on this ray is less than on any other ray and hence the 2-3 characteristic is at a larger angle to the streamline. Actually, the crossflow Mach number at the shock ($\xi = 0$) is lower, but the solution at the shock does not make use of characteristic 2-3. Secondly, at the shock the streamline direction is directed more towards a line of constant η than at any other point in the flow (with the same η coordinate). This in turn rotates the characteristic 2-3. Thirdly, the first ray is near the edge of the region, so that characteristic 2-3 has only the region between $\xi = 0.05$ and $\xi = 0$ in which to strike the line $\eta = \eta_0$.

As the flow moves towards $\phi = 180°$ the solution for point 3 on the rays on the body side of $\xi = 0.05$ progressively fail, but at a relatively slow rate, due to the three effects described above. It is apparent that on any ray, η = constant, where there exists a region in which solutions at points 3 are

undetermined, solutions can be found on both sides of such a region, i.e., at the shock and close to the body.

In order to obtain solutions at point 3 when characteristic 2-3 does not intercept the line $\eta = \eta_0$ (Fig. 6), the equations of motion (2.20) - (2.24), have been rearranged to give explicit expressions for u_η, v_η, w_η, and p_η.

$$p_\eta = \rho \pi \sin\theta \left[w \left(\frac{I}{\rho a^2} + J \right) - H\right] / \left[\frac{w^2}{a^2} - 1 \right] \tag{5.28}$$

$$w_\eta = \frac{H}{F} - \frac{p_\eta}{\rho w} \tag{5.29}$$

$$v_\eta = G/F \tag{5.30}$$

and

$$u_\eta = \left[(v^2 + w^2) - E\, u_\xi\right]/F \quad , \tag{5.31}$$

where A to F are as defined in Section 2.3, and G to J are defined by equation (6.7).

These equations have been integrated from n,m to point 3 (Fig. 6), using a fourth order Runge Kutta scheme. The ξ derivatives have been obtained using a fifth order centered difference scheme. The ξ derivatives must also be calculated at the intermediate points.

However, since the inner point 3's and the conditions at the shock can be determined first, in the conventional manner, the determination of the ξ derivatives is considerably more constrained (and probably more accurate) than the corresponding calculation of the η derivatives in the windward region. Using this technique no difficulty has been experienced in obtaining well-behaved solutions well beyond the point at which an internal

shock has to be introduced in order to satisfy the boundary condition of no circumferential flow through the leeward symmetry plane. In addition, the embedded GTT method has served as a useful model for the method used in the leeward region (described in the next section).

6.0 LEEWARD REGION

Close to the surface the characteristics solution indicates that the crossflow Mach number is rising with increasing ϕ for ϕ close to 180° even though w is falling slowly. The increase in the crossflow Mach number is essentially due to the reduction in pressure. However, since w and $v = 0$ at the surface at $\phi = 180°$, the crossflow has somehow to beome subsonic. In the outer region (close to the shock) this occurs without a shock because $(v^2 + w^2)$ drops more rapidly than does a^2.

It is of value to manipulate the Bernoulli equation in order to show up the significant difference between conical and two dimensional flow, due to the role of u, the radial velocity component. In general one can obtain

$$\left[1 + \frac{\gamma-1}{2} M^2\right]^{\gamma/\gamma-1} = \frac{p_o}{p} \qquad (6.1)$$

where M = total velocity/sound speed and p_o is the stagnation pressure. For two dimensional flow any reduction in M implies an increase in p. For conical flow M can be split up as follows,

$$M^2 = \frac{u^2 + v^2 + w^2}{a^2} = \frac{u^2}{a^2} + \frac{v^2 + w^2}{a^2} = M_r^2 + M_{cr}^2 . \qquad (6.2)$$

It turns out that the radial Mach number is not greatly different from the free stream Mach number, and that any changes in pressure generally occur due to changes, albeit small, in M_r; even though the value of M_{cr} determines the character of

the governing differential equations. In the outer flow the pressure falls continuously (while M_{cr} is greater than one) as ϕ increases even though M_{cr} is falling at the same time. The 'slack' is taken up by an increase in M_r. Thus examination of the characteristics solution suggests the occurrence of an internal shock attached to the body but probably terminating before the outer shock is reached.

By analogy with the windward region it appears feasible to integrate from the internal shock to the leeward line of symmetry, and then to adjust the position of the internal shock to satisfy the boundary condition of zero circumferential velocity at the leeward symmetry plane.

Two major problems present themselves that were not present for the windward region. Firstly, the occurrence of a vortical singularity is to be expected on the line $\phi = 180°$. The location of the vortical singularity is given by $v = 0$ away from the body. Since v is not much affected by the internal shock (the internal shock is almost normal to the body throughout the region and very weak opposite the vortical singularity), the location of the vortical singularity can be located fairly closely by extrapolating the characteristics solution. However, at the vortical singularity jumps in entropy, radial velocity u and density, ρ are to be expected (see Section 3.1). Thus one would like to integrate away from such a singularity, but to do so would make it difficult to relate the location of the internal shock to the $w = 0$ leeward boundary condition.

The second problem is that, because the internal shock does not extend all the way to the outer shock there is no convenient

mechanism (i.e., the location of the internal shock) for "adjusting" the circumferential velocity at $\phi = 180°$.

Once the crossflow Mach number just inside the outer shock becomes subsonic (Fig. 7) the shock shape is no longer determined by solely upstream (smaller ϕ) conditions. However, because this sonic line/shock intersection typically occurs fairly close to $\phi = 180°$ (e.g., for $M_\alpha = 7$, $\alpha = 30°$, $\theta_b = 20°$, $\phi_{sonic}/shock = 165°$) and since the shock slope must be zero at $\phi = 180°$, the shock location between the sonic line/shock intersection and $\phi = 180°$ has been extrapolated. This immediately gives values for the flow variables at the shock from the shock relations (2.13). It is thought that any error introduced by extrapolating the shock location will be purely local and have small effect on either the location of the internal shock, the location of the vortical singularity or the conditions at the body. It would be feasible to introduce an initially unknown intermediate outer shock location and to determine this at the same time as the location of the internal shock is determined. It seems unlikely that the improvement in the solution would justify the extra effort and computing time required.

The derivatives in the ξ direction have been computed using centered, fifth order finite difference representations like equation (4.2). This was judged to be a reasonable compromise between realizable accuracy and the exponential growth of small disturbances to be expected from Telenin's (1964) analysis. As indicated in Section 2.3, the region between the internal shock and the line $\phi = 180°$ has been transformed into a rectangle.

To do this a boundary between the internal shock and the external shock is required. Once an internal shock location has been specified, a line of constant ϕ, from the end of the internal shock to the outer shock, has been used for the additional boundary (Fig. 7).

The transformed equations, given in Section 2.3, can be arranged to give the explicit variation of the τ derivatives:

$$p_\tau = [F(J + \frac{I}{\rho a^2}) - (D\,G + \frac{B\,H}{\sin\theta})]/[\frac{F^2}{a^2} - (D^2 + \frac{B^2}{\sin^2\theta})] \quad , \tag{6.3}$$

$$w_\tau = \frac{H}{F} - \frac{B}{\rho\,F\sin\theta}\,p_\tau \quad , \tag{6.4}$$

$$v_\tau = \frac{G}{F} - \frac{D}{\rho\,F}\,p_\tau \tag{6.5}$$

$$u_\tau = [(v^2 + w^2) - E\,u_\xi]/F \tag{6.6}$$

where

$$A = \frac{(1-\xi)}{\sigma}\,\theta_{s_\phi} \quad , \quad B = \frac{1}{\lambda} \quad , \quad C = -\frac{1}{\sigma} \quad ,$$

$$D = -\frac{\phi_{is_\theta}}{\lambda}(1-\tau) \quad , \quad E = C\,V + \frac{A}{\sin\theta}\,w \quad ,$$

$$F = D\,V + \frac{B}{\sin\theta}\,w \quad , \tag{6.7}$$

$$G = w^2\cot\theta - u\,v - \frac{C}{\rho}\,p_\xi - E\,V_\xi \quad ,$$

$$H = -u\,w - v\,w\cot\theta - \frac{A}{\rho\sin\theta}\,p_\xi - E\,w_\xi \quad ,$$

$$I = a^2\,E\,\rho_\xi - E\,p_\xi \quad ,$$

and

$$J = -2u - v \cot\theta - C\, v_\xi - \frac{A}{\sin\theta}\, w_\xi - \frac{E}{\rho}\, \rho_\xi \quad .$$

As with the windward region, the density is determined from the Bernoulli equation (2.10). Whereas in the windward region iteration on one set of integrations is required to fix the outer shock location, in the leeward region three sets of integrations are iterated. Firstly the shock location is iterated, integrating towards $\phi = 180°$; secondly the w_ϕ derivatives at $\phi = 180°$ are iterated, integrating towards the shock; and finally the shock location is again iterated, integrating towards $\phi = 180°$. In principle the set of three integrations could be repeated indefinitely until the solution no longer changed. However, the required computing time for this small region of the overall flow field would then become disproportionately large compared with the computing time required to obtain solutions in the windward and shoulder regions. The reason for three sets of integrations is related to the two special problems described at the beginning of Section 6.

The general procedure has been to specify an internal shock location and to obtain the flow conditions behind it from the shock relations in the following form,

$$\begin{aligned} u_s &= u_1 \\ v_s &= (w_1 \cos\varepsilon + v_1 \sin\varepsilon)\sin\varepsilon - v_{ns}\cos\varepsilon \\ w_s &= (w_1 \cos\varepsilon + v_1 \sin\varepsilon)\cos\varepsilon + v_{ns}\sin\varepsilon \\ \rho_s &= \rho_1\, v_{n_1}/v_{ns} \quad , \quad p_s = p_1 + \rho_1\, v_{n_1}^2 - \rho_s\, v_{ns}^2 \quad , \end{aligned} \tag{6.8}$$

where

v_{n_1}, the upstream normal velocity, $= w_1 \sin \varepsilon - v_1 \cos \varepsilon$

v_{ns}, the downstream normal velocity, $=$

$$= (1 - \mu^2(u_1^2 + (w_1 \cos \varepsilon + v_1 \sin \varepsilon)^2))/v_{n_1} \quad ,$$

and $\cot \varepsilon = \phi_{is_\theta} \sin \theta_s$ with ε having the same sense as in Section 2.2.

Conditions 1 are the upstream conditions and are obtained from the characteristic solution. In the region between the internal and the external shock the flow variable values at $\tau = 0$ are obtained by interpolating the characteristics solution. From the outer extremities of the internal shock (Fig. 7) the location of the left running characteristic is obtained and followed until it intersects the sonic line. The region between the characteristic/sonic line boundary and the arbitrary upstream outer boundary of the leeward region cannot be affected by the internal shock. Consequently the flow in this region is determined solely from the underlying characteristics solution. However, the flow variables in this region can affect the behavior behind the shock, thus it is necessary to lay out the leeward region across this area and to interpolate function values on the leeward grid in this outer region (Fig. 7) so that the ξ derivatives, required to compute the flow behind the shock, can be evaluated.

For the rays (constant ξ) which do not pass through the internal shock and lie downstream of the characteristic/sonic line boundary, the w velocity given by the characteristics

solution up to the characteristic/sonic line boundary is extrapolated so that it is zero at $\phi = 180°$. w_τ is constructed using a third order finite difference scheme and equations (6.3) to (6.7) are rearranged to depend on w_τ rather than p_τ. Equation (6.4) is not used. On the rays of constant ξ that do pass through the internal shock all the flow variables are initially assumed unknown.

Since the ray that coincides with the surface is a streamline, equations (6.3) to (6.7) can be considerably simplified thereon, the result is

$$u_\tau = \frac{w \sin \theta_b}{B} \quad , \tag{6.9}$$

$$w_\tau = - \lambda \sin \theta_b [u(2-w^2/a^2) - v_\xi/\sigma]/[1 - \frac{w^2}{a^2}] \quad , \tag{6.10}$$

$$p = S_s \rho^\gamma \tag{6.11}$$

$$\frac{\gamma p}{(\gamma-1)\rho} + \frac{1}{2}(u^2 + w^2) = B \quad . \tag{6.12}$$

As in Section 4, S_s is the entropy parameter at the surface and can be most easily determined by its value just downstream of the internal shock. The main difference between these equations and those used in Section 4 is that here no assumption is made about the pressure; instead, the continuity equation (2.20) is rearranged to give (6.10).

The general procedure has been to simultaneously integrate the ten rays of constant ξ using a fourth order Runge-Kutta scheme in the direction of increasing τ until the line $\phi = 180°$

is almost reached. Since w_τ is well behaved at $\phi = 180°$, an extrapolation is made to determine the value of w at $\phi = 180°$. This is required because F in equations (6.3) to (6.6) goes to zero as τ goes to one. Powell's (1964) method is used to adjust the internal shock location until w becomes zero on $\phi = 180°$. As in the windward region the location of the internal shock is specified by its location at one of the rays and by the shock slope at all the other rays. It is known, *a priori*, that the local shock slope must be normal to the surface in order to preserve the boundary condition of zero normal flow at the surface. A step size of $\Delta\tau = 0.2$ has been used in the leeward region. It will be noted that in this initial integration no account is taken of the vortical singularity.

Each time a solution is found for the internal shock location that allows the boundary condition of $w = 0$ at $\phi = 180°$, a check is made to see if the internal shock should extend further into the flow. The shock location and slopes are extrapolated until the next ray of constant ξ is reached. At that point the upstream normal velocity is computed from the characteristics solution. If it is supersonic a fresh set of integrations is made toward $\phi = 180°$ until convergence is obtained, including the extra ray. The process of obtaining a converged solution and checking the upstream normal shock velocity is repeated, including an extra ray each time, until the upstream normal shock velocity becomes subsonic.

The v velocity distribution from the converged solution of the first integration is extrapolated to $\phi = 180°$ and this

determines the location of the vortical singularity. Since the line $\phi = 180°$ is a streamline the equations of motion (2.20) to (2.24) can be simplified to

$$u_\xi = - v \sigma \tag{6.13}$$

$$p = S \rho^\gamma \tag{6.14}$$

$$\frac{\gamma p}{(\gamma-1)\rho} + \frac{1}{2}(u^2 + v^2) = B \tag{6.15}$$

and

$$w_\tau = - \lambda \sin\theta[u(2-v^2/a^2) - \frac{v_\xi}{\sigma}(1-v^2/a^2)] - v \cot\theta \quad . \tag{6.16}$$

The similarity with equations (6.9) to (6.12) and (4.14) to (4.17) may be noted. The equations have been written in this form so that if the v distribution along $\theta = 180°$ is obtained by extrapolating the initial τ integration then equations (6.13) to (6.16) can be solved to yield the gradient w_τ. One knows that the entropy undergoes a jump as the vortical singularity is traversed. Equations (6.13) to (6.16) were integrated from the outer shock to the vortical singularity. The correct jump in entropy parameter is obtained by differencing its value just inside the outer shock and its value used in solving the surface equations (6.9) to (6.12). Once this jump is known equations (3.7) give the appropriate jumps in u and ρ. As demonstrated in Section 3.1, p is continuous at the vortical singularity. Once all the conditions are obtained on the body side of the vortical singularity the integration proceeds to the body surface. At this point one has a close approximation to the flow conditions at

$\phi = 180°$.

For the second set of integrations the location of the internal shock is held fixed at the position determined by the first integration. The equations are then integrated from $\phi = 180°$ towards the characteristics/sonic line boundary (Fig. 7) and the internal shock with the intention of matching the w distribution at the characteristics/sonic line boundary. Powell's method is used to iterate on the w_τ variation at $\phi = 180°$ until the w distribution matches at the characteristic/sonic line boundary. Each time the iteration scheme chooses a new set of values for w_τ, equations (6.13) to (6.16) are integrated along $\phi = 180°$ from the outer shock to the body to obtain appropriate initial conditions. The purpose of this second set of integrations is to obtain the correct w distribution in the outer region and to obtain the correct behavior in the region of the vortical singularity.

It is found that the u distribution from the second set of integrations agrees well with u distributions at the upstream edge of the leeward region given by the characteristics solution. This is not entirely surprising since the u velocity component is parallel to the internal shock and hence unaffected by it.

A third set of integrations is then made from the internal shock to the leeward symmetry line. The third set of integrations is the same as the first set in that its purpose is to relocate the internal shock until the boundary condition of zero w at $\phi = 180°$ is satisfied. It is different in that the u distribution obtained from the second set of integrations is assumed

throughout the leeward region. Also, on rays that do not pass through the internal shock the w distribution of the second set of integrations is assumed. Results of the third set of integrations indicate that the change in internal shock location from that found after the first set of integrations is typically less than half a degree. Thus the final solution satisfies both the conditions of zero circumferential velocity at $\phi = 180°$ and also has the correct behavior at the vortical singularity.

7.0 DISCUSSION OF NUMERICAL COMPUTATIONS

7.1 Scope

Results have been obtained in the free stream Mach number range, 3 to 16, nose cone angles from 5° up to 30° and angles of incidence up to 50°. The limitations on the scope of these results has been physical rather than numerical. Thus for angles of attack equal to 50° viscous effects will dominate the flow field behavior, particularly for more slender cones. For Mach numbers above 16 real gas effects will become significant. For $M_\infty \sin \alpha$ too small the crossflow will be completely subsonic and the present methods will not be applicable. For cone nose angles too large the flow will no longer be attached.

Jones (1968) used the technique of fixing the free stream Mach number and cone nose angle and then incrementing the incidence from zero, using an extrapolation of the solution for the outer shock location at the previous (lower) incidence as the starting point for the current iteration. In the present study the incidence, free stream Mach number and the nose angle have been incremented from previously converged solutions. This has often been more convenient since it has then been possible to maintain a fixed ϕ_{max} for the GTT method and still completely span the subsonic crossflow region. The alternative of incrementing from zero incidence would either require partially spanning the elliptic region (see Section 7.4) or starting with $\phi_{max} = 180°$ and progressively decreasing ϕ_{max} as the incidence is increased. In practice it was found to be more efficient to increment in positive steps of incidence and free stream Mach number and negative steps of cone

nose angle. Thus for the cases shown in Figs. 11 and 12, i.e., $M_\infty = 3.86$, $\alpha = 10°$, $\theta_b = 5°$ and $M_\infty = 16$, $\alpha = 15°$, $\theta_b = 7°$ converged solutions were first obtained for $\theta_b = 10°$ and then θ_b was reduced in steps of 1°.

ϕ_{max}, the boundary of the windward region, was also incremented in a similar manner, e.g., the solutions for $M_\infty = 3.86$, $\alpha = 10°$, $\theta_b = 5°$ (Fig. 11) were for $\phi_{max} = 100°$ and the solutions for $M_\infty = 7$, $\alpha = 45°$, $\theta_b = 30°$ (Figs. 24, 25, 26) were for $\phi_{max} = 72°$. It has been shown (Section 4) that if ϕ_{max} extends too far into the supersonic crossflow region the expressions for P_ζ etc. (equations (4.9) to (4.11)) can become indeterminate. Initially a solution was obtained in the windward region for $M_\infty = 7$, $\alpha = 45°$, $\theta_b = 30°$ with $\phi_{max} = 90°$. However, this solution led to a physically unrealistic outer shock location in the windward region. Consequently ϕ_{max} was reduced to 72° and a reasonable solution was obtained. Thus it seems generally desirable to keep ϕ_{max} as close to the windward sonic line as possible, while still being completely in the supersonic crossflow region.

7.2 Accuracy and Execution Time

The accuracy of the GTT method is difficult to assess because of the unstable nature of the scheme (see Section 4). The total computational error results partly from round-off error, which is a property of the computer used, and partly from the truncation error of representing the ϕ and θ derivatives by finite difference expressions. Conventionally a stable numerical scheme ensures that round-off error is negligible compared with

truncation error. In the GTT method the round-off error will grow like $\exp(N \cdot \xi)$ where N is the number of rays in the ξ direction (Fig. 5).

The present results were obtained with $N = 5$. Comparisons with other numerical schemes (Section 7.3) and experimental results (Section 7.4) suggest that the choice of $N = 5$ has kept the round-off error small. The truncation error in the representation of the η derivatives is of order $\Delta\eta^4$ where $\Delta\eta = 0.125$. The integration in the ξ direction used a fourth order Runge Kutta scheme and a step size, $\Delta\xi = 0.1$.

In the leeward region the truncation error in the representation of the ξ derivatives was $\Delta\xi^4$ with $\Delta\xi = 0.1$. The integration in the τ direction used a fourth order Runge Kutta scheme and a step size, $\Delta\tau = 0.2$. Due to the small circumferential extent of the leeward region, $\Delta\tau = 0.2$ is approximately equivalent to $\Delta\eta = 1/90$.

In the shoulder region a second order characteristics scheme was used with step sizes $\Delta\xi = 0.1$ in the interior, $\Delta\xi = 0.05$ adjacent to the shock and the body and $\Delta\eta$ between 0.001 and 0.02.

The execution time depends on how well the outer shock shape in the windward region is chosen initially. Thus starting from a known solution at $M_\infty = 7$, $\theta_b = 30°$ and $\alpha = 30°$, solutions to the windward region were generated for $\alpha = 31°$ to $43°$ in steps of $1°$ in 6.2 seconds on a CDC 7600. Since converged solutions may often not exist close to the required conditions it would seem desirable to start from an empirical estimate of the

outer shock location perhaps based on the work of Williams (1969) and Eastman and Omar (1965). This has not been done in the present study.

The execution time for the shoulder region depends on the extent to which the program reduces the step size in the ϕ direction. For the case $M_\infty = 7$, $\alpha = 30°$ and $\theta_b = 20°$ the execution time was 3 seconds on a CDC 7600. In the leeward region all three integrations are iterative so that execution time can vary considerably. However, for $M_\infty = 7$, $\alpha = 30°$ and $\theta_b = 20°$ the execution time was 3 seconds on a CDC 7600.

No particular effort has been made to ensure the overall computer program is as efficient as possible. However, an overall execution time of 7 seconds for the case $M_\infty = 7$, $\alpha = 30°$ and $\theta_b = 20°$ compares favorably with an estimated execution time of 60 seconds for the shock capturing technique applied to the same conditions.

7.3 Comparison with Other Numerical Methods

Comparisons have been made mainly with the shock capturing method of Kutler and Lomax (1970). The data, produced by the shock capturing method, on which Figs. 8, 9 and 10 are based, was supplied privately by Kutler (1973). However, the location and extent of the internal shock and the occurrence (or not) of a vortical singularity are based solely on the interpretation of the present author.

The shock capturing method is a second order method for which the truncation error is $O(h^2)$. The step sizes for the shock capturing data were $\Delta\eta = 1/18$ and $\Delta\xi = 1/11$. The locations

of the shock waves and sonic lines for the two methods are indicated in Fig. 8. The location of the outer shock and the windward sonic lines are in good agreement. The largest difference in the location of the outer shock was 0.6% at $\phi = 90°$. At $\phi = 180°$ the difference in the location of the outer shock was 0.3%. However, it is apparent that the location and extent of the internal shock and the leeward sonic lines do not agree. Generally the shock capturing method predicts an earlier and more localized internal shock than does the present method.

The pressure distribution at the body (Fig. 9), predicted by the two methods is in substantial agreement. Outside the leeward region the largest difference in c_p is 0.0007 at $\phi = 0°$. Even at $\phi = 180°$ the difference in c_p is only 0.0027. The other flow variables generally agree to the order of 1/2% outside the leeward region. Inside the leeward region significant differences do occur mainly as a result of the vortical singularity. In the present method the correct jump conditions at the vortical singularity are retained whereas the dissipative nature of the shock capturing method effectively removes the vortical singularity (Fig. 10). Since the leeward line of symmetry is a streamline, entropy should be constant along it, with a jump at the vortical singularity. It can be seen that, for the shock capturing method, the entropy is nowhere constant along the leeward line of symmetry. Similarly the variations of u and ρ are also significantly altered by the presence of the vortical singularity. It is interesting that the pressure distribution which is continuous through the vortical singularity shows qualitative similarity.

It is not suggested that the different treatment of the vortical singularity is responsible for the discrepancy in the location of the internal shock. In the present method the change in the internal shock location between the first integration (Section 6), which takes no account of the discontinuity at the vortical singularity and the third integration which does, was only 1/2°. The difference in the internal shock locations shown in Fig. 8 is approximately 5°.

Another comparison with other numerical methods is shown in Fig. 12. For this condition $M_\infty = 16$, $\alpha = 15°$ and $\theta_b = 7°$, the results of the Lockheed modified shock capturing technique (1972) and the 'Moretti' code due to Abbett (1970) were provided privately by Lyons (1974). Results using the present method lie well within the spread of the other two codes.

7.4 Comparison with Experiments

An attempt was made to consider the case $M_\infty = 3.86$, $\alpha = 10$ $\theta_b = 5°$ for which experimental data has been obtained by Amick (1961). It turned out that the crossflow Mach number parameter, $M_\infty \sin\alpha$ was too low for supersonic crossflow and it was not possible to completely span the elliptic region. The result for the pressure distribution is shown in Fig. 11. It is apparent that the GTT method only gives a poor solution on the last ray and that this seems to have had little effect on the other rays. This suggests that it might be permissible to only partially span the subsonic crossflow region as long as the solution adjacent to the 'open' side is disregarded.

The major experimental comparison has been with the

results of Tracy (1963). The results of Fig. 13 indicate good agreement for the outer shock except in the leeward region, where viscous effects are significant for the case considered. The circumferential location of the internal shock is not predicted very accurately. In view of the viscous/inviscid interaction in this region (see Section 3.1) this is not surprising. Perhaps what is surprising is the reasonable agreement on the orientation and the normal extent of the internal shock. The pressure distribution is compared in Fig. 14. The tendency for the GTT method to underpredict the pressure on the windward line of symmetry was also apparent in the comparisons Jones (1968) made with the experimental results of Rainbird (1968).

8.0 FLOW FIELD BEHAVIOR

8.1 Detailed Flow Field Description for Large Incidence

For the case $M_\infty = 7$, $\alpha = 30°$ and $\theta_b = 20°$ detailed solutions have been obtained and compared with results from the shock capturing method (Section 7.3). For the same case, Figs. 15 to 18 show contour plots of entropy parameter, p/ρ^γ, crossflow Mach number, pressure and normal velocity, respectively.

Since entropy is constant along streamlines Fig. 15 shows the streamline pattern for an inclined cone. The streamlines shown appear to be discontinuous at the internal shock because the entropy is discontinuous in crossing any shock wave. The general character of the flow is well illustrated: the streamlines sweep around the body, are pulled away from the body by the internal shock and converge on the vortical singularity. The contours of crossflow Mach number M_{cr} shown in Fig. 16, indicate a general acceleration of the flow in the circumferential direction. Initially M_{cr} increases more rapidly at the outer shock, but once the flow becomes supersonic at the body ($\phi \approx 75°$) the flow at the body accelerates leading to a minimum in M_{cr} approximately half way between the shock and body. At the outer shock M_{cr_ϕ} becomes negative at approximately $\phi = 115°$. This point of maximun M_{cr} occurs at progressively larger ϕ as the body surface is approached. For $\xi > 0.7$, M_{cr_ϕ} remains positive until an internal shock occurs. The region $\xi > 0.7$ also defined the region for which v_θ is positive. For further discussion see Section 8.6.

The pressure contours shown in Fig. 17 indicate an initial rapid decrease in pressure with ϕ. The flow continues to

expand in the supersonic crossflow region until either an internal shock occurs (close to the body) or the crossflow again becomes subsonic (close to the shock). The pressure jump across the internal shock and the recompression in the leeward region are small. The contours of normal velocity shown in Fig. 18 suggest a new way of determining whether the vortical singularity will occur away from the body. Examination of the contour $v = 0$, which is connected to the vortical singularity, shows that it originates at the body at approximately $\phi = 110°$. Thus at $\phi \approx 110°$, v_θ changes sign. Use of this criterion to predict lift-off of the vortical singularity is described in Section 8.6.

8.2 Effect of Incidence on the Entropy Layer

For small angles of attack there is a narrow region adjacent to the body surface across which the entropy changes markedly (see Fig. 19, $\alpha = 10°$). This entropy layer has been studied analytically (see Section 3.1 for references) and numerically by Ndefo (1969), Jones (1968) and Klunker et al. (1971). The formation of a localised entropy layer is a result of the vortical singularity being attached to the body. Thus for the cases $\alpha = 30°$ and $40°$ shown in Fig. 19, the vortical singularity had moved off the surface and the corresponding entropy distribution is more nearly linear, particularly for large angles of attack.

8.3 Effect of Mach Number

For the results shown in Figs. 20 to 25 no attempt has been made to obtain solutions in the leeward region. The results shown in Figs. 20 and 21 have been obtained at constant α and

θ_b, with $\alpha = 15°$ and $\theta_b = 10°$. The results indicate that increasing the Mach number causes the outer shock to lie closer to the body and the crossflow to become sonic earlier in the ϕ direction, particularly close to the outer shock. Close to the body the circumferential location at which the flow becomes sonic is relatively insensitive to Mach number. This insensitivity to Mach number of the conditions at the body surface in the windward region is reflected in the pressure distribution shown in Fig. 21. Thus, at the body, the effect of increasing Mach number is restricted to an increase in the expansion of the flow in the supersonic region.

8.4 Effect of Incidence

The results shown in Figs. 22 and 23 were obtained at $M_\infty = 7$ and $\theta_b = 20°$. The major effect of increasing the incidence is the rapid movement of the outer shock away from the body on the leeward side. The movement of the windward sonic line with increasing incidence is towards the windward line of symmetry particularly close to the body. The pressure distribution shown in Fig. 23 indicates that the pressure in the windward region increases with incidence. On the leeward side once the crossflow becomes supersonic there is no detectable pressure variation with incidence. For the results at $\alpha = 20°$ the crossflow is everywhere subsonic. The difference in pressure distribution between a subsonic crossflow and a supersonic crossflow is particularly marked on the leeward side of the cone.

8.5 Effect of Nose Angle

The results shown in Figs. 24 to 26 have been obtained at $M_\infty = 7$ and $\alpha/\theta_b = 1.5$. The results for the outer shock and windward sonic line locations for $\theta_b = 10°$ and $20°$ are consistent with the results of Fig. 20; that is, the outer shock moves towards the body and the windward sonic line moves towards the windward line of symmetry as the crossflow Mach number parameter, $M_\infty \sin \alpha$, is increased.

The results for $\theta_b = 30°$ follow no such trend. The outer shock location for $\theta_b = 30°$ appears relatively wider at $\phi = 90°$ and considerably foreshortened at 180°. The wider outer shock at $\phi = 90°$ is consistent with the positive normal velocities for that location (Fig. 26). This is in marked contranst to the results for $\theta_b = 10°$ and $20°$, both of which show negative normal velocity components at $\phi = 90°$. The tendency for distance between the outer shock and the body to be a maximum other than at $\phi = 180°$ has been previously noted by Babenko (1964) for subsonic crossflows about inclined cones with nose angles equal to 30° and greater. The variation of pressure distribution with increasing nose angle (Fig. 25) is qualitatively the same as the variation of pressure distribution with incidence (Fig. 23).

The tendency for the normal velocity to become positive, at the body, at smaller values of ϕ as the nose angle is increased is believed to be related to the movement of the vortical singularity away from the surface, as will be demonstrated in the next section.

8.6 Vortical Singularity Lift-Off

Previous analyses of the vortical lift-off (Melnik, 1967, and Jones, 1969) have been concerned with the behavior at the leeward line of symmetry. Melnik found a criterion for $p_{\phi\phi}$ at $\phi = \pi$ such that the vortical singularity would lift off. Once the vortical singularity has left the surface there must be a contour $v = 0$ which is connected to the vortical singularity and which intercepts the body at some ϕ less than π (see Fig. 18). At this upstream point (in the crossflow direction) v_θ at the surface changes from a negative value upstream to a positive value downstream. The criterion that $v_\theta = 0$ at the surface will be used in this report to indicate that the vortical singularity is away from the body in the leeward symmetry plane. This criterion would break down if the $v = 0$ contour rejoined the body before $\phi = \pi$, i.e., v_θ becomes negative again and the vortical singularity then would remain attached to the body. It will be shown that this possibility is remote, if not impossible.

To examine the behavior of v_θ it is convenient to start with the equations of motion at the surface written in θ,ϕ coordinates. These are similar to equations (6.9) to (6.12) and are

$$u_\phi = w \sin \theta_b \tag{8.1}$$

$$p_\theta = \rho w^2 \cot \theta_b \tag{8.2}$$

$$w w_\phi + \frac{1}{\rho} p_\phi + u w \sin \theta_b = 0 \tag{8.3}$$

$$v_\theta + \frac{1}{\sin \theta_b} w_\phi + \frac{w}{\rho \sin \theta_b} \rho_\phi + 2u = 0 \qquad (8.4)$$

$$p_\phi = a^2 \rho_\phi \quad . \qquad (8.5)$$

From (8.3), (8.4) and (8.5), ρ_ϕ and w_ϕ can be eliminated to give

$$v_\theta = - u - \frac{p_\phi}{\rho w \sin\theta_b} [M_{cr}^2 - 1] \quad . \qquad (8.6)$$

Advantage has been taken of the fact that $M_{cr} = w/a$ at the surface. If the crossflow is everywhere subsonic it is an observed fact that p_ϕ only becomes positive close to $\phi = \pi$ and only for conditions of relatively large $M_\infty \sin \alpha$ and small θ_b. If the crossflow becomes supersonic p_ϕ is everywhere negative up to the termination of the supersonic crossflow region. It has been observed that in the leeward subsonic region p_ϕ can become positive. At the internal shock p_ϕ is positive. In addition, quantities u, ρ, w and $\sin \theta_b$ are always positive. Thus equation (8.6) demonstrates the change in character of the dependence of v_θ on p_ϕ when the crossflow changes from subsonic to supersonic. This result is the basis of the present analysis.

Equation (8.3) can be rearranged to give

$$\frac{p_\phi}{\rho w \sin \theta_b} = - (u + \frac{w_\phi}{\sin \theta_b}) \quad . \qquad (8.7)$$

Substitution of (8.7) into (8.6) gives

$$v_\theta = - u + (u + \frac{w_\phi}{\sin \theta_b})(M_{cr}^2 - 1) \qquad (8.8)$$

or

$$v_\theta = u\,(M_{cr}^2 - 2) + \frac{w_\phi}{\sin\theta_b}(M_{cr}^2 - 1) \quad . \tag{8.9}$$

Since the growth or decline of M_{cr} is relevant to the present investigation, differentiating $M_{cr} = w/a$ with respect to ϕ leads to

$$M_{cr_\phi} = -\frac{p_\phi}{\rho a w}\left[1 + \frac{\gamma-1}{2} M_{cr}^2\right] - \frac{u}{a}\sin\theta_b \quad , \tag{8.10}$$

$$M_{cr_\phi} = \frac{w_\phi}{a}\left[1 + \frac{\gamma-1}{2} M_{cr}^2\right] + \left(\frac{\gamma-1}{2}\right) M_{cr}^2 \frac{u}{a}\sin\theta_b \quad , \tag{8.11}$$

$$M_{cr_\phi} = \frac{w_\phi}{a} + \frac{\gamma-1}{2} M_{cr}^2 (w_\phi + u\sin\theta_b) \quad , \tag{8.12}$$

or

$$M_{cr_\phi} = \frac{\sin\theta_b}{a(M_{cr}^2 - 1)}\left[u\left(2 - \left(\frac{3-\gamma}{2}\right) M_{cr}^2\right)\right.$$

$$\left. + v_\theta\left(1 + \frac{\gamma-1}{2} M_{cr}^2\right)\right] \quad . \tag{8.13}$$

Examination of (8.10) indicates that M_{cr} can decrease without the need for p to increase, due to the influence of second term (compare Section 6). Differentiating equation (8.8) with respect to ϕ and substituting for M_{cr_ϕ} from (8.13) leads to

$$v_{\theta_\phi} = w\sin\theta_b[M_{cr}^2 - 2] + \frac{2\,M_{cr}}{[M_{cr}^2 - 1]^2}\sin\theta_b\,\frac{(u + v_\theta)}{a}$$

$$\times\left[u\left(2 - \left(\frac{3-\gamma}{2}\right) M_{cr}^2\right) + v_\theta\left(1 + \frac{\gamma-1}{2} M_{cr}^2\right)\right]$$

$$+ \frac{w_{\phi\phi}}{\sin\theta_b}[M_{cr}^2 - 1] \quad . \tag{8.14}$$

This can be recast in the form

$$v_{\theta_\phi} = w \sin\theta_b [M_{cr}^2 - 2] - \frac{p_\phi}{\rho w \sin\theta_b} 2 M_{cr} M_{cr_\phi}$$

$$- \frac{w_{\phi\phi}}{\sin\theta_b} [1 - M_{cr}^2] \quad . \tag{8.15}$$

Typically, at the surface M_{cr} increases with ϕ in the windward region, reaches a maximum for ϕ in the range $\phi = 100$ to $130°$, and decreases to 0 at $\phi = \pi$ either smoothly or discontinuously through an internal shock (Fig. 16). The maximun value of M_{cr} is a function of the crossflow Mach number parameter, $M_\infty \sin\alpha$. w will follow a similar pattern, i.e., w_ϕ will be positive at $\phi = 0$, will become zero at some intermediate ϕ (approximate range $\phi = 120$ to $130°$) and will be negative thereafter. It is expected that $w_{\phi\phi}$ will not become positive.

The behavior of v_θ and M_{cr_ϕ} at the surface will be examined as a function of the parameter $w_\phi/u \sin\theta_b$ and M_{cr}. It can be seen that, from equation (8.9), the condition $v_\theta = 0$ is given by

$$\frac{w_\phi}{u \sin\theta_b} = \frac{(2 - M_{cr}^2)}{(M_{cr}^2 - 1)} \quad . \tag{8.16}$$

From equation (8.11), the condition that $M_{cr_\phi} = 0$ is given by

$$\frac{w_\phi}{u \sin\theta_b} = \frac{-1}{1 + \frac{2}{(\gamma-1)M_{cr}^2}} \quad . \tag{8.17}$$

Equations (8.16) and (8.17) are shown in Fig. 27, and are used to define regions in which v_θ and M_{cr_ϕ} remain positive, etc.

For a completely subsonic crossflow, it is apparent from

Fig. 27, that v_θ can only become positive if p_ϕ is positive. The smallest p_ϕ required to produce positive v_θ occurs at $M_{cr} = 0$. Physically this corresponds to $\phi = \pi$. For v_θ to be positive at $\phi = \pi$ it is necessary that $v_{\theta\phi}$ be large and positive for $\phi < \pi$. For ϕ only slightly less than π, M_{cr_ϕ} will be negative. Examination of equation (8.15) indicates that, for p_ϕ negative, only the last term will contribute to the growth of v_θ. For completely subsonic flow w reaches a maximum at around $\phi = 120°$ and $w_{\phi\phi}$ is generally small throughout. Thus it is most unlikely that v_θ will become positive for this case. Examination of the tabulated data of Babenko (1964) and Jones (1969) indicates that p_θ does not become positive anywhere except for crossflow Mach numbers approaching one and even then only for cases in which θ_b is small. This is consistent with equation (8.7).

The next case to be considered is when a small region of supersonic flow occurs adjacent to the body. As long as the flow remains supersonic p_ϕ will remain negative. From Fig. 27 it can be seen that, for $w_\phi/u \sin\theta_b$ positive or only slightly negative, M_{cr_ϕ} will be positive; however, v_θ remains negative, if $1 \leq M_{cr} \lesssim 1.5$. Once $w_\phi/u \sin\theta_b$ falls below AB (Fig. 27), M_{cr_ϕ} becomes negative and the supersonic crossflow region eventually terminates. If v_θ is negative at $M_{cr} = 1$, then equation (8.6) indicates that no discontinuity will occur and v_θ will be negative as the leeward subsonic crossflow region is entered. One result of the local region of supersonic crossflow is that w does not reduce as rapidly with ϕ as it would in a purely

subsonic crossflow. Therefore, in the present case, once the crossflow is again subsonic, w_ϕ becomes large and negative in order to reduce to zero at $\phi = \pi$. For small θ_b this will probably lead to positive v_θ (Fig. 27) just prior to $\phi = \pi$.

This is essentially the case that Melnik and Jones have studied. In this report this case will be referred to as a subsonic lift-off of the vortical singularity since v_θ first becomes positive in a region of subsonic crossflow. It should be noted that the localised region of supersonic flow upstream of lift-off is essential to reduce the pressure so that substantial positive p_ϕ is required to achieve pressure recovery to the required conditions at $\phi = \pi$. It was noted above that subsonic lift-off of the vortical singularity is only likely to occur for small nose angles. This is confirmed by examination of Jones' (1969) tabulated data.

The final case to be considered is that for which the crossflow becomes supersonic at a sufficiently small ϕ that a substantial region of supersonic crossflow exists in which w_ϕ is positive or close to zero. Examination of Fig. 27 indicates that for $M_{cr_\phi} \approx 1.5$ the range of values of $w_\phi/u \sin\theta_b$ which give a negative v_θ is small. The condition that p_ϕ is negative to sustain supersonic flow sets a lower limit, DE, of $w_\phi/u \sin\theta_b = -1$. If $w_\phi/u \sin\theta_b$ is greater than line AB but v_θ is negative, the effect of positive M_{cr_ϕ} will cause a shift to the right. As long as $w_\phi/u \sin\theta_b$ reduces slowly enough to allow M_{cr_ϕ} to remain positive, eventually a region of positive v_θ will be entered. As M_{cr} approaches ∞ the permissible

range of values of $w_\phi/u \sin\theta_b$ which will cause a negative v_θ shrinks to zero. Thus unless $w_\phi/\sin\theta_b$ is in region ABDE v_θ will eventually become positive. Examination of the numerical data suggests that for $M_{cr} \approx 2$ to 3, w_ϕ can become negative but is so small in magnitude that $w_\phi/u \sin\theta_b$ lies well above the line ABC. If M_{cr_ϕ} remains positive with increasing ϕ then the supersonic crossflow region will be terminated by an internal shock in order that the symmetry condition at $\phi = \pi$ is satisfied. If M_{cr_ϕ} is negative, the supersonic crossflow region will be terminated by an internal shock as long as v_θ remains positive. At $M_{cr} = 1$, v_θ remains continuous, even if an internal shock occurs, because the internal shock must be locally normal to the body surface. If v_θ remains continuous and positive then at $M_{cr} = 1$, $p_\phi = +\infty$ (equation (8.6)), i.e., an internal shock occurs.

On the subsonic side of the internal shock the positive v_θ requires a positive p_ϕ. Examination of the numerical data confirms that p_ϕ remains positive to $\phi = \pi$. This case will be referred to as a supersonic lift-off of the vortical singularity since the location where v_θ first becomes positive is in a region of supersonic crossflow. Examination of Fig. 27 indicates that in cases where w_ϕ is negative but close to values that make $v_\theta = 0$, a larger θ_b is more likely to produce a positive v_θ. This would be the case for $M_{cr} > \sqrt{2}$. This is in contrast to the subsonic vortical lift-off which was more likely to occur for smaller θ_b.

The above analysis has shown the changing character of the surface flow with ϕ depends on the value of w_ϕ compared with the value of M_{cr}. Although M_{cr} is expected to depend on the parameter $M_\infty \sin \alpha$ it is not clear what causes w_ϕ to become negative at a particular ϕ location. Examination of the numerical data suggests that w_ϕ at the surface is strongly influenced by the flow away from the body.

The following tentative conclusions will now be drawn concerning the lift-off of the vortical singularity and the connection between this and the occurrence of supersonic crossflow and an internal shock. Firstly it appears that if the crossflow is completely subsonic no vortical lift-off will occur. Secondly, if the flow exhibits a local area of supersonic crossflow but v_θ remains negative in that region no internal shock will occur and there is a strong probability that a subsequent subsonic lift-off of the vortical singularity will occur. In this case the vortical singularity will be close to the surface. Thirdly, if the supersonic crossflow region extends far enough for v_θ to become positive then the supersonic crossflow region will be terminated by an internal shock and a supersonic lift-off of the vortical singularity will occur. In this case the vortical singularity will occur further from the body.

9.0 CONCLUSION

A composite numerical scheme has been described which is based in part on the GTT method and in part on the method of characteristics. The numerical method has been designed specifically for the problem of a cone inclined at large angle of attack to a supersonic inviscid free stream such that a substantial region of supersonic crossflow occurs. As such it produces results which compare favorably with the results of other numerical methods, notably the shock capturing technique, and with experimental data. The numerical method is the order of ten times faster than the shock capturing method and appears to be the first numerical method to satisfactorily take account of both the internal shock and the vortical singularity which occurs away from the body for the large angles of attack considered here. The limitations on the method appear to be physical rather than numerical, e.g., at too large an angle of attack the flow field is dominated by viscous effects, at too small an angle of attack the crossflow will be everywhere subsonic.

The numerical method has been used to examine the flow variation with free stream Mach number, M_∞, angle of attack, α, and cone nose angle, θ_b. The results at large angle of attack are in broad agreement with previous studies at smaller angles of attack made by Babenko (1964). It appears, from the numerical studies and from an analysis of the equations of motion at the surface, that if the flow is everywhere subsonic the vortical singularity will not leave the surface of the cone. Further, that for a very narrow band of conditions, $M_{cr} \approx 1$, $\alpha/\theta_b \approx 1.1$ and θ_b small

the vortical singularity will just leave the surface and no internal shock will occur. For all other conditions of larger M_{cr} the supersonic crossflow region will terminate with an internal shock and the vortical singularity will occur well away from the body surface.

REFERENCES

Abbett, M. J. (1970), "Inviscid Equilibrium Air Flow about Blunted Cones at Incidence--Analysis and Users Manual, Aerotherm Corp. Report UM-70-20.

Abramowitz, M. and Stegun, I. A. (1964), "Handbook of Mathematical Functions," National Bureau of Standards, Applied Math. Series No. 55, p. 18.

Amick, J. L. (1961), "Pressure Measurements on Sharp and Blunt 5° and 15° Half-Angle Cones at Mach Number 3.86 and Angles of Attack to 100°," NASA TN-D753.

Avduevskii, V. S. and Medvedev, K. I. (1966), "Study of the Laminar Boundary Layer Separation on a Cone at an Angle of Attack," Izv. AN SSSR Mekhanika Zhidkosti i Gaza 3, 117-119.

Babaev, D. A. (1962), "Numerical Solution of the Problem of Supersonic Flow Past the Upper Surface of a Delta Wing," Zhur. Vychislitel'noi Mat. & Mat. Fiz. 2, 2, 278-289.

Babaev, D. A. (1963), "Numerical Solution of the Problem of Supersonic Flow Past the Lower Surface of a Delta Wing," AIAA J. 1, 9, 2224-2231.

Babenko, K. I., Voskresenskii, G. P., Lyubimov, A. N. and Rusanov, V. V. (1964), "Three Dimensional Flow of Ideal Gas Past Smooth Bodies," AN SSR Matem. Inst. im V. A. Steklova Moskova (NASA TT F-380, 1966).

Bashkin, V. A. (1968), "Calculation of the Equations of a Laminar Boundary Layer by the Method of Integral Relations," Zh. Vychisl. Mat. Mat. Fiz. 8, 6, 1280-1290.

Bazzhin, A. P. (1971), "Some Results of Calculations of Flows Around Conical Bodies at Large Incidence Angles," Proceedings of the Second International Conference on Numerical Methods (ed. M. Holt), published as Lecture Notes in Physics No. 8, Springer-Verlag, Berlin.

Bazzhin, A. P., and Chelysheva, I. F. (1967), "Application of the Straight-Line Method to the Calculation of Flow Past Conical Bodies at Large Angles of Attack," Izv. AN SSSR Mekhanika Zhidkosti i Gaza 2, 3, 119-123.

Bazzhin, A. P., Trusova, O. N. and Chelysheva, I. F. (1968), "Calculation of Perfect Gas Flows Around Elliptic Cones at Large Angles of Attack," Izv. AN SSSR Mekhanika Zhidkosti i Gaza 3, 4, 45-51.

Belotserkovskii, O. M. (1966), "Supersonic Gas Flow Around Blunt Bodies--Theoretical and Experimental Investigations," Computer Center of the Academy of Sciences USSR, Moscow (NASA TT F-453, 1967).

Belotserkovskii, O. M. and Chushkin, P. I. (1965), "The Numerical Solution of Problems in Gas Dynamics," in Basic Developments in Fluid Dynamics (ed. M. Holt), Vol. 1, Academic Press, New York, pp. 89-126.

Berger, S. A. (1971), Laminar Wakes, American Elsevier Publishing Co., New York, p. 82.

Boericke, R.R. (1971), "Laminar Boundary Layer on a Cone at Incidence in Supersonic Flow," AIAA J. 9, 3, 462-468.

Briggs, B. R. (1960), "The Numerical Calculation of Flow Past Conical Bodies Supporting Elliptic Conical Shock Waves at

Finite Angles of Incidence," NASA TN D-340.

Brook, J. W. (1964), "The Calculation of Non-linear Supersonic Conical Flows by the Method of Integral Relations," Grumman Aircraft Engineering Corp. FDL-TDR-64-7.

Cheng, H. K. (1962), "Hypersonic Flows Past a Yawed Circular Cone and Other Pointed Bodies," J. Fluid Mech. 12, 2, 169-191.

Chushkin, P. I. and Shchennikov, V. V. (1960), "The Calculation of Certain Conical Flows without Axial Symmetry," AN SSSR Inzh. Fiz. Zh. 3, 7, 88-94 (Grumman Research Translation TR-20, 1962).

Dwyer, H. A. (1971), "Boundary Layer on a Hypersonic Sharp Cone at Small Angle of Attack," AIAA J. 9, 2, 277-284.

Eastman, D. W. and Omar, M. E. (1965), "Flow Fields about Highly Yawed Cones by the Inverse Method," AIAA J. 3, 9, 1782-1784.

Feldhuhn, R. H., Winkelmann, A. E. and Pasiuk, L. (1971), "An Experimental Investigation of the Flowfield around a Yawed Cone," AIAA J. 9, 6, 1074-1081.

Ferri, A. (1951), "Supersonic Flow Around Circular Cones at Angles of Attack," NACA TR-1045.

Fowell, L. R. (1956), "Exact and Approximate Solutions for the Supersonic Delta Wing," J. Aeronaut. Sci. 23, 8, 709-720,770.

Gilinskii, S. M., Telenin, G. F. and Tinyakov, G. P. (1964), "A Method of Computing Supersonic Flow Around Blunt Bodies, Accompanied by a Detached Shock Wave," Izv. AN SSR, Mekhan. i mashinostr. 4, 9-28 (NASA TT F-297, 1965).

Gonidou, R. (1968), "Supersonic Flow Around Cones at Incidence," NASA TT F-11473.

Helliwell, W. S. and Lubard, S. C. (1973), "An Implicit Method for Three-Dimensional Viscous Flow with Application to Cones at Angle of Attack," Aerospace Corp. Report TR-0074(4450-64)-1.

Holt, M. (1954), "A Vortical Singularity in Conical Flow," Quart. J. Mech. and Appl. Math. 7, 4, 438-455.

Holt, M. and Blackie, J. (1956), "Experiments on Circular Cones at Yaw in Supersonic Flow," J. Aeronaut. Sci. 23, 10, 931-936.

Holt, M. and Ndefo, D. E. (1970), "A Numerical Method for Calculating Steady Unsymmetrical Supersonic Flow Past Cones," J. Comp. Phys. 5, 3, 463-486.

Jones, D. J. (1968), "Numerical Solutions of the Flow Field For Conical Bodies in a Supersonic Stream," N.R.C. of Canada, Aero. Rept. LR-507.

Jones, D. J. (1969), "Tables of Inviscid Supersonic Flow about Circular Cones at Incidence, $\gamma = 1.4$," AGARDograph 137, Parts 1 and 2.

Jones, D. J., South, J. C. and Klunker, E. B. (1972), "On the Numerical Solution of Elliptic Partial Differential Equations by the Method of Lines," J. Comp. Phys. 9, 496-527.

Klunker, E. B., South, J. C. and Davis, R. M. (1971), "Calculation of Nonlinear Conical Flows by the Method of Lines," NASA TR-374.

Kutler, P. (1973), Data for Figs. 8 to 10, Private Communication.

Kutler, P. and Lomax, H. (1970), "The Computation of Supersonic Flow Fields about Wing-Body Combinations by "Shock-Capturing" Finite Difference Techniques," Proceedings of the Second International Conference on Numerical Methods in Fluid

Dynamics, p. 24-29, publ. as Lecture Notes in Physics, No. 8 (ed. M. Holt), Springer-Verlag, Berlin.

Kopal, Z. (1947), "Tables of Supersonic Flow Around Yawing Cones," M.I.T., Dept. of Elect. Eng., Center of Analysis, Tech. Rept. 3.

Kopal, Z. (1949), "Tables of Supersonic Flow Around Cones of Large Yaw," M.I.T., Dept. of Elect. Eng., Center of Analysis, Tech. Rept. 5.

Liskovets, O. A. (1965), "The Method of Lines (A Review)," Differentsial'nye Uravneniya 1, 12, 1662-1678.

Lockheed Missile and Space Co. (1972), "A Three Dimensional, Shock Capturing, Finite Difference Code."

Lyons, J. M. (1974), Data for Fig. 12, Private Communication.

Maslen, S. H. (1951), "Supersonic Conical Flow," NACA TN 2651.

Melnik, R. E. (1967), "Vortical Singularities in Conical Flow," AIAA J. 5, 4, 631-637.

Moore, F. K. (1953), "Laminar Boundary Layer on Cone in Supersonic Flow at Large Angle of Attack," NACA TR 1132.

Moretti, G. (1967), "Inviscid Flowfield about a Pointed Cone at an Angle of Attack," AIAA J. 5, 4, 789-791.

Munson, A. G. (1965), "The Vortical Layer on an Inclined Cone," J. Fluid Mech. 20, 4, 625-643.

Ndefo, E. (1968), "Supersonic Flow Past a Yawed Cone Calculated by a Direct Method," Univ. of Calif., Berkeley, Aero. Sci. Rept. AS-68-2.

Ndefo, D. E. (1969), "A Numerical Method for Calculating Steady Unsymmetrical Supersonic Flow Past Cones," Univ. of Calif.,

Berkeley, Aero. Sciences Rept. AS-69-11.

Powell, M. J. D. (1964a), "An Efficient Method for Finding the Minimum of a Function of Several Variables without Calculating Derivatives," The Computer Journal 7, 155-162.

Powell, M. J. D. (1964b), "A Method for Minimizing a Sum of Squares of Non-Linear Functions without Calculating Derivatives," Computer J. 7, 4, 303-307.

Rainbird, W. J. (1968), "The External Flow Field about Yawed Circular Cones," AGARD Conference Proceedings No. 30: Hypersonic Boundary Layers and Flow Fields, Paper No. 30.

Stocker, P. M. and Mauger, F. E. (1962), "Supersonic Flow Past Cones of General Cross-Section," J. Fluid Mech. 13, 3, 383-389.

Stone, A. H. (1948), "On Supersonic Flow Around a Slightly Yawing Cone," Part I, J. Math. and Phys. 27, 1, 67-81.

Stone, A. H. (1952), "On Supersonic Flow Around a Slightly Yawing Cone," Part II, J. Math. and Phys. 30, 200-213.

Telenin, G. F. and Tinyakov, G. P. (1964), "A Method of Calculating Three-Dimensional Flow Past a Body with a Detached Shock Wave," Dokl. AN SSR 154, 5, 1056-1058.

Tracy, R. R. (1963), "Hypersonic Flow over a Yawed Circular Cone," Graduate Aero. Labs., Calif. Inst. of Technology, Pasadena, Calif., Memo. No. 69.

Van Dyke, M. D. (1958), "The Supersonic Blunt-Body Problem - Review and Extension," J. Aeronaut. Sci. 25, 8, 485-496.

Williams, J. B. (1969), "A Correlation of the Windward Shock Angle on Yawed Cones," AIAA J. 7, 7, 1398.

Woods, B. A. (1962), "The Flow Close to the Surface of a Circular Cone at Incidence to a Supersonic Stream," Aero. Quart. 13, 2, 115-128.

Yahalom, R. (1971), "An Experimental Investigation of Supersonic Flow past Yawed Cones," Univ. of Calif., Berkeley, Aero. Sci. Rept. AS-71-2.

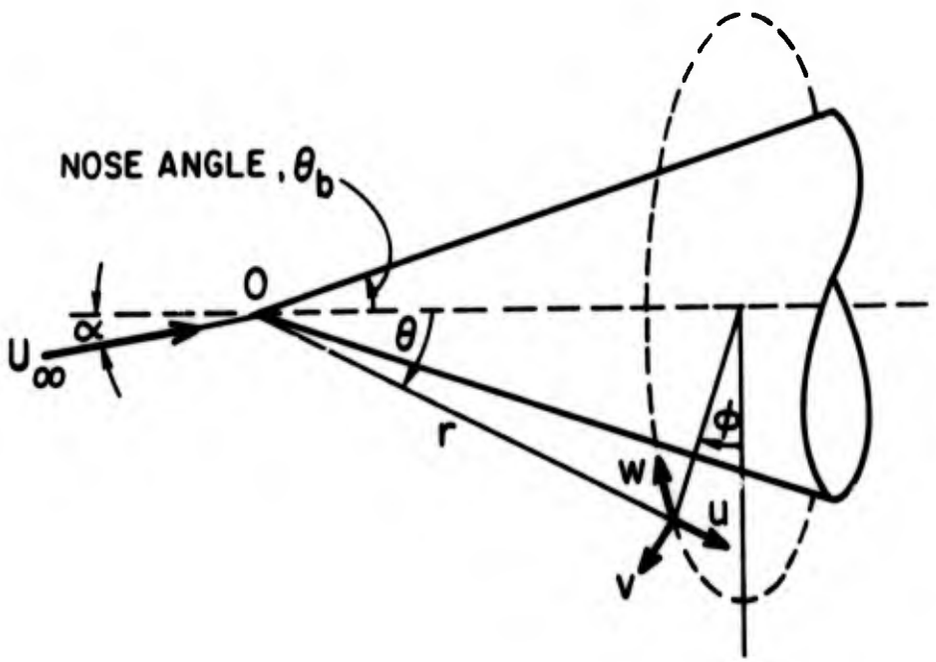

FIG. 1 COORDINATE SYSTEM AND VELOCITIES

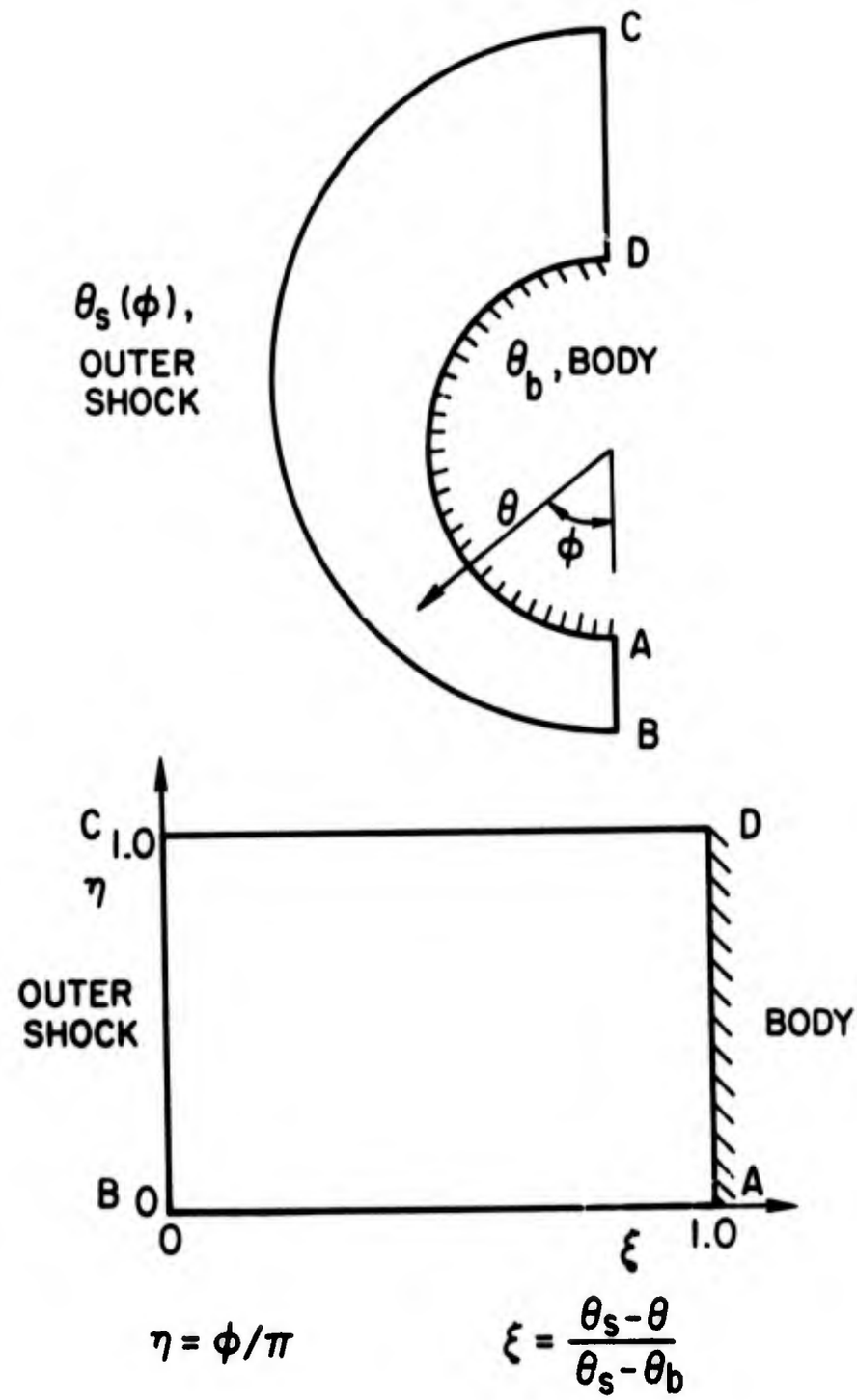

FIG. 2 COORDINATE TRANSFORMATION USED IN THE WINDWARD (SECTION 4) AND SHOULDER (SECTION 5) REGIONS

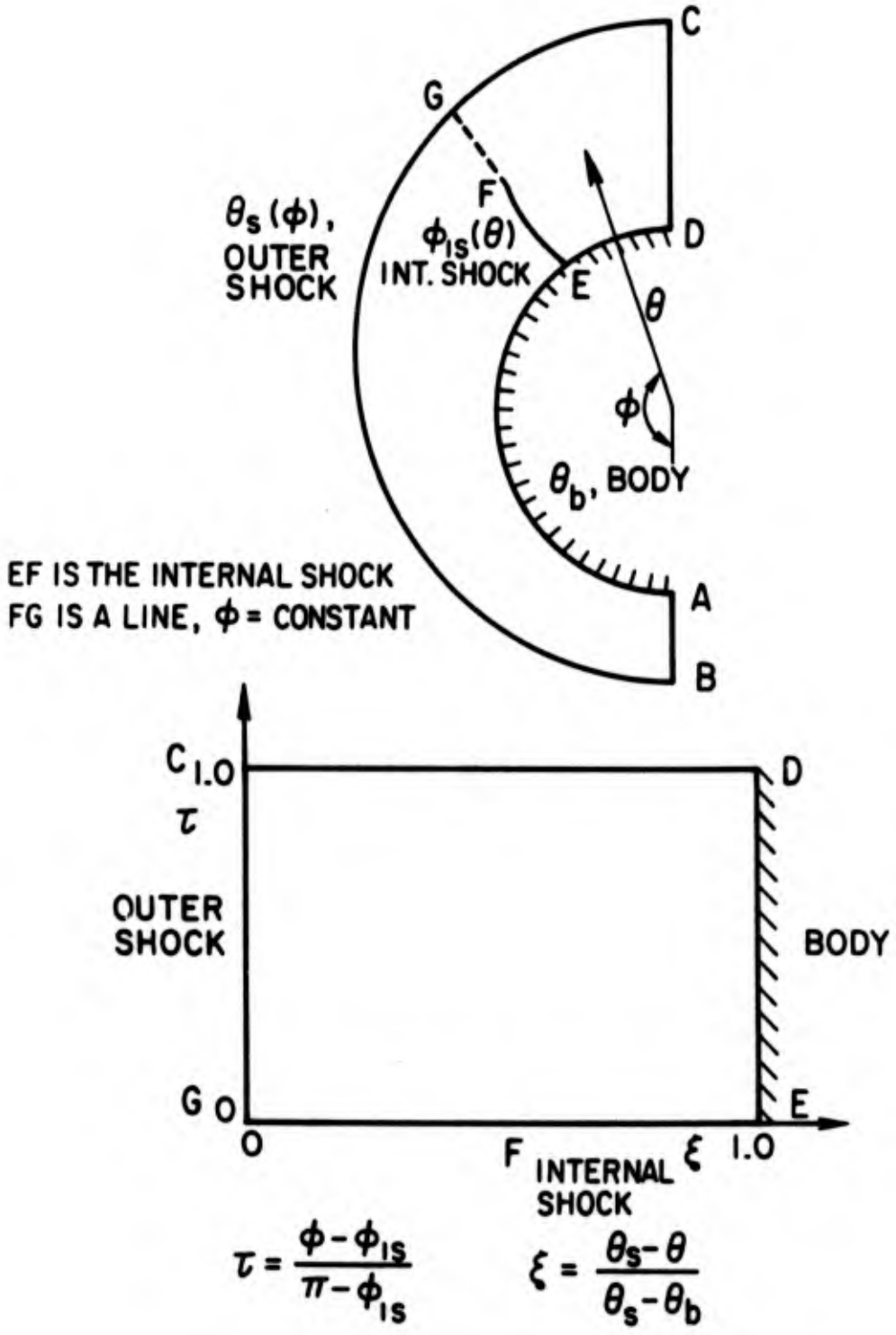

FIG. 3 COORDINATE TRANSFORMATION USED IN THE LEEWARD REGION (SECTION 6)

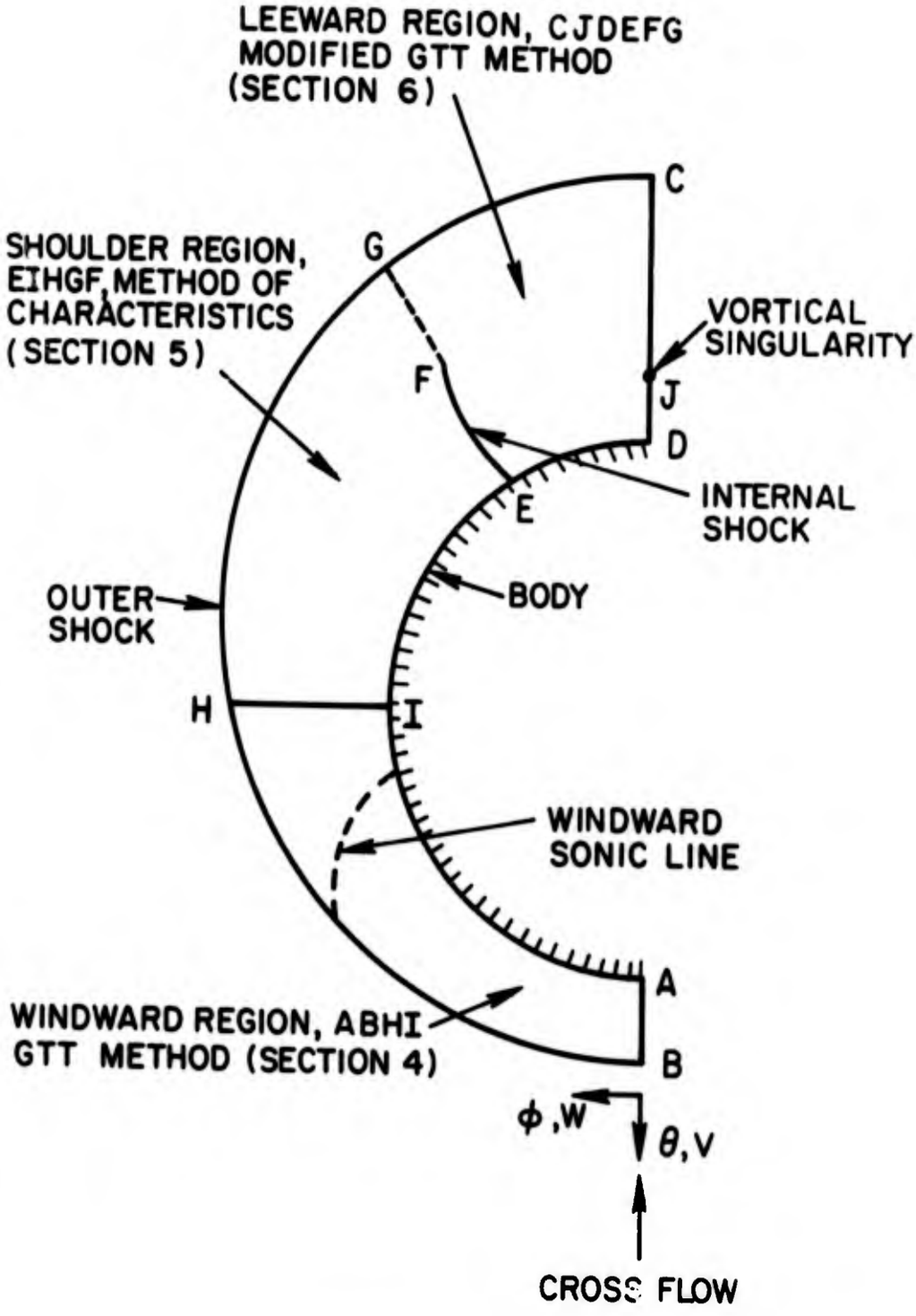

FIG. 4 CLASSIFICATION OF THE DIFFERENT FLOW REGIONS ON THE BASIS OF THE NUMERICAL METHOD USED

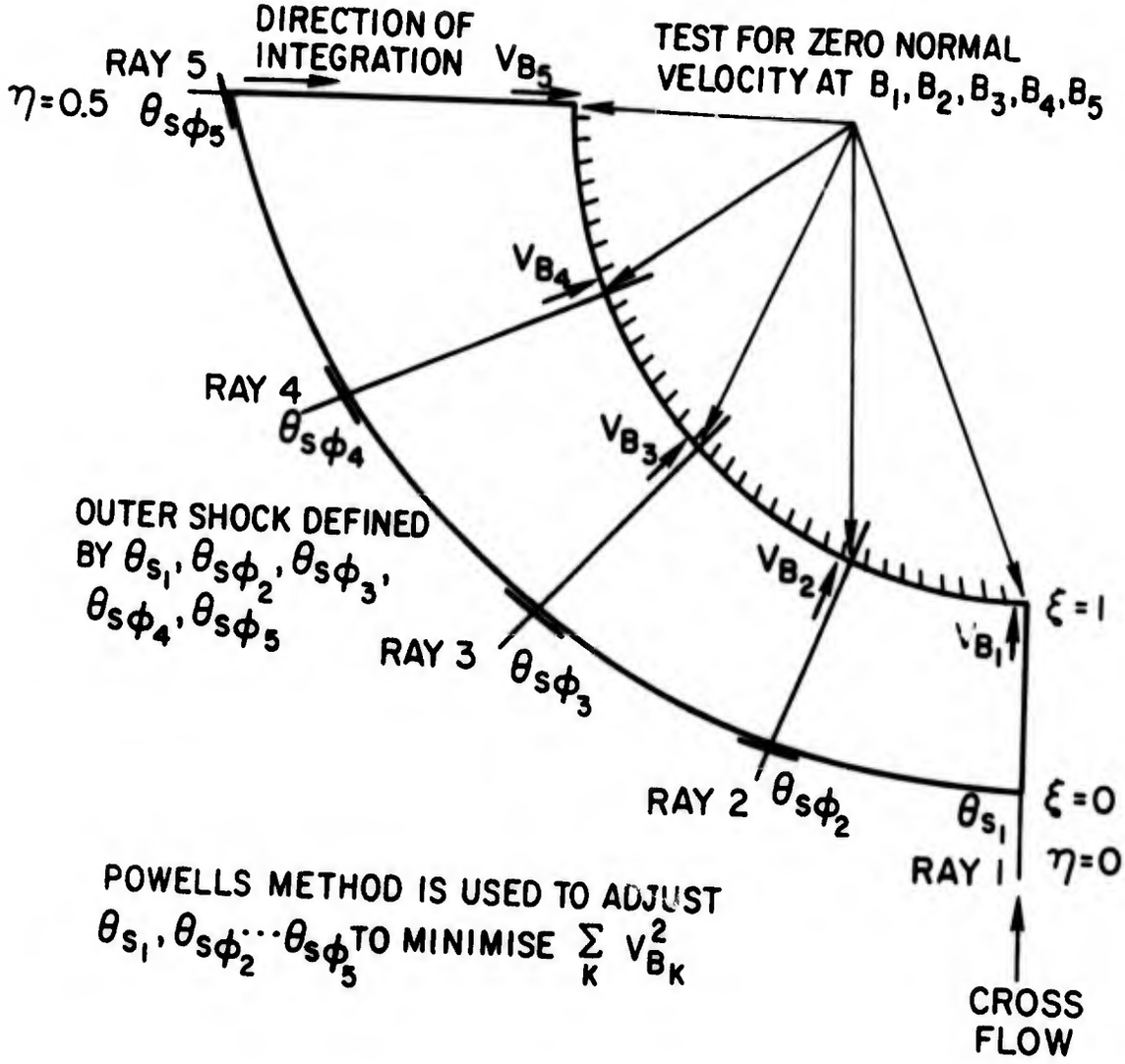

FIG. 5 SCHEMATIC REPRESENTATION OF THE NUMERICAL METHOD USED IN THE WINDWARD REGION (SECTION 4)

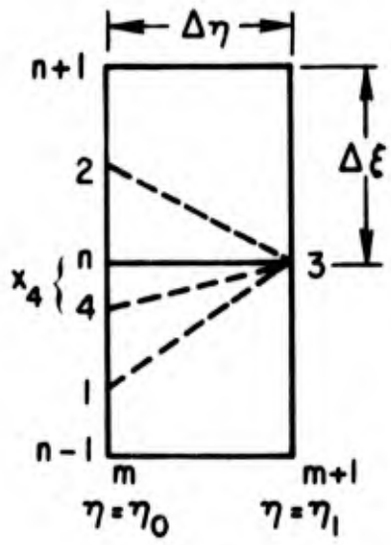

(a) POINT 3 IS AN INTERIOR POINT

1 3 } ARE CHARACTERISTIC
2 3 } DIRECTIONS
} THROUGH
4 3 IS STREAMLINE DIRECTION } POINT 3

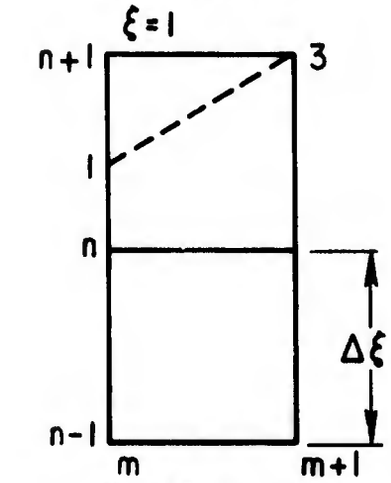

(b) POINT 3 IS AT THE SHOCK

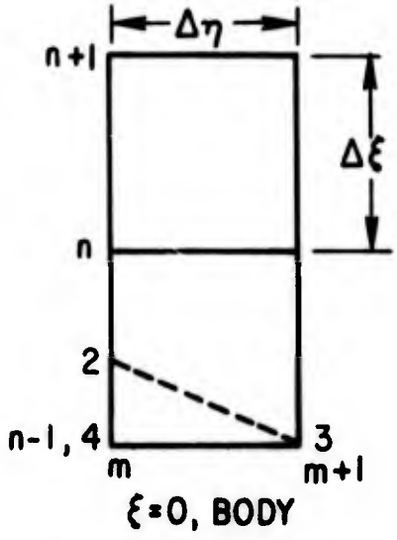

(c) POINT 3 IS AT THE BODY

FIG.6 SCHEMATIC REPRESENTATION OF THE NUMERICAL METHOD USED IN THE SHOULDER REGION (SECTION 5)

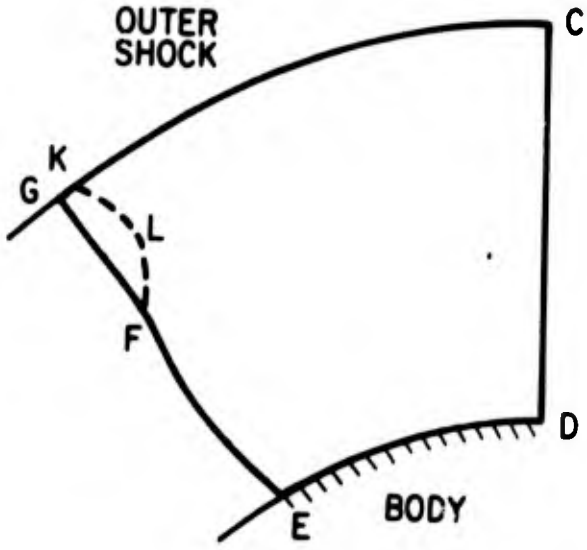

SOLUTION IN FGKL IS DETERMINED SOLELY BY THE CHARACTERISTICS SOLUTION

KL IS PART OF LEEWARD SONIC LINE

FL IS THE OUTER CHARACTERISTIC PATH THROUGH THE END OF THE INTERNAL SHOCK

POWELLS METHOD IS USED TO ADJUST THE LOCATION OF E F UNTIL THE VELOCITY COMPONENT NORMAL TO C D IS ZERO FOR THE 1st AND 3rd INTEGRATIONS

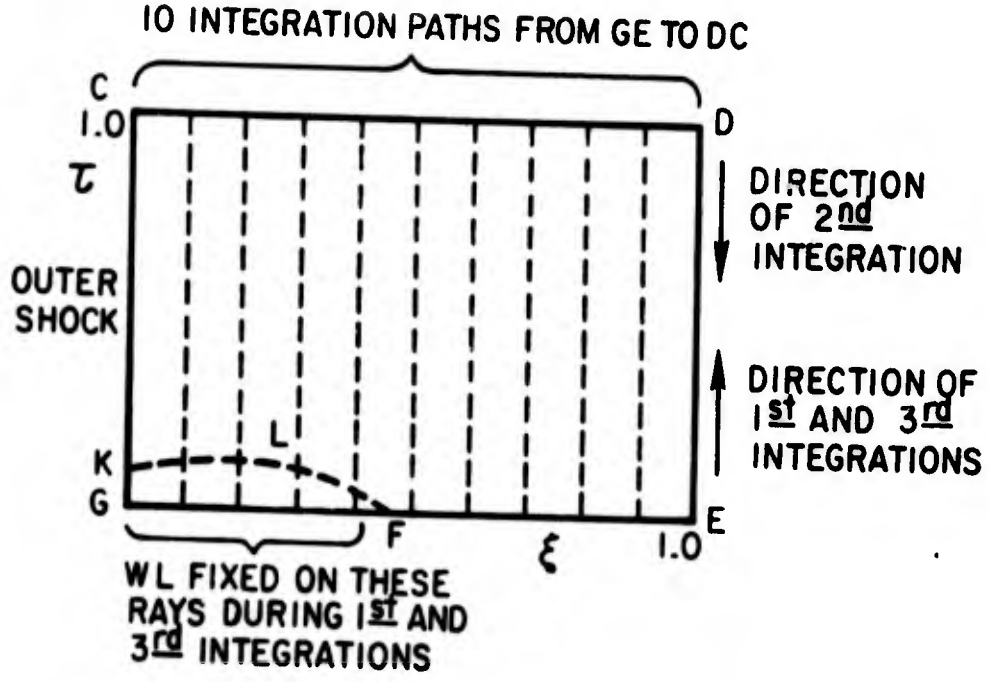

FIG. 7 SCHEMATIC REPRESENTATION OF THE NUMERICAL METHOD USED IN THE LEEWARD REGION (SECTION 6)

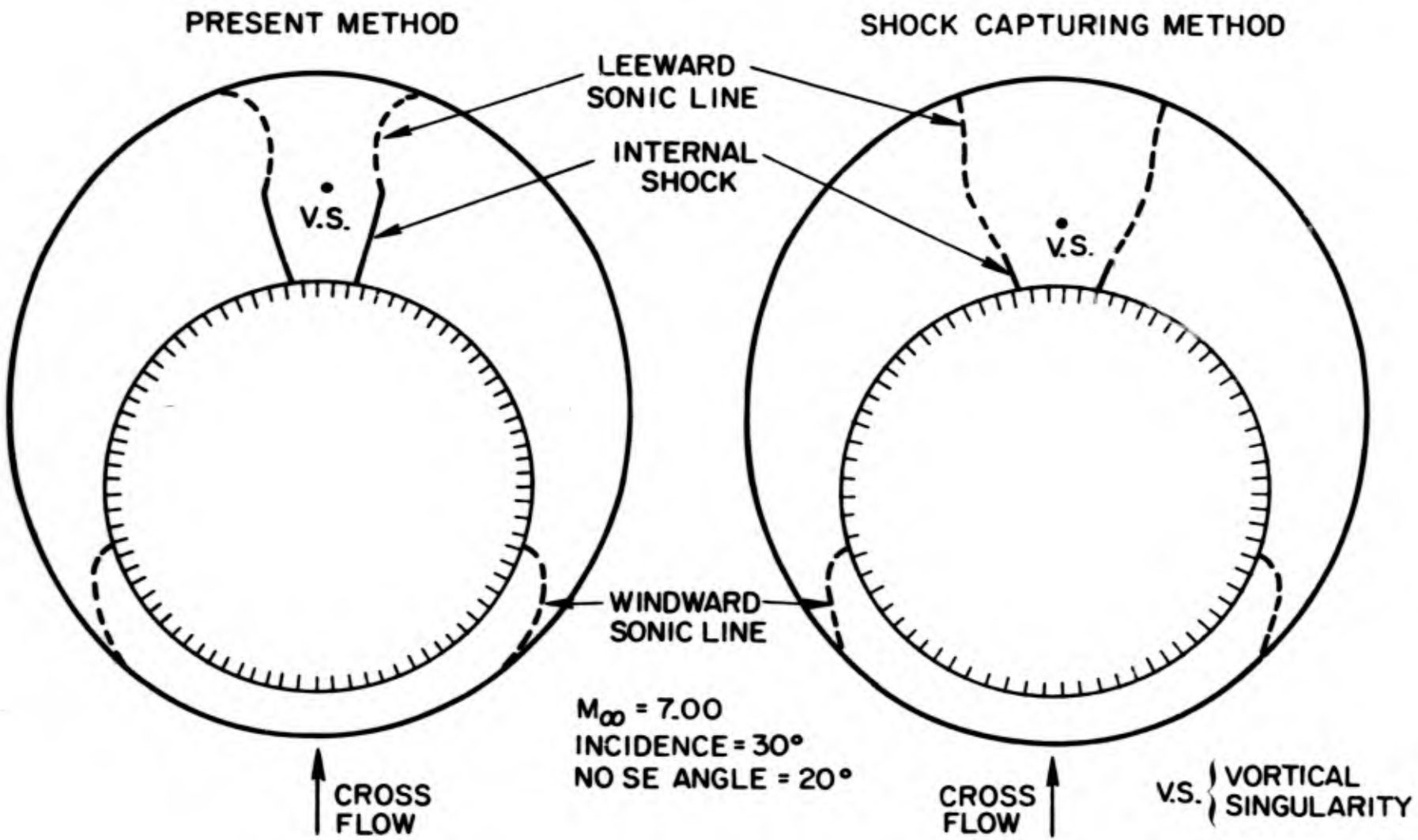

FIG. 8 COMPARISON WITH SHOCK CAPTURING METHOD- SHOCK WAVE AND SONIC LINE LOCATIONS

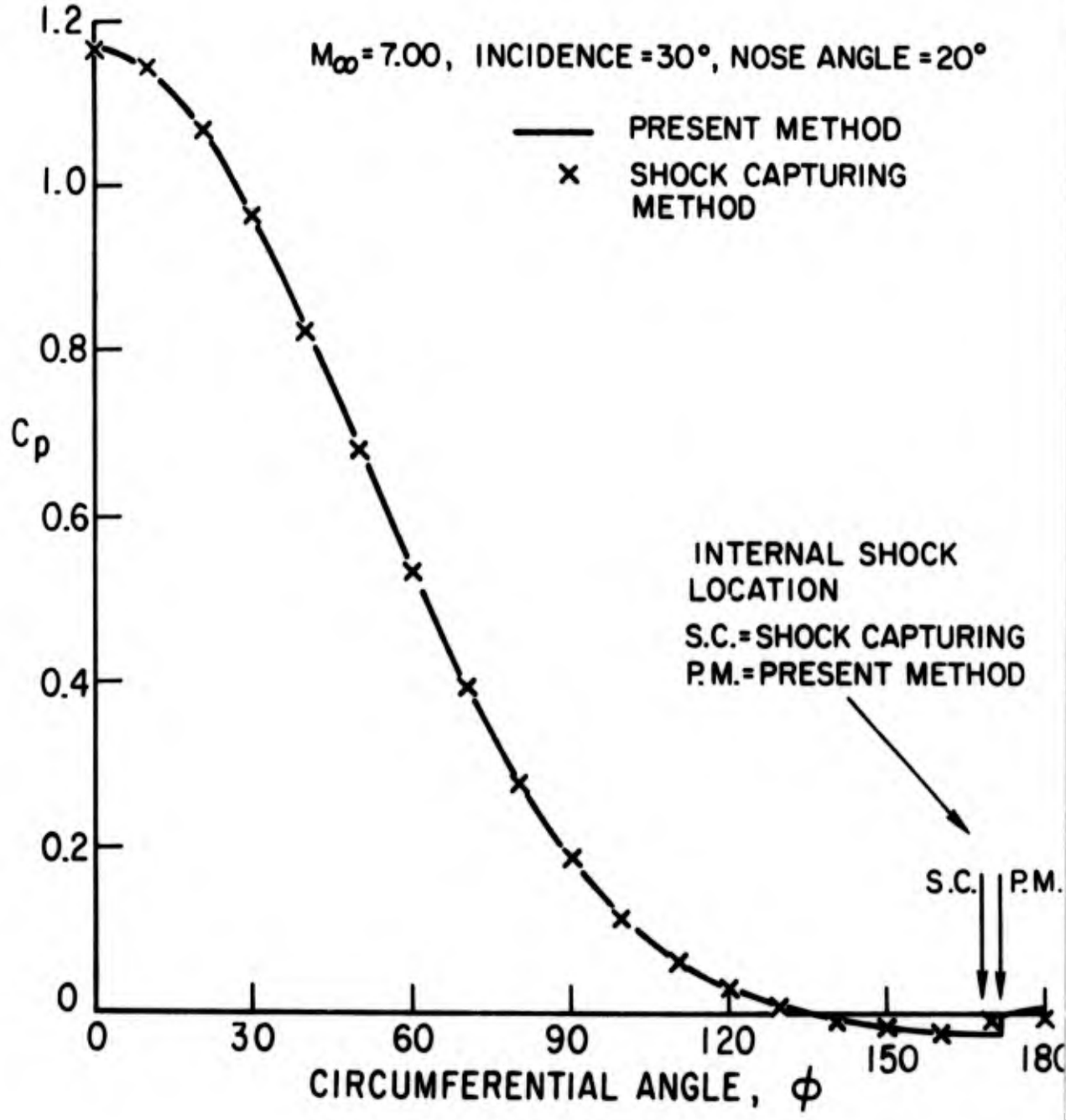

FIG. 9 COMPARISON WITH SHOCK CAPTURING METHOD – PRESSURE DISTRIBUTION

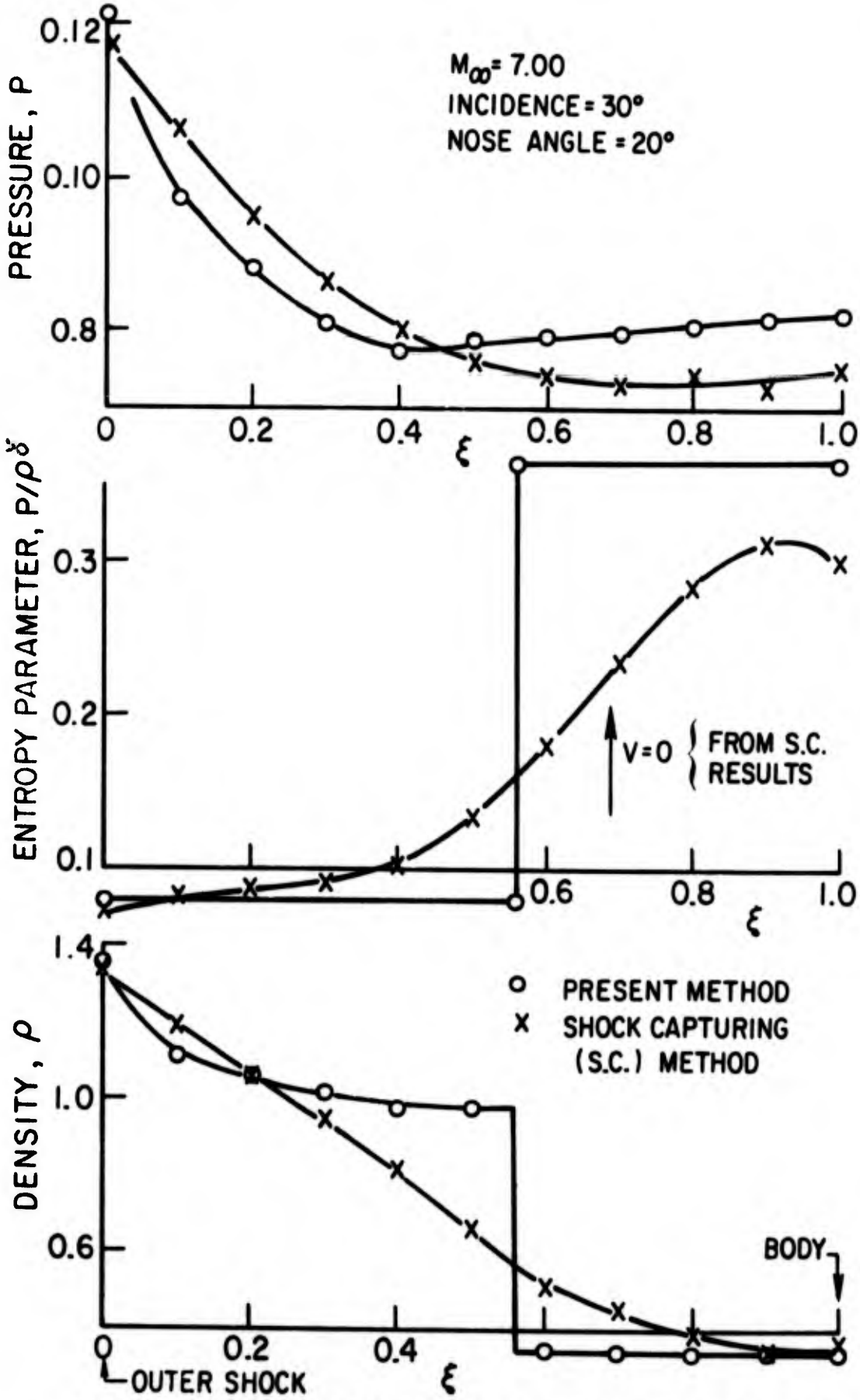

FIG. 10 FLOW VARIATION ALONG LEEWARD LINE OF SYMMETRY

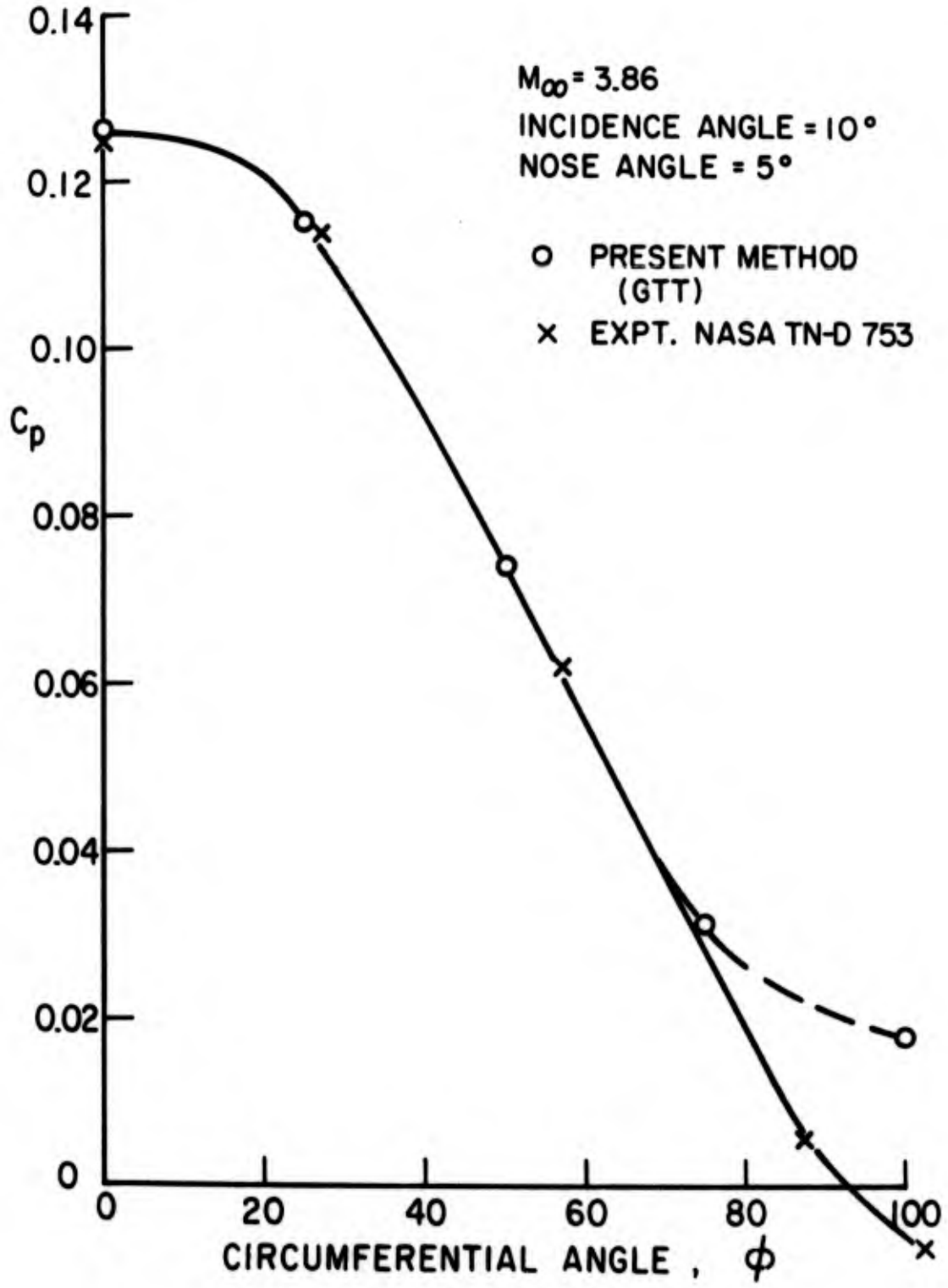

FIG. 11 PRESSURE DISTRIBUTION FOR A CASE WHERE THE CROSS FLOW IS COMPLETELY SUBSONIC

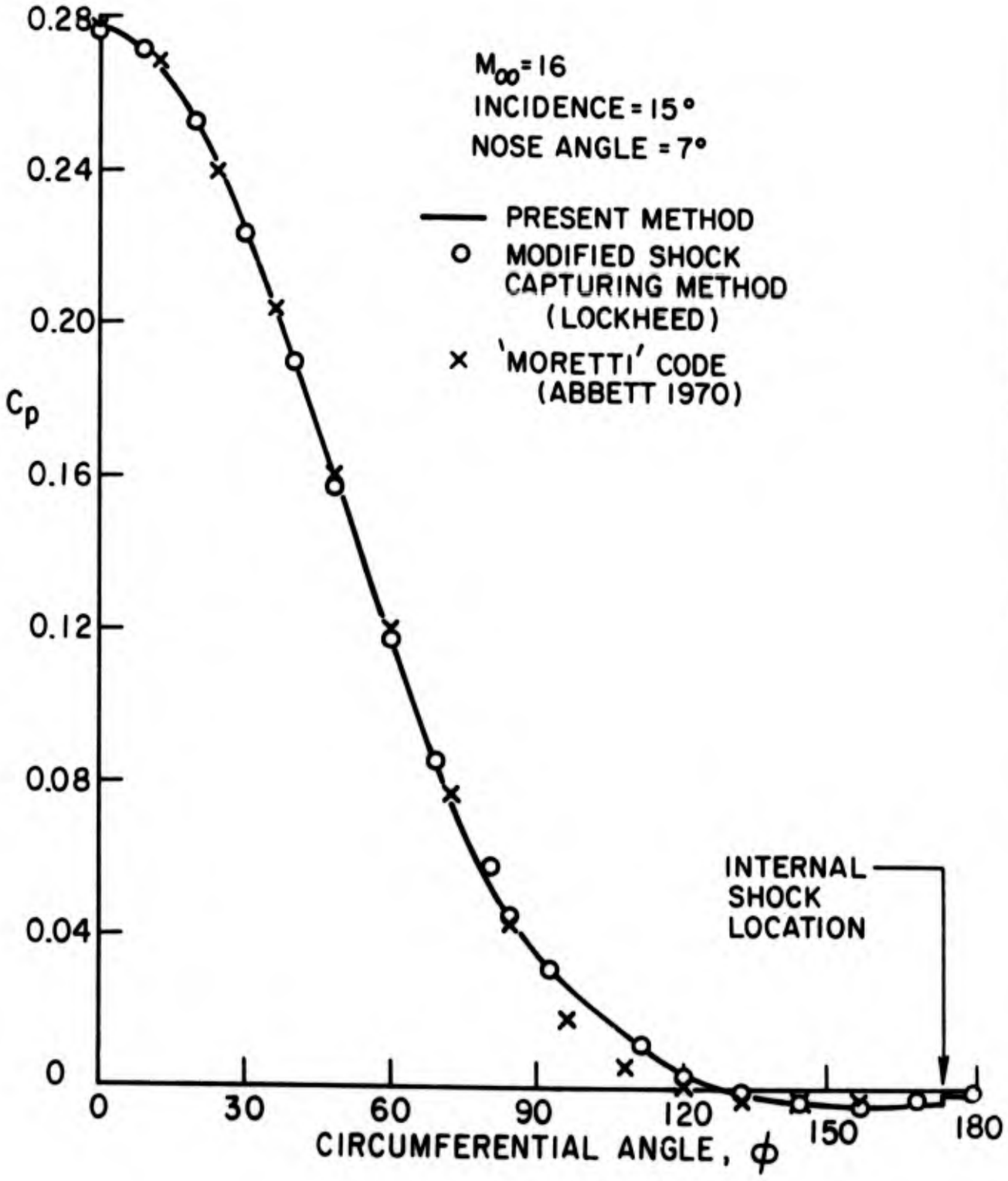

FIG. 12 PRESSURE DISTRIBUTION FOR LARGE FREESTREAM MACH NUMBER

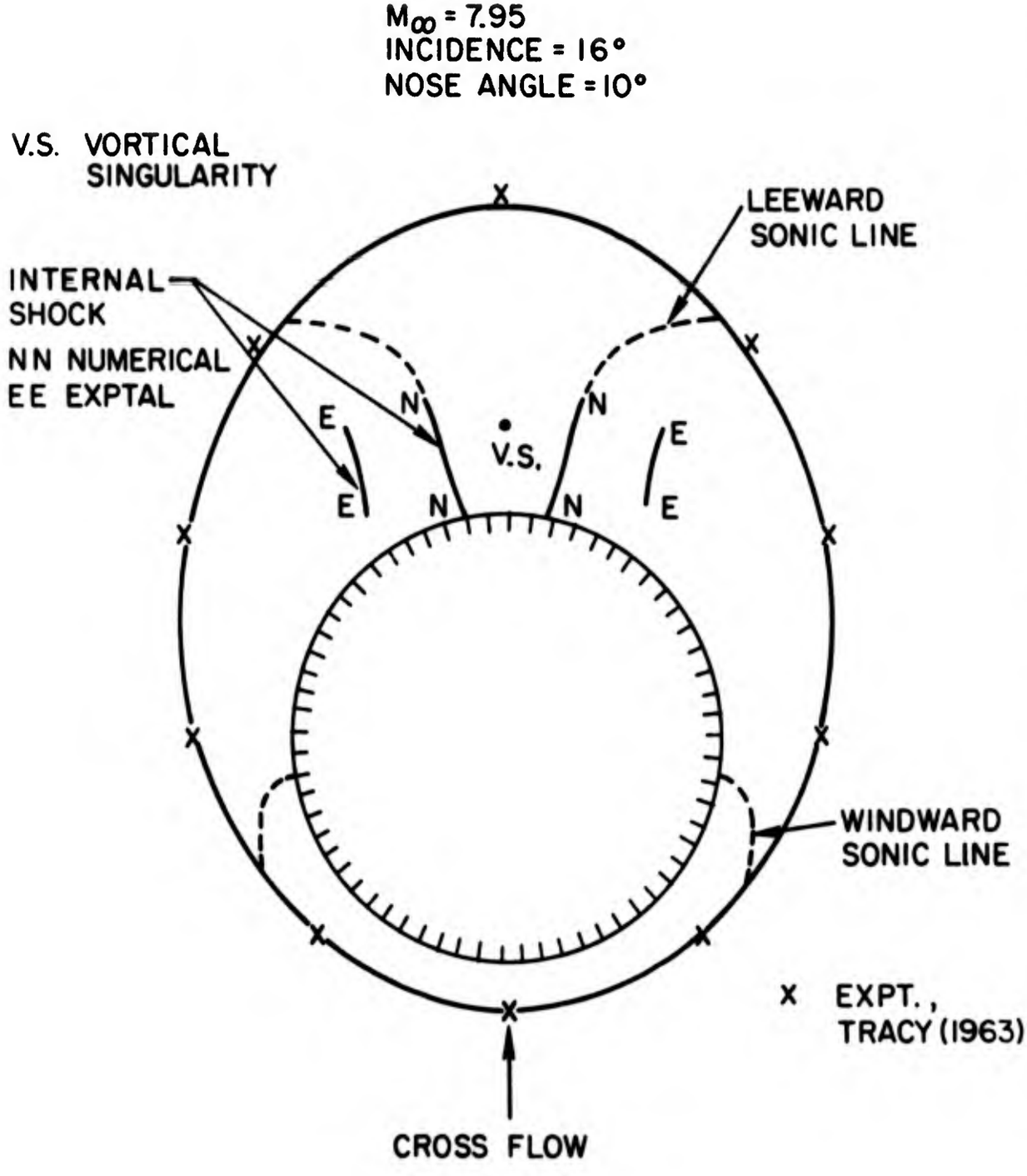

FIG. 13 COMPARISON WITH EXPERIMENT-SHOCK WAVE AND SONIC LINE LOCATIONS

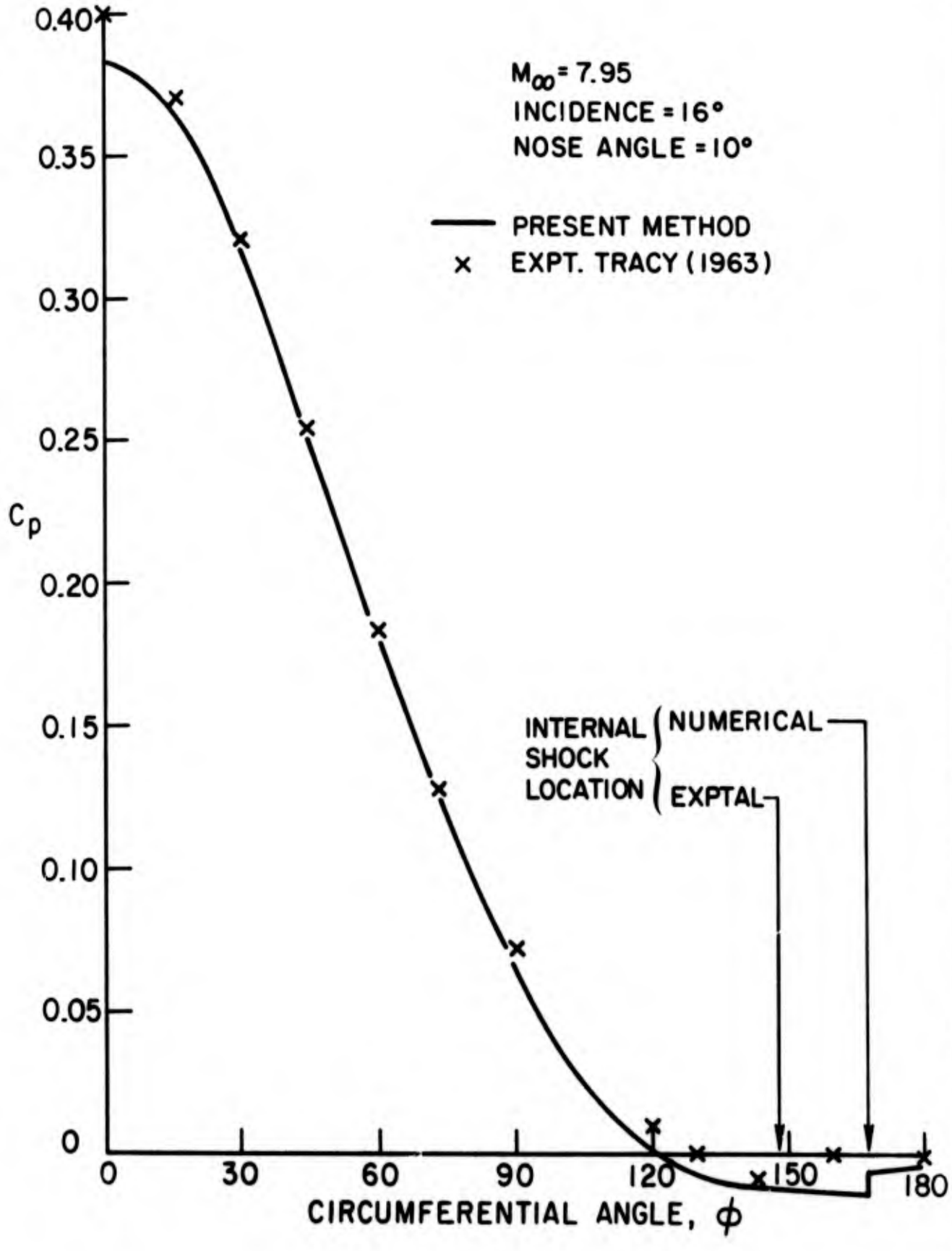

FIG. 14 COMPARISON WITH EXPERIMENT-PRESSURE DISTRIBUTION

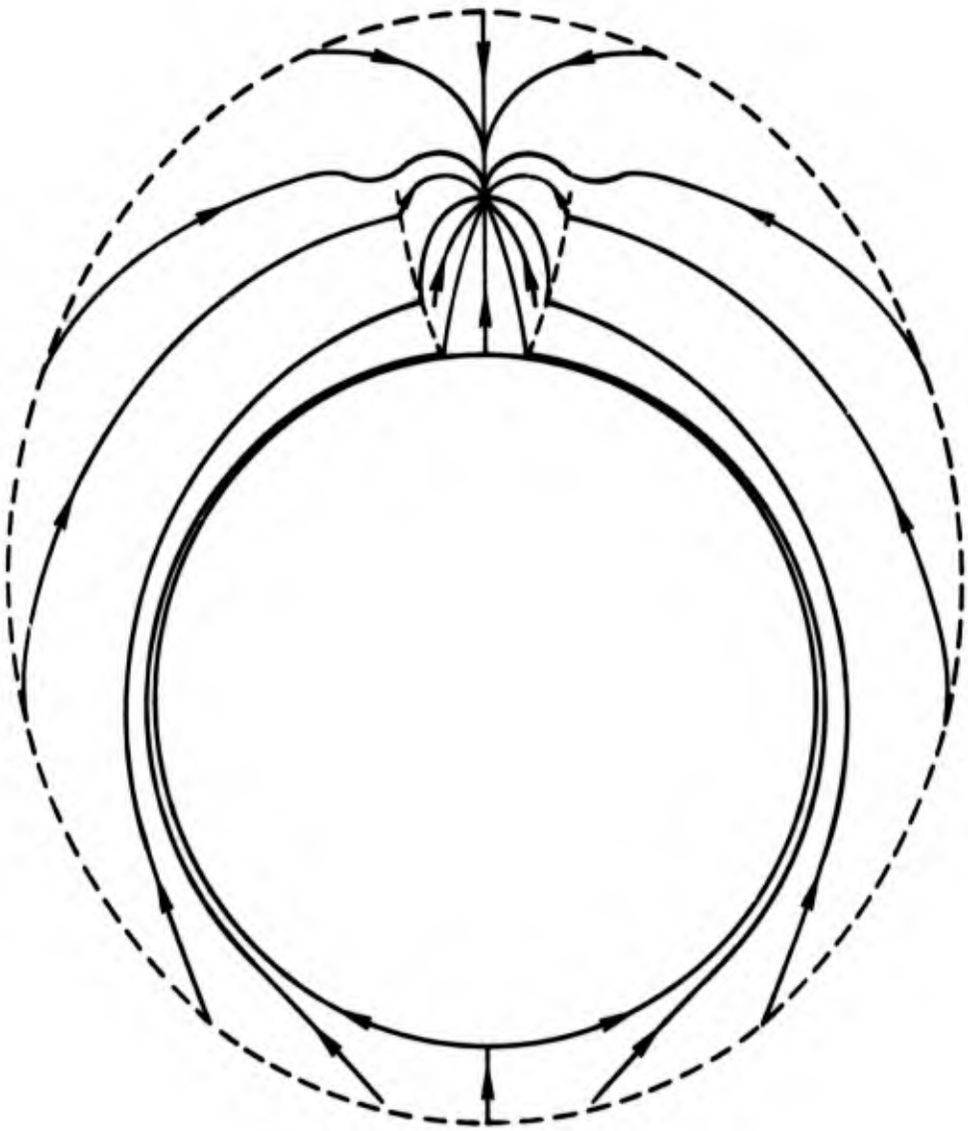

FIG. 15 STREAMLINE PATTERN AT $M_\infty = 7$, INCIDENCE = 30°, NOSE ANGLE = 20°

$$M_{cr} = \left[\frac{v^2 + w^2}{a^2} \right]^{1/2}$$

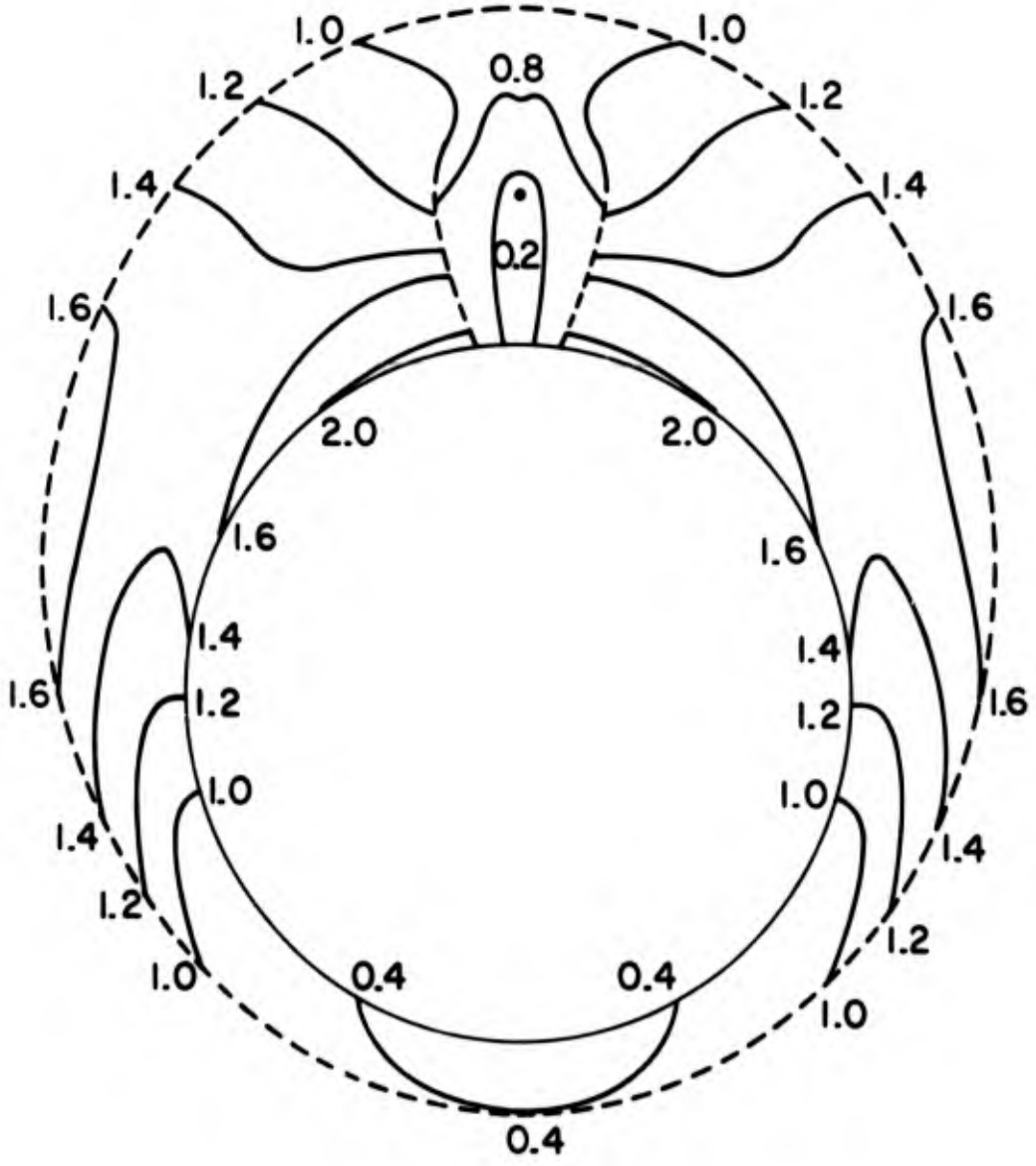

FIG. 16 CONTOURS OF CROSS FLOW MACH NUMBER AT $M_\infty = 7$, INCIDENCE = 30° AND NOSE ANGLE = 20°

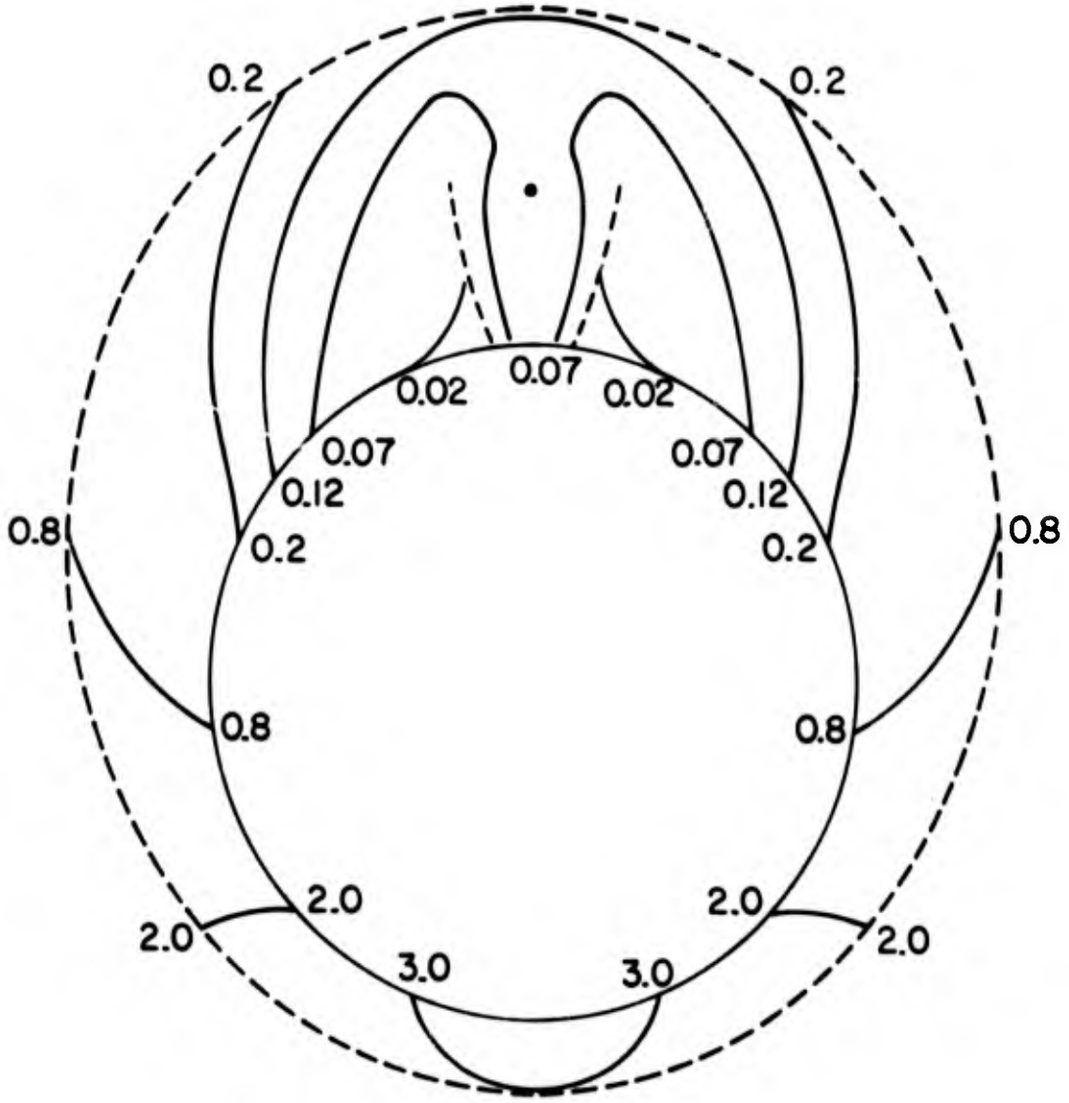

FIG. 17 CONTOURS OF PRESSURE AT $M_\infty = 7$, INCIDENCE=30°, AND NOSE ANGLE = 20°

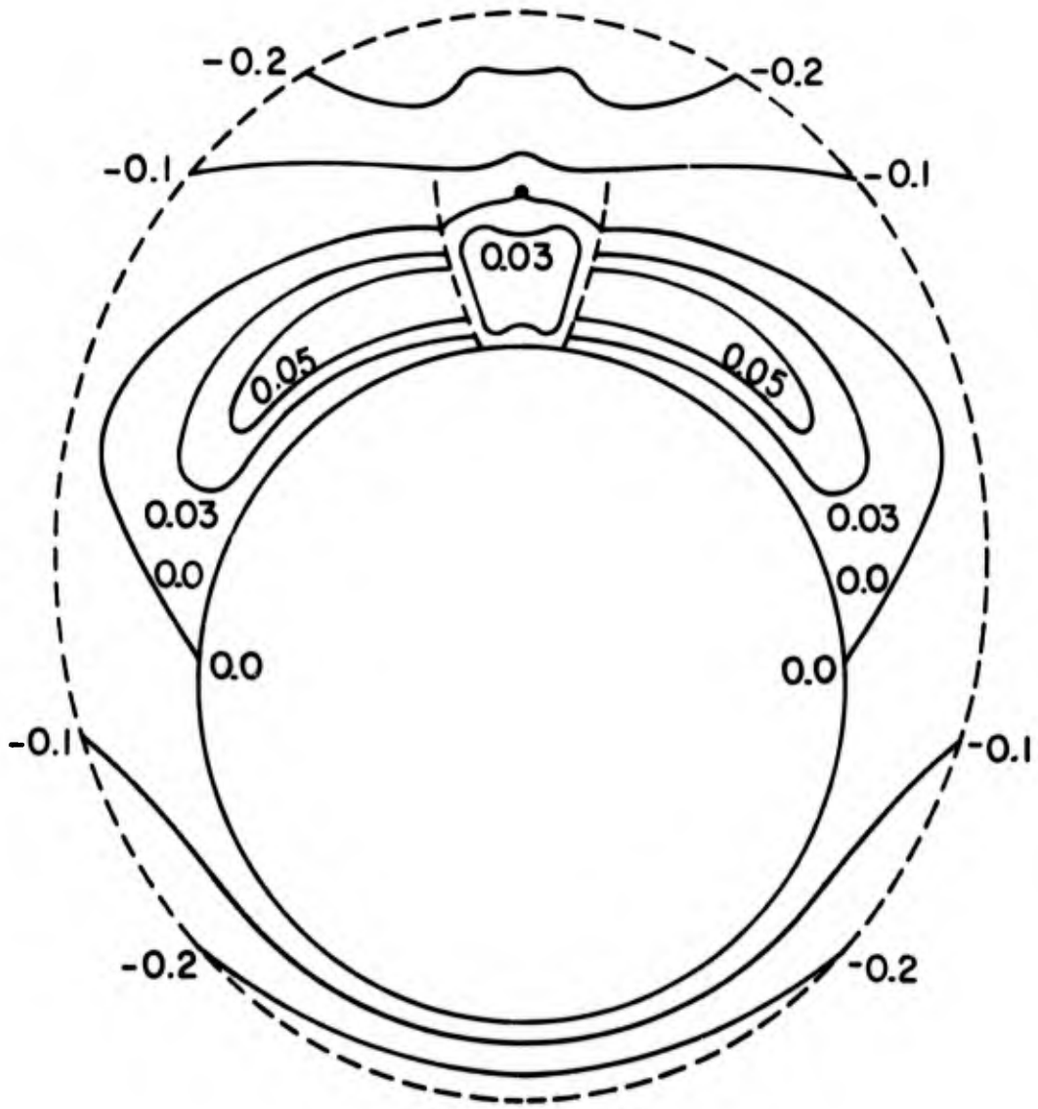

FIG. 18 CONTOURS OF NORMAL VELOCITY COMPONENT AT $M_\infty = 7$, INCIDENCE = 30° AND NOSE ANGLE = 20°

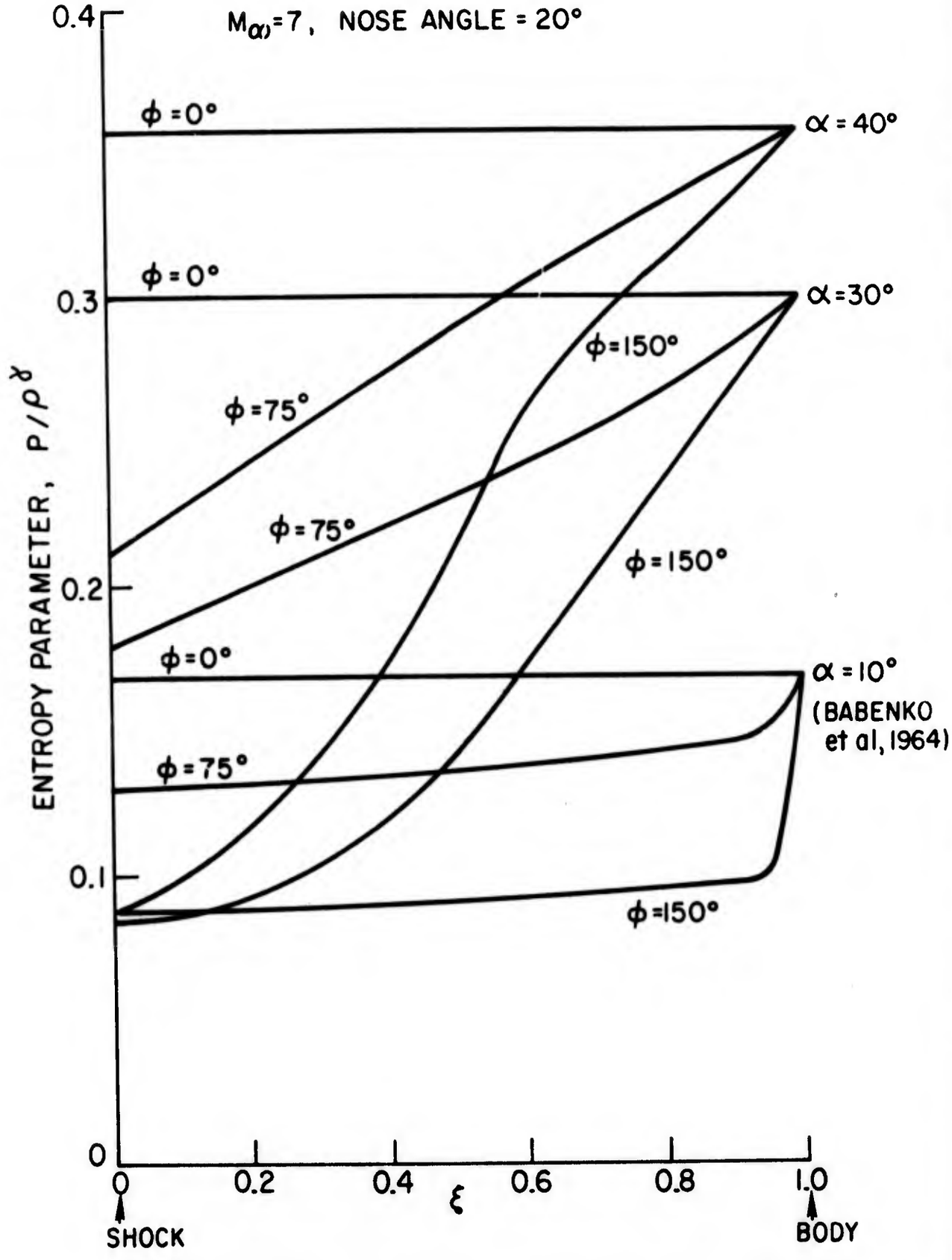

FIG. 19 EFFECT OF INCIDENCE ON THE ENTROPY LAYER

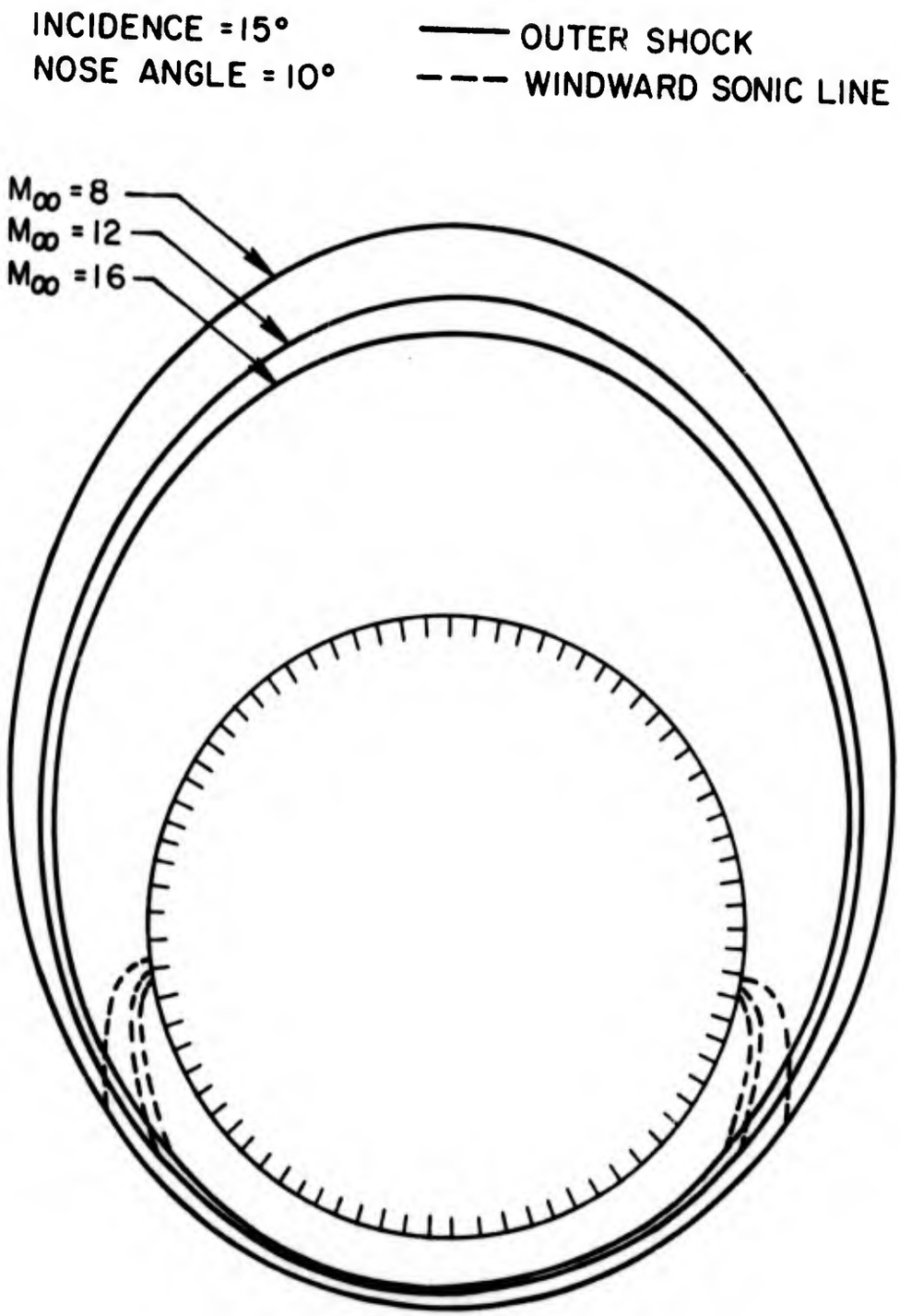

FIG. 20 VARIATION OF SHOCK SHAPE WITH MACH NUMBER

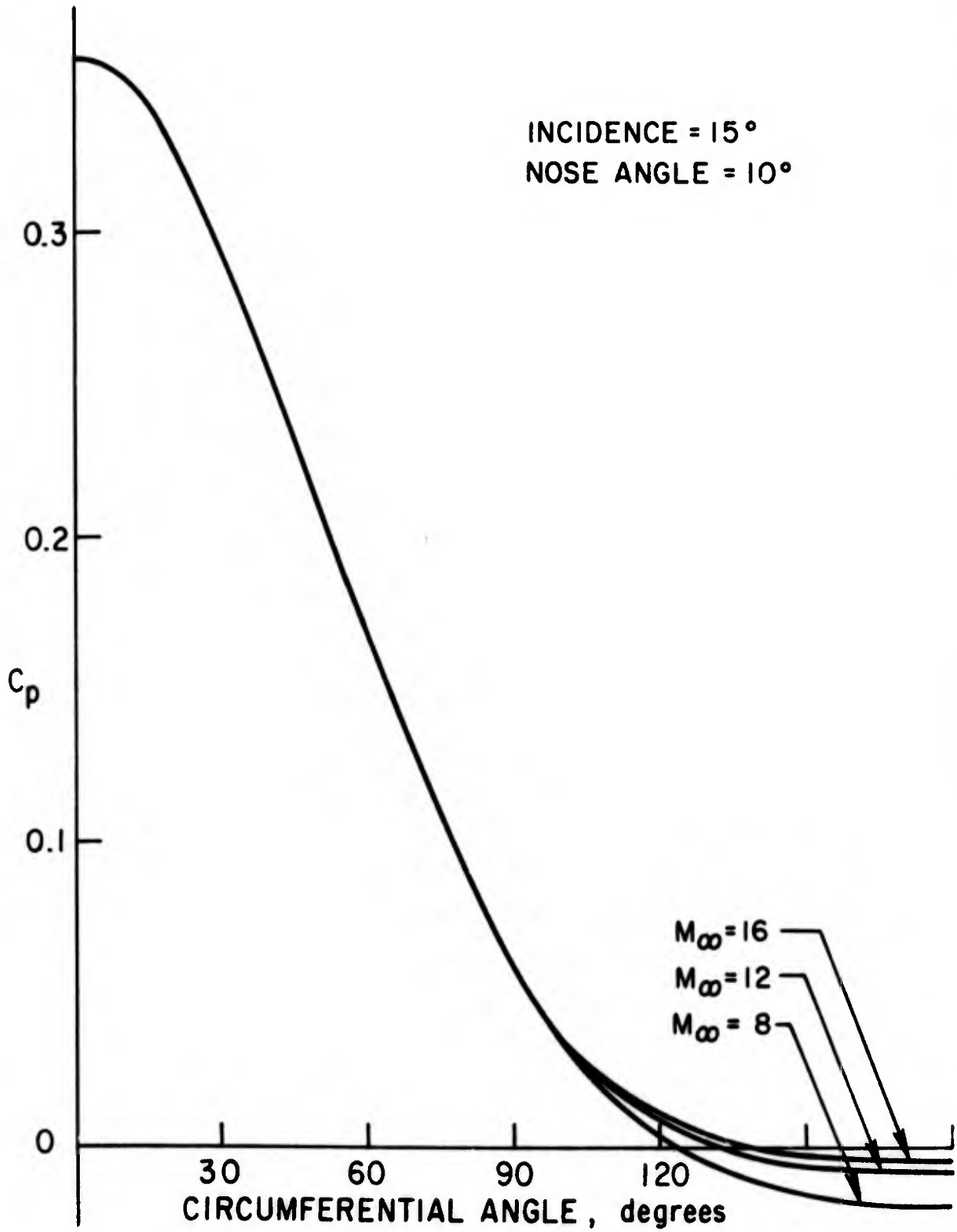

FIG. 21 VARIATION OF PRESSURE DISTRIBUTION WITH MACH NUMBER

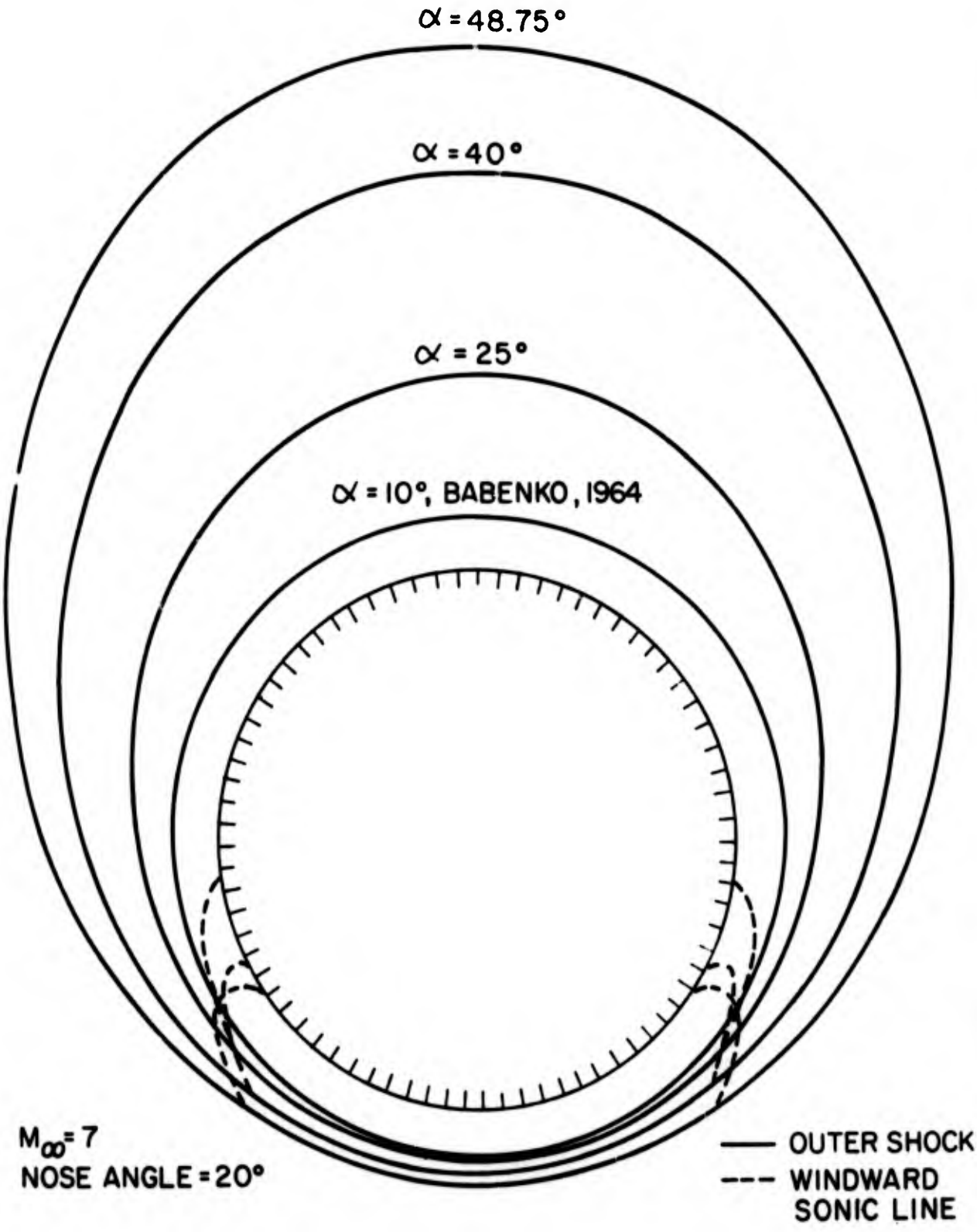

FIG. 22 VARIATION OF SHOCK SHAPE WITH INCIDENCE

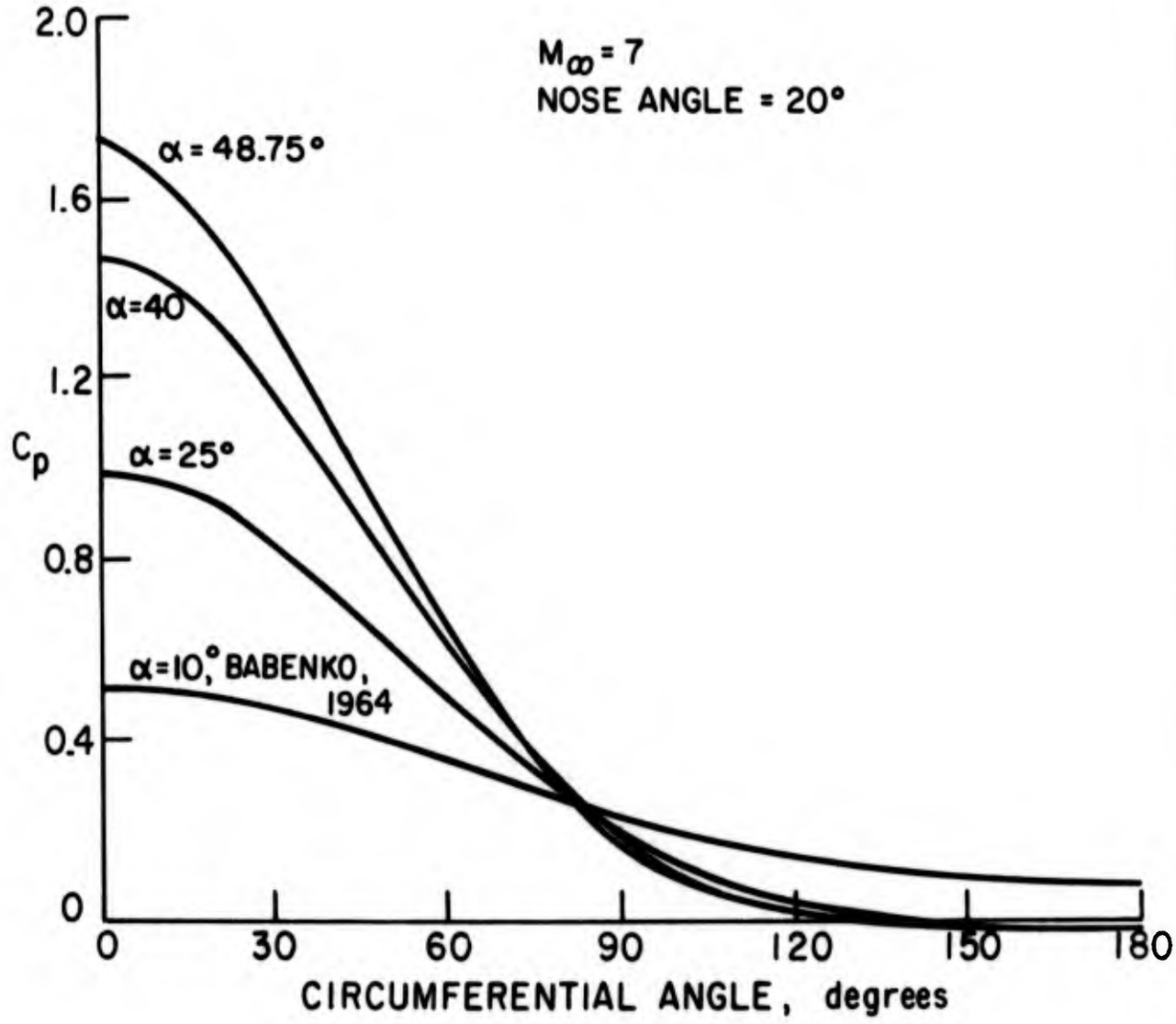

FIG. 23 VARIATION OF PRESSURE DISTRIBUTION WITH INCIDENCE

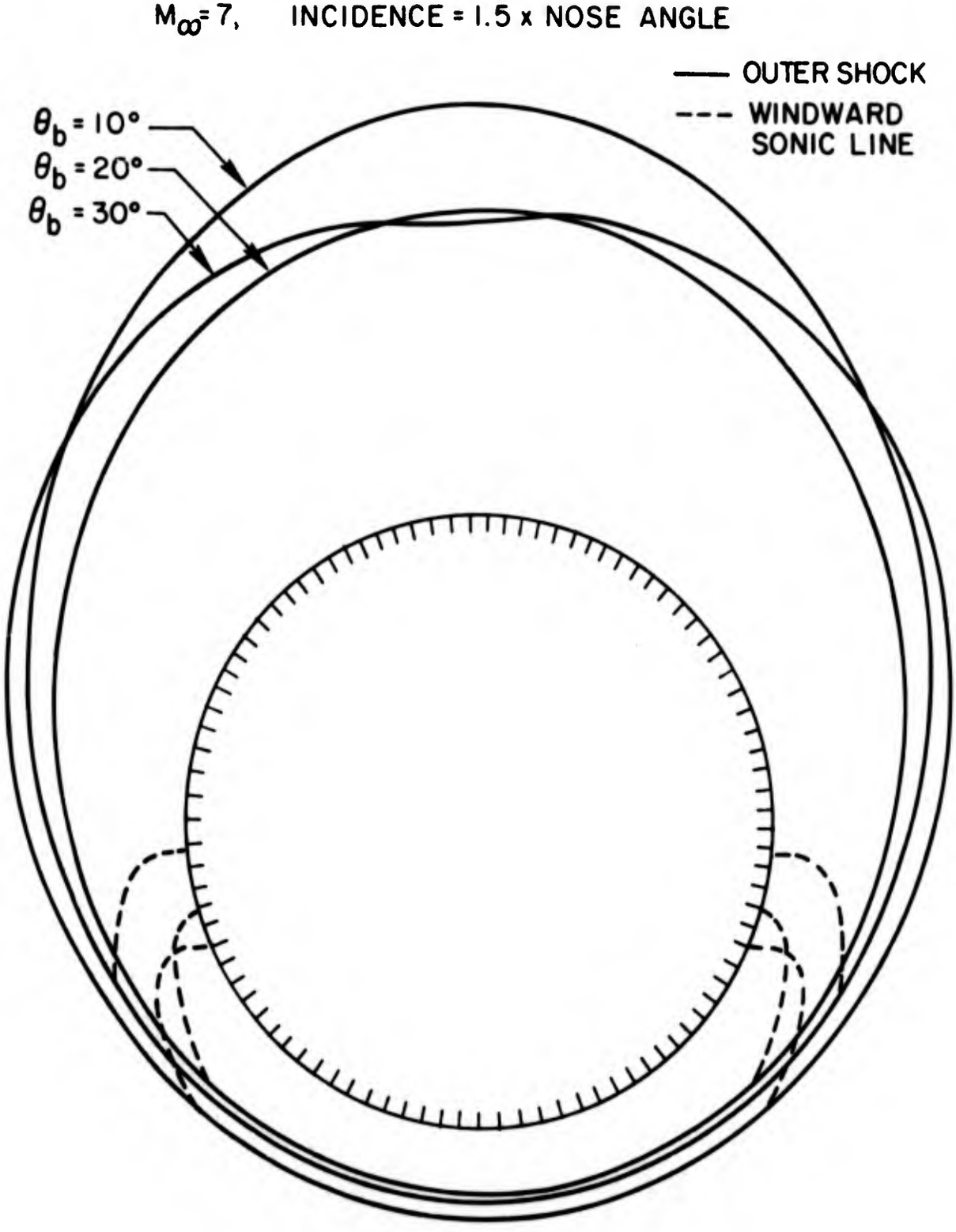

FIG. 24 VARIATION OF SHOCK SHAPE WITH NOSE ANGLE, θ_b

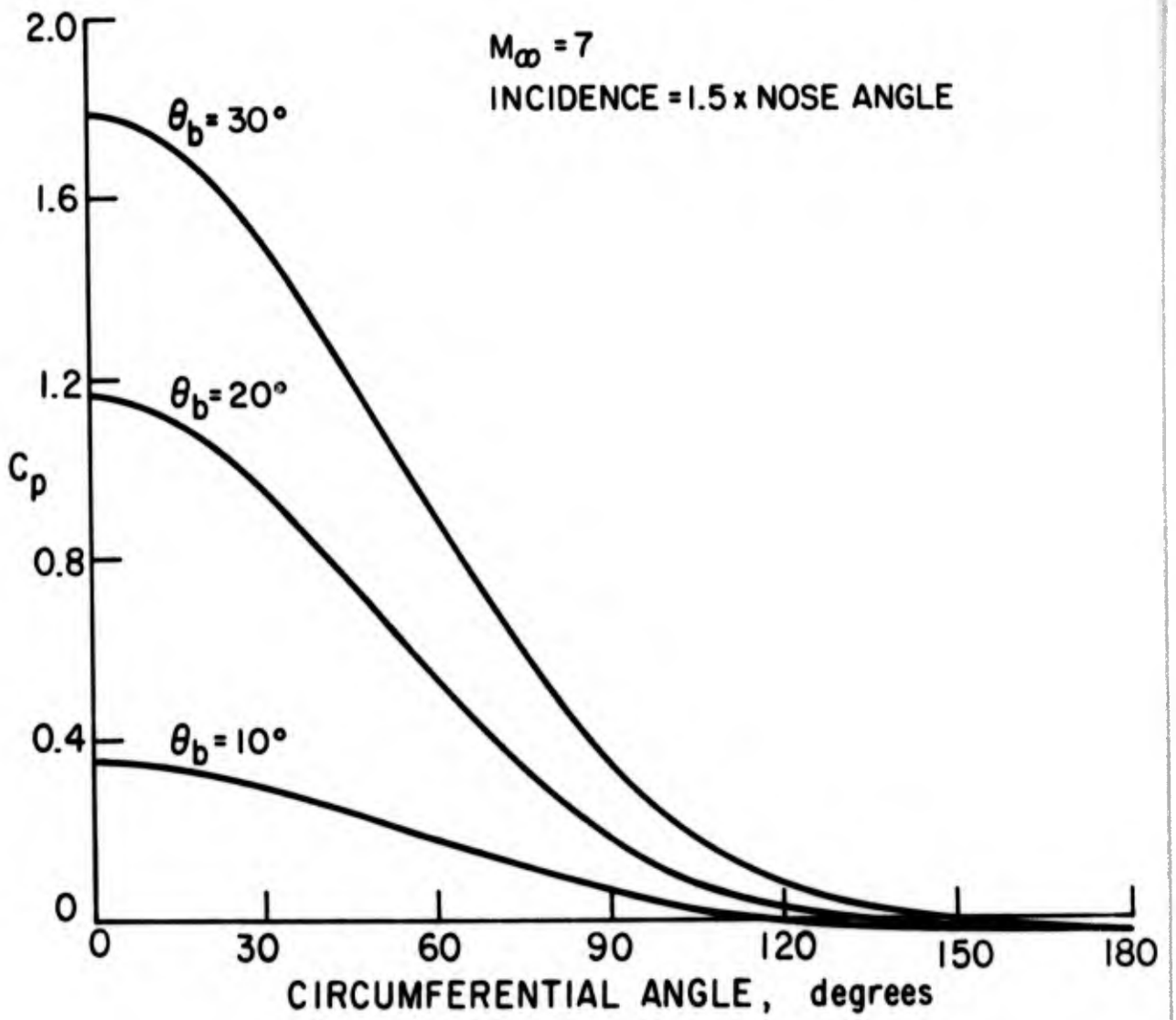

FIG. 25 VARIATION OF PRESSURE DISTRIBUTION WITH NOSE ANGLE, θ_b

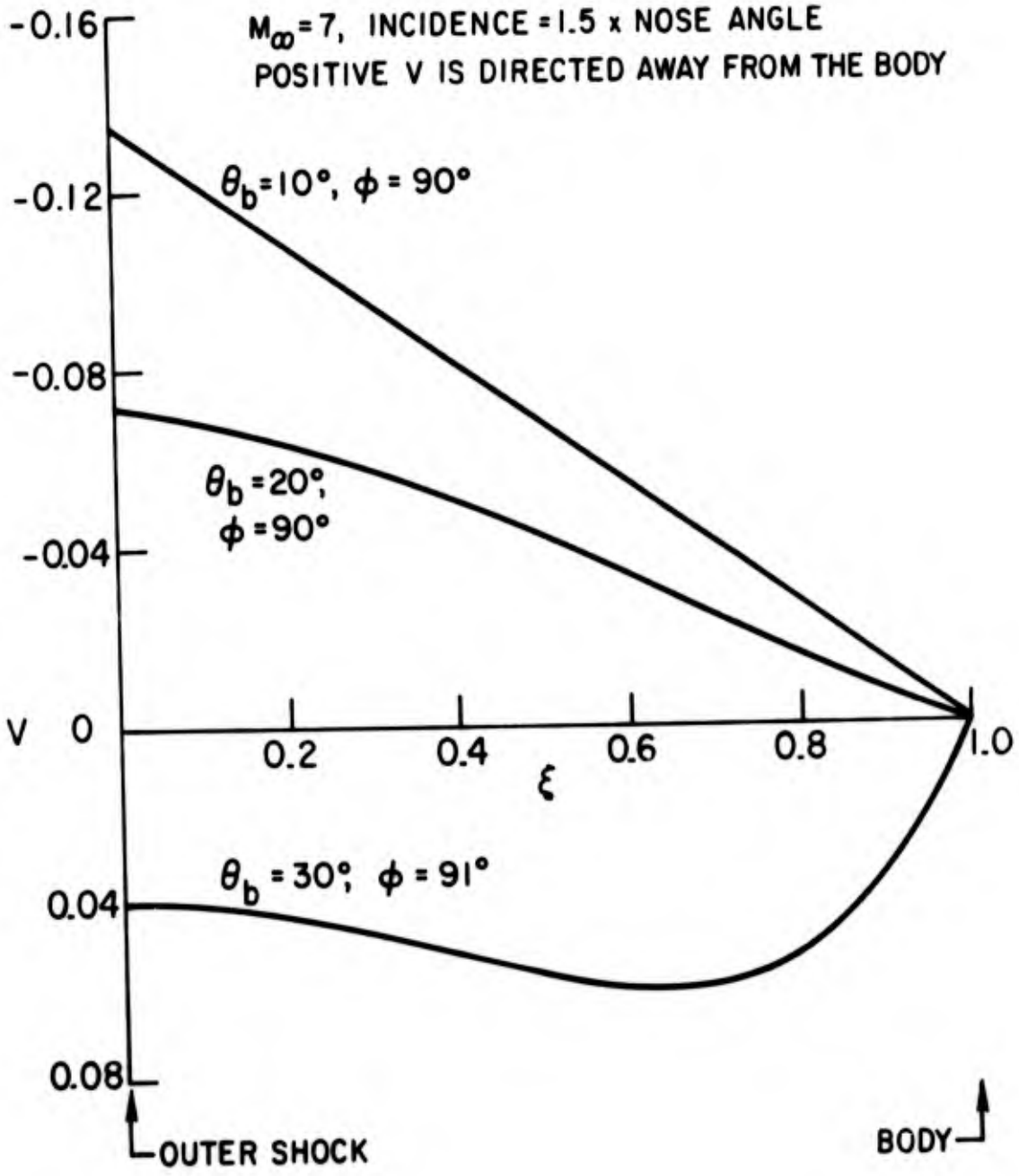

FIG. 26 VARIATION OF NORMAL VELOCITY COMPONENT WITH ξ FOR VARIOUS NOSE ANGLES

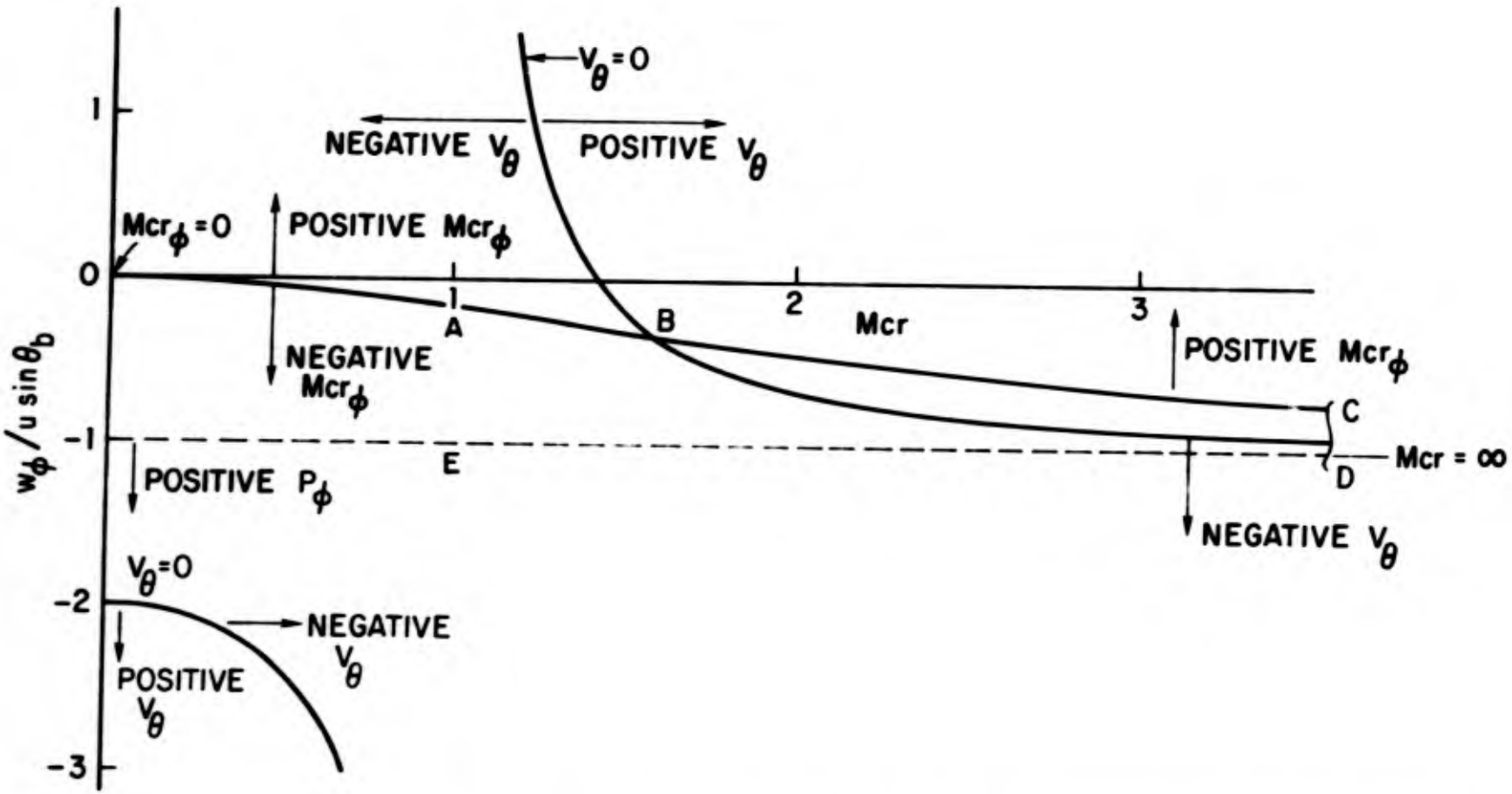

FIG. 27 VARIATION OF THE CIRCUMFERENTIAL VELOCITY GRADIENT PARAMETER AT THE SURFACE WITH CROSS FLOW MACH NUMBER

APPENDIX A. DESCRIPTION OF POWELL'S METHOD

Powell's method (1964b) has been used to adjust the location of the outer shock to minimize the normal velocity at the body in the windward region; and to adjust the location of the internal shock to minimize the circumferential velocity in the leeward symmetry plane. In this appendix the description of Powell's method will be given in terms of its application to the windward region. The location of the outer shock, which Powell's method adjusts, was actually specified (see Section 4) in terms of one shock location and four shock slopes. For ease of notation the present description will be made with the outer shock defined by five locations $\theta_{s_1} \ldots \theta_{s_5}$ (Fig. 5).

Let

$$F(\underline{\theta_s}) = \sum_{k=1}^{5} v_k(\underline{\theta_s})^2 \quad , \tag{A.1}$$

where $\underline{\theta_s}$ has components $\theta_{s_1}, \theta_{s_2} \ldots \theta_{s_5}$, v_k are the normal velocities at the body. Powell's method seeks to choose the components of θ_s such that F is a minimum. Physically it is expected that $F_{min} = 0$. If $\underline{\theta_s}$ is considered to be an estimate of the shock location to make $F(\underline{\theta_s})$ a minimum, and if $(\underline{\theta_s} + \underline{\delta})$ is the actual minimum such that

$$F(\underline{\theta_s} + \underline{\delta}) = 0 \quad , \tag{A.2}$$

then differentiating (A.2) leads to

$$\sum_{k=1}^{5} \frac{\partial v_k(\theta_s + \underline{\delta})}{\partial \theta s_i} \cdot v_k(\underline{\theta_s} + \underline{\delta}) = 0 \quad , \quad i = 1, \ldots 5 \quad . \tag{A.3}$$

Expanding (A.3) as a Taylor series in $\underline{\delta}$ about $\underline{\theta_s}$ and neglecting terms above the first derivative gives

$$\sum_{j=1}^{5} \left\{ \sum_{k=1}^{5} \frac{\partial v_k(\underline{\theta_s})}{\partial \theta_{s_i}} \cdot \frac{\partial v_k(\underline{\theta_s})}{\partial \theta_{s_j}} \right\} \delta_j = - \sum_{k=1}^{5} \frac{\partial v_k(\underline{\theta_s})}{\partial \theta_{s_i}} \cdot v_k(\underline{\theta_s})$$

$$i = 1,2,\ldots 5 \quad . \qquad \text{(A.4)}$$

Powell (1964b) demonstrates that neglect of derivatives higher than the first requires that the magnitude of v_k should be of the same order as the corrections $\underline{\delta}$. In practice this leads to a requirement that the estimate of the shock location $\underline{\theta_s}$ be reasonably close to the converged solution. Powell's method is attractive because it evaluates terms like $\partial v_k(\underline{\theta_s})/\partial \theta_{s_j}$ numerically rather than analytically.

Rather than attempting to obtain $\underline{\delta}$ directly from (A.4), the method treats $\underline{\delta}$ purely as a direction in which to search; that is, a scalar λ_m is sought with which to minimize $(\underline{\theta_s} + \lambda\, \underline{\delta})$.

An auxiliary function $\underline{d}$ is defined such that each component of $\underline{d_i}$ is an independent direction. Approximate derivatives, ${\gamma_i}^k$, of v_k in the ith direction are assumed to be of the form

$${\gamma_i}^k = \sum_{j=1}^{5} \frac{\partial v_k}{\partial \theta_{s_j}} (\underline{\theta_s}) \cdot {d_i}^j \quad , \quad \begin{matrix} i = 1,2,\ldots 5 \\ k = 1,2,\ldots 5 \end{matrix} \quad . \qquad \text{(A.5)}$$

It is assumed that $\underline{\delta}$ can be written in the form

$$\underline{\delta} = \sum_{i=1}^{5} q_i\, \underline{d_i} \quad . \qquad \text{(A.6)}$$

Substitution of (A.5) and (A.6) into (A.4) then leads to

$$\sum_{j=1}^{5} \{ \sum_{k=1}^{5} \gamma_i^k \gamma_j^k \} q_j = p_i \quad , \quad i = 1,2,\ldots 5 \ . \quad (A.7)$$

where

$$p_i = - \sum_{k=1}^{5} \gamma_i^k \cdot v_k(\underline{\theta}_s) \quad .$$

On the first iteration $\underline{d}_i$ is chosen to have the form

$$\underline{d}_i = (0,\ldots , s_i,\ldots 0) \quad (A.8)$$

where s_i is a scaling factor.
The initial evaluation of γ_i^k is given by

$$\gamma_i^k = s_i \cdot [v_k(\theta_{s_1},\ldots \theta_{s_i} + \epsilon_i,\ldots \theta_{s_5}) - v_k(\underline{\theta}_s)]/\epsilon_i \ . \quad (A.9)$$

s_i in equations (A.8) and (A.9) is chosen to satisfy

$$\sum_{n=1}^{5} \gamma_i^{k2} = 1 \quad . \quad (A.10)$$

For each step in the iteration the value of λ_m to minimize $(\underline{\theta}_s + \lambda \underline{\delta})$ is sought following a procedure laid down by Powell (1964a) in a companion paper. Essentially the method consists of evaluating $F(\underline{\theta}_s + \lambda_n \underline{\delta})$ for three values of λ_n, and fitting a quadratic through the corresponding distribution of F_n to establish a fresh estimate λ_m. At each step the value of λ_n which makes F_n a local maximum is discarded. Once λ_m for the current iteration has been found an estimate of $\partial F/\partial \lambda$ is found

so that, after scaling, $\underline{\delta}$ and $\partial F/\partial\lambda$ can replace the largest $\underline{d}_i$ and the corresponding γ_i^k. If λ_1 and λ_2 are the values of λ which give the smallest and next smallest values of F, then

$$\frac{\partial F}{\partial \lambda} \approx \frac{[v_k(\underline{\theta}_s + \lambda_1 \underline{\delta}) - v_k(\underline{\theta}_s + \lambda_2 \underline{\delta})]}{\lambda_1 - \lambda_2} = u_k(\underline{\delta}) \quad . \qquad (A.11)$$

An improved estimate of $\partial F/\partial\lambda$ is given by

$$v_k(\underline{\delta}) = u_k(\underline{\delta}) - \mu \cdot v_k(\underline{\theta}_s + \lambda_m \underline{\delta}) \quad , \qquad (A.12)$$

where

$$\mu = \sum_{k=1}^{5} u_k(\delta) \cdot v_k(\underline{\theta}_s + \lambda_m \underline{\delta}) / \sum_{k=1}^{5} [v_k(\underline{\theta}_s + \lambda_m \underline{\delta})]^2 \quad . \qquad (A.13)$$

$\underline{\delta}$ and $v_k(\underline{\delta})$ are scaled so as to preserve equation (A.10) after $\underline{\delta}$ has replaced $\underline{d}_t$, where t is obtained from

$$|p_t \cdot q_t| = \max |p_i \cdot q_i| \quad , \quad 1 \leq i \leq 5 \quad . \qquad (A.14)$$

The scaled version of $v_k(\underline{\delta})$ replaces γ_t^k and $\underline{\theta}_s + \lambda_m \underline{\delta}$ becomes the new $\underline{\theta}_s$ for the next iteration. Most of the computing time required for Powell's method is in the initial evaluation of γ_i^k by equation (A.9). Powell (1964b) indicates that the advantages of the method are that, firstly, only for the initial step are more function evaluations required than in the generalized least squares method, thereafter the approximate derivatives can be obtained from the local minimization along a line, Powell (1964a).

The second advantage is that replacing $\underline{d}_t$ with the current $\underline{\delta}$ should keep the vectors $\underline{d}_i$ linearly independent. In practice if the initial choice for the outer shock was not close enough to the correct outer shock location it was possible to reach the situation in which $\underline{\delta} = 0$ and $F_{min} \neq 0$.